FACULTY OF SCIENCE
UNIVERSITY OF COPENHAGEN

Long-distance Communication with Atomic Quantum Memories

Simulation and Analysis of DLCZ-type Repeaters using three different Quantum Memories

Jonatan Bohr Brask

Supervisor: Anders Søndberg Sørensen

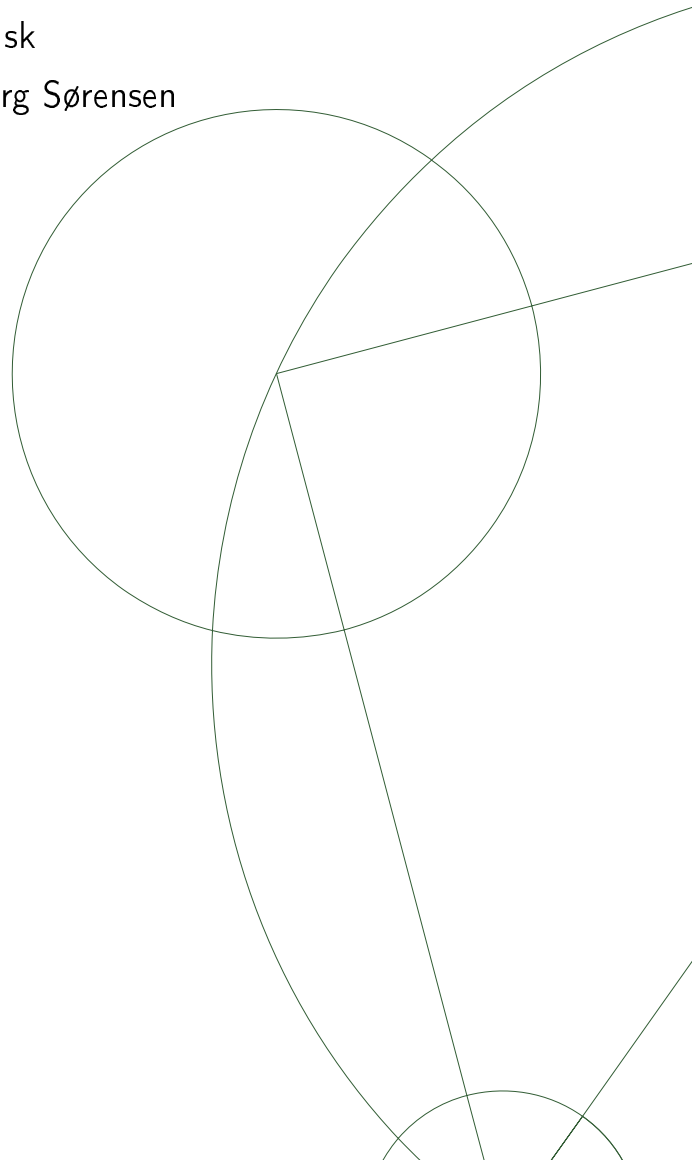

A Thesis Presented for the Degree of
Cand. Scient. in Physics

Niels Bohr Institute
University of Copenhagen
Denmark

12th September 2006

Preface

The work in this master thesis was carried out during the period September 2005 to July 2006. During this time, the project evolved a lot from the initial idea. The original motivation for the work was to investigate if the quantum memory which had been recently developed and tested in experiment in the quantum optics laboratory at the Niels Bohr Institute, would perform well in a DLCZ-type repeater protocol (see the introduction). This problem was graduately generalised to the development of a broader model which also encompass other quantum memories and to include modifications of the protocol. Only late in the work process did the project appear in the form presented here.

The thesis is intended for an audience of other master students of physics or readers of equivalent background in science. An introduction to most specialised concepts is provided in the beginning of the thesis, but a good understanding of quantum mechanics is required for a serious reading, and some experience with quantum harmonic oscillators, for example from quantum optics, is probably helpful.

Working on this project has been very rewarding although time-consuming and demanding at times. During my work I had the good opportunity to attend a few workshops and symposia with scientists in the field, and it has been interesting to get a close view at contemporary research in quantum physics.

Many people have been helpful and encouraging to me during work and writing. First of all I would like to thank my supervisor Anders Søndberg Sørensen for never tiring of my questions, spending many hours on discussions and explanations and for encouraging me to participate in quantum information events in and around the Niels Bohr Institute.

I also want to thank Christine Muschik of the Max-Planck-Institut für Quantenoptik, Germany for kindly sharing her work on one of the atomic quantum memories considered in the thesis.

Thanks is due to Eugene Polzik, Jacob Sherson and all the people of the quantum optics laboratory at the Niels Bohr Institute for helpful discussions and for sharing their expert knowledge on experimental quantum optics.

For the Sisyphean labour of proofreading, for critical comments and much optimism on my behalf I owe many thanks to Oxana Mishina, and thank you also to Morten Helmstedt for correcting my English.

Contents

Chapter 1

Introduction

Within the last three decades, a new field of science on the borderlines between physics, mathematics and computer science has sprung up. The field of *quantum information theory* was founded, when it was realised that information encoded in physical systems of quantum mechanical nature has properties which are fundamentally different from those of information encoded in systems described by classical physics.

A computer based on quantum mechanics - a *quantum computer* - is a potentially very powerful tool, because the laws of quantum mechanics can be exploited to solve some computational problems which are presently considered intractable on any classical computer. Important examples include efficient simulation of quantum mechanical systems, and prime factoring of large integers. Historically, Richard Feynmann was one of the first people to suggest a computer based on quantum mechanics, and his idea was to use it for simulations of quantum systems [13]. The field of quantum information theory only took flight in 1996 however, when Shor realised that prime factoring of large integers can be solved efficiently by a quantum computer [29]. This drew much funding to the field because most modern cryptosystems used e.g. by banks, public authorities and on the internet — most prominently the widespread RSA algorithm — are based on the assumption that prime factoring is computationally intractable[1].

More recently, much effort has been put into the study of quantum information and much has been understood in terms of information theory and computation. However progress has been largely theoretical. The physical implementation of a full scale quantum computer is very difficult, due to the harsh requirements to isolation of the quantum systems, low noise levels and efficient and controllable interaction. Experiments have been performed which test basic operations needed in the computer such as quantum teleportation, but only very small quantum computers has been built to date (on the order of 10 qubits), and only a few quantum algorithms have been implemented. Much therefore still remains to be done in this field, and the work in this thesis should be viewed against the broader background

[1] This has never been proven, but no efficient classical algorithm has been found to date.

of quantum information theory and the long-term goal of implementation of full scale quantum computation.

In this thesis we focus on physical implementation of long-distance quantum communication. Quantum communication already has commercial applications, in quantum cryptographic hardware[2], and we can also envision applications in experiments on quantum mechanics or in the future information exchange between quantum computers. The basic situation we consider is shown in fig. 1.1

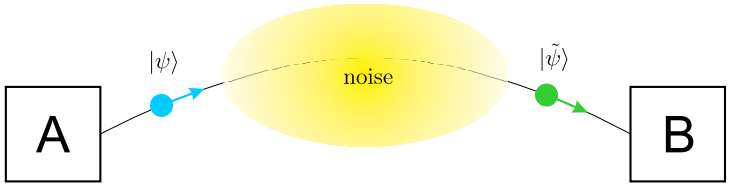

Figure 1.1: Quantum communication over a noisy channel.

A signal encoded into quantum bits (*qubits*) is exchanged between two parties A and B. For a realistic channel, there will be some noise during transmission, and the received state will not be identical to the one which was sent. If nothing is done to correct noise, the quality of the received signal will decrease exponentially with the length of the channel, and the rate at which information can be transferred from sender to receiver will also drop exponentially. For example qubits can be encoded in the polarisation of photons which are sent through an optical fibre. Depolarisation then leads to a degradation of the signal quality and absorption leads to a decreased rate. For short communication ranges one may try to compensate this by improving the quality of fibre, but such an approach is not scalable. As signal quality drops exponentially with the communication length, the demands to the properties of the fibre quickly become impossible to satisfy as the length is increased. The exponential decrease in signal quality and communication rate is the main problem which must be overcome for quantum communication to become viable.

If A and B share a pair of entangled qubits, then, as explained in the chapter on background theory, they can exchange information without loss by means of quantum teleportation. Therefore the general problem of communication over noisy channels can be reduced to the specific problem of establishing an entangled pair between the two ends of a channel. *Quantum repeaters* are protocols which have been designed to solve this problem. In this thesis we are concerned with a particular type of quantum repeaters, originally proposed by Duan, Lukin, Cirac and Zoller in [8] and for this reason termed DLCZ-type repeaters. The DLCZ-type repeater is a probabilistic protocol in which quantum memories (i.e. memories for qubits) play an integral role. In the original proposal by DLCZ the quantum memories were atomic memories which allowed storage of quantum states of light, and indeed this is true for all the systems that we shall look at. However the

[2]See e.g. http://www.magiqtech.com/.

mathematical description of the protocol is broader and we try to emphasise this throughout the thesis.

In the thesis three different quantum memories - all based on atomic storage of light states - are inserted into the same DLCZ-type protocol. The first memory is the original proposal by DLCZ, the second memory was proposed by Muschik *et al* in [21] and the third memory has been demonstrated in experiment at the quantum optics laboratory of the Niels Bohr Institute, with results reported in [18]. The aim of the work has been to investigate how well the DLCZ-type protocol performs for each of these memories. For all three systems, the two important parameters for repeater operation are addressed: the quality of the generated entanglement and the achievable communication rates. We examine how these quantities depend on the parameters of the memories that are used, and verify that sub-exponential scaling with the channel length can be achieved for both of them.

To be able to analyse the three protocols, a mathematical framework for DLCZ-type repeaters is developed. We construct a model in terms of harmonic oscillators and develop mathematical methods for both analytical and numerical treatment of the repeater systems. In particular the idea of a generating function for Bogoliubov transformations, due to A.S. Sørensen, is implemented and extended, and a pertubative model for DLCZ-type repeaters using a general parametrised quantum memory is presented. The mathematical tools are implemented in *Mathematica* programs. By means of the programs, interesting properties of the three repeater systems are approached largely by numerical simulations, but also by analytical calculations. The tools developed for analysis have a broader application than just the three systems we examine, and they constitute a substantial part of the work behind this thesis.

In addition to analysis of DLCZ-type repeaters using the three specific quantum memories — and slightly apart from the main focus of the thesis — we also consider a modification of the repeater protocol to include mixing of parallel channels. The idea was to speed up the communication rate. Channel mixing is explained at the end of the thesis, and some preliminary results are also presented.

Summing up, the essential work presented in this thesis consists of:

- A model for DLCZ-type repeaters and quantum memories based on harmonic oscillators, together with mathematical tools for making numerical and analytic predictions.

- A pertubative approach to DLCZ-type repeaters using a general parametrised quantum memory.

- For each of three specific atomic quantum memories, an analysis of the performance of the original DLCZ protocol employing this memory.

- A preliminary look at the effect of channel mixing for DLCZ-type repeaters.

Thesis outline

The thesis is divided into eight chapters, with the following structure:

Chapter 1 (this chapter) Introduces the main objectives of the work and outlines the thesis.

Chapter 2 Provides the reader with necessary background knowledge from quantum mechanics and quantum information theory.

Chapter 3 Explains the concept of quantum repeaters in detail, in particular the DLCZ-type repeater.

Chapter 4 Explains the generating function method, which is the back bone in all our analytical and numerical calculations.

Chapter 5 Describes a pertubative approach to DLCZ-type repeaters using a general quantum memory

Chapter 6 Describes each of the three quantum memories which are used for repeaters and presents the results from analytical and numerical analysis of each of them.

Chapter 7 Concludes on the results from chapter 5 and chapter 6 and outlines future work.

Chapter 8 Describes the idea of channel mixing and reports on preliminary results.

Chapter 2

Background Theory

The purpose of this chapter is to provide the reader with the necessary theoretical background to understand how quantum repeaters work and to understand the models we are going to use for their analysis. In the first section of the chapter we describe various elements of quantum mechanics. In the second section we give an introduction to quantum computing and quantum communication.

2.1 A bit of Quantum Mechanics

The reader is assumed to be familiar with quantum mechanics in the Dirac bra-ket formulation and should also have met with most of the contents of this section before, but as these are concepts which will be used extensively in the main body of the thesis we make a short reminder here. We do not present proofs of any of the claims in this section. Such proofs may be found in the literature, e.g. [12, 22, 27].

2.1.1 The Density Operator

In the usual formulation the states of a quantum system are vectors in a Hilbert space describing the system: $|\psi\rangle \in \mathcal{H}$. Observables are Hermitean operators on this space and the states evolve in time by unitary transformations. Recall that the quantum state with state vector $|\psi\rangle$ may equally well be described by an operator, called the *density operator*, defined as:

$$\rho \equiv |\psi\rangle \langle\psi| \tag{2.1.1}$$

All information about the physical system contained in $|\psi\rangle$ is also contained in ρ and everything which may be calculated from $|\psi\rangle$ can also be calculated from ρ.

In a given basis $\{|e_i\rangle\}$ for $\mathcal{H}$ we may write:

$$\rho = \sum_{i,j} |e_i\rangle \langle e_i| \rho |e_j\rangle \langle e_j| = \sum_{i,j} |e_i\rangle \langle e_i|\psi\rangle \langle\psi|e_j\rangle \langle e_j| \tag{2.1.2}$$

hence, in this basis the density operator is represented by the *density matrix* with elements $\langle e_i| \rho |e_j\rangle$. We shall not distinguish between the operator and its matrix representation and we will use the terms density matrix and density operator interchangeably.

The action of an operator A on $\mathcal{H}$ on the density matrix is given by:

$$A\rho A^\dagger \tag{2.1.3}$$

If we perform a measurement of the observable O with eigenvalues o_i then the probability of obtaining each possible outcome and the associated post-measurement density matrix are given by[1]:

$$P(o_i) = \mathrm{Tr}(P_i\rho) \qquad \text{and} \qquad \frac{P_i\rho P_i^\dagger}{\mathrm{Tr}(P_i\rho)} \tag{2.1.4}$$

where P_i is the projection operator onto the eigenspace associated with o_i. It follows that the expectation value of O is simply $\mathrm{Tr}(O\rho)$.

When the system is composite, consisting e.g. of subsystems A and B, then the density operators for the subsystems can be derived from that of the joint system by taking the partial trace:

$$\rho_A = \mathrm{Tr}_B(\rho) \qquad \rho_B = \mathrm{Tr}_A(\rho) \tag{2.1.5}$$

the operators ρ_A, ρ_B are also called *reduced density operators*. Predictions about measurements on the subsystems can be made from ρ_A, ρ_B in exactly the same way as described for ρ above.

Two properties characterise the set of density operators: An operator ρ on $\mathcal{H}$ is a density operator associated with some state (or mixture, see the next section) if and only if it is positive and has unit trace:

$$\langle\psi|\rho|\psi\rangle \geq 0 \;\forall\; |\psi\rangle \in \mathcal{H} \qquad \mathrm{Tr}(\rho) = 1 \tag{2.1.6}$$

It follows from the positivity that any density operator is also Hermitean.

2.1.2 Mixed and Pure States

One reason that we use the density operator formalism is that it applies also to incoherent mixtures of states and hence is more general than the state vector formalism.

Suppose that our knowledge of the quantum system is limited so that we are unable to ascribe to it a single state, but rather each state from the set $\{|\psi_i\rangle\}$ is known to occur with probability p_i, where $\sum_i p_i = 1$. When more than one of

[1] Strictly speaking, these formulae are valid only for projective measurement. Generalised measurements with measurement operators which are not necessarily orthogonal projections and outcomes which are not eigenvalues of an observable may be defined, but since we deal only with the projective case in this thesis, we take (2.1.4) as our definition [22].

the p_i are non-zero, the system is described by a statistical or incoherent mixture of states. We say that the system is in a *mixed state*. When all but one of the p_i vanish the system is in a *pure state*.The density operator is defined for mixed states in the following way:

$$\rho \equiv \sum_i p_i \rho_i = \sum_i p_i \left|\psi_i\right\rangle \left\langle\psi_i\right| \tag{2.1.7}$$

All the properties listed in sec. 2.1.1 hold also for this definition.

Statistical averages over a mixture are very easily calculated from ρ. Whenever we apply a linear map to (2.1.7) we get simply the weighted sum of this map applied to each of the pure state density matrices ρ_i, i.e. the mean. For example, for the expectation value:

$$\mathrm{Tr}(O\rho) = \sum_i p_i \mathrm{Tr}(O\rho_i) = \sum_i p_i \left\langle O\right\rangle_i = \left\langle O\right\rangle \tag{2.1.8}$$

It is also easy to test whether the state is pure or mixed since for any density matrix, ρ is pure if and only if $\mathrm{Tr}(\rho^2) = 1$.

We see that we have a nice handle on doing computations for systems which behave probabilistically, and this will come in handy when we begin our study of implementations of the repeater.

2.1.3 Fidelity

A measure of the closeness of quantum states is something we shall need extensively. Such a measure is provided by the *fidelity*. The fidelity of an arbitrary state ρ with respect to a pure state $|\psi\rangle$, we define to be:

$$F(\rho, \psi) \equiv \mathrm{Tr}(\rho|\psi\rangle\langle\psi|) = \langle\psi|\rho|\psi\rangle \tag{2.1.9}$$

Fidelity can also be defined in the case where both states are mixed, but this definition will suffice for our purposes[2].

It is not hard to prove that:

$$0 \leq F(\rho, \psi) \leq 1 \tag{2.1.10}$$

with $F(\rho, \psi) = 0$ if and only if the support of ρ is on a subspace orthogonal to $|\psi\rangle$, and $F(\rho, \psi) = 1$ if and only if $\rho = |\psi\rangle\langle\psi|$. Furthermore, it follows from the cyclic property of the trace that the fidelity is preserved under unitary transformations:[3]

$$F(U\rho U^\dagger, U|\psi\rangle) = F(\rho, |\psi\rangle) \tag{2.1.11}$$

[2]Note though, that (2.1.9) does not generalise directly since $\mathrm{Tr}(\rho\rho) < 1$ if ρ is not pure. To ensure $F(\rho, \rho) = 1$ for mixed states, a root is included in the definition. In [22] $F(\rho, \sigma) \equiv \mathrm{Tr}\sqrt{\rho^{1/2}\sigma\rho^{1/2}}$.

[3]We shall write $F(\rho, \psi)$ or $F(\rho, |\psi\rangle)$ alternately as is more convenient.

In the case where both states are mixed, but can be simultaneously diagonalised, $F(\rho, \sigma)$ can be given a geometric interpretation. Writing $\rho = \sum_i \lambda_i |e_i\rangle\langle e_i|$ and $\sigma = \sum_i \kappa_i |e_i\rangle\langle e_i|$ we have:

$$F(\rho, \sigma) = \sum_i \lambda_i \kappa_i \tag{2.1.12}$$

which is simply the inner product of the vectors consisting of the eigenvalues of the states. In the general case no such interpretation has been found[4], but the simple trace definition (2.1.9) means that the fidelity is easy to work with and to evaluate, and so it remains a valuable tool [22].

It is apparent that the fidelity is not a metric, since a metric is minimal for identical states. There are other distance measures which do yield metrics on the set of density operators and have simple geometric interpretations, but we prefer the fidelity because of its simplicity and because it is the common measure in the literature on quantum repeaters [3, 6, 8, 21].

2.1.4 Entanglement

While the sections above dealt with the mathematical formalism of quantum mechanics, this section is about a genuine physical phenomenon.

Whenever a quantum system consists of several parts there is a possibility for those parts to be correlated in a highly non-classical manner. The phenomenon is called *entanglement*. In quantum communication entanglement is completely essential for information transfer and the entire purpose of the repeater is to generate and distribute entanglement among different locations. Hence this concept is central for the work in this thesis.

Formally entanglement is defined as follows:

> Let $|\psi_{AB}\rangle$ denote the joint state of systems A and B. Then, whenever this state cannot be written as a product of states of the subsystems $|\psi_{AB}\rangle = |\psi_A\rangle \otimes |\psi_B\rangle$, it is said to be *entangled* or *non-separable*.

A state which is not entangled is called *separable*. Entangled states between any number of participants is possible, but here we will consider only bipartite entanglement - that is entanglement between just two systems.

The easiest way to understand entanglement is by example. Say that we have two identical quantum systems described by two-dimensional Hilbert spaces $\mathcal{H}_A$ and $\mathcal{H}_B$. Each of these have a basis and, keeping a foresighted eye on the section about qubits below, we denote the elements $\{|0\rangle_A, |1\rangle_A\}$ and $\{|0\rangle_B, |1\rangle_B\}$ respectively. We can then define four important examples of entangled states.

[4]Some attempts have been made in the case of qubit states, e.g. [4].

The so-called *Bell states*:

$$\begin{aligned} \left|\Phi^+\right\rangle &= \frac{|00\rangle_{AB} + |11\rangle_{AB}}{\sqrt{2}} \qquad \left|\Phi^-\right\rangle = \frac{|00\rangle_{AB} - |11\rangle_{AB}}{\sqrt{2}} \\ \left|\Psi^+\right\rangle &= \frac{|01\rangle_{AB} + |10\rangle_{AB}}{\sqrt{2}} \qquad \left|\Psi^-\right\rangle = \frac{|01\rangle_{AB} - |10\rangle_{AB}}{\sqrt{2}} \end{aligned} \tag{2.1.13}$$

We can use one of the Bell states to illustrate the correlations between entangled systems. Suppose the state of the composite system is $|\psi_{AB}\rangle = |\Psi^-\rangle$ and we make a projective measurement on A onto the basis, i.e. we measure the observable:

$$M_A = \lambda_0 \left|0\right\rangle_{AA}\left\langle 0\right| + \lambda_1 \left|1\right\rangle_{AA}\left\langle 1\right| \qquad \lambda_0, \lambda_1 \in \mathbb{R} \tag{2.1.14}$$

The possible outcomes of this measurement are the eigenvalues λ_0, λ_1. They each occur with probability $\frac{1}{2}$ and the corresponding post measurement states are[5]:

$$\lambda_0 : \frac{P_0|\Psi^-\rangle}{\sqrt{1/2}} = |01\rangle_{AB} \qquad \lambda_1 : \frac{P_1|\Psi^-\rangle}{\sqrt{1/2}} = -|10\rangle_{AB} \tag{2.1.15}$$

where $P_0 = |0\rangle_{AA}\langle 0|$ and $P_1 = |1\rangle_{AA}\langle 1|$ are the projection operators onto the eigenspaces corresponding to λ_0, λ_1[6]. Note that there is perfect correlation between the measurement outcomes and the state of system B after the measurement. If λ_0 was obtained, then the post measurement state of B is $|1\rangle$, if λ_1 was obtained the state is $|0\rangle$. As soon as the measurement on A has been performed we know with certainty what would be the outcome of a similar subsequent measurement on B.

In itself there is nothing non-classical about this kind of correlation. We would obtain the same result if we were to pick at random from a large ensemble of paper slips, half of which were labelled 10 and the other half 01. However similar correlations are found also when $|\Psi^-\rangle$ are measured in other bases, and by comparing expectation values from different measurements, it is possible to obtain statistics which would be impossible for a classical system. More precisely the so-called CHSH inequality can be broken. It is outside the scope of this thesis to go into details, but essentially the CHSH inequality is valid for variables which are classical in the sense that they have values which are fixed prior to measurement (the assumption of realism), and hence by breaking it one shows that this cannot be the case for quantum variables. Here we are touching upon the foundations of quantum mechanics, the theory of hidden variables and the famous EPR paradox. Readers who would like know more about this are referred to the articles of John Bell [1]. See for example "Bertlmann's socks and the nature of reality" for a discussion of entanglement.

[5] To obtain the probabilities one can find the reduced density matrix for system A: $\rho_A = \mathrm{Tr}_B(\left|\Psi^-\right\rangle\left\langle\Psi^-\right|)$. Then $P(\lambda_0) = \mathrm{Tr}_A(|0\rangle_{AA}\langle 0|\,\rho_A)$ and similarly for λ_1, c.f. sec. 2.1.1.

[6] Defined this way, the projection operators act only on system A; the operators in (2.1.15) are really $P_{0A} \otimes \mathbb{1}_B, P_{1A} \otimes \mathbb{1}_B$. However it is convention to keep the identity operator implicit.

Since entanglement is of such importance, it would be useful to have first a way of testing for entanglement and second a measure of the degree of entanglement possessed by a given state.

The definition above does not lend itself very well to testing, since proving non-existence of the states $|\psi_A\rangle, |\psi_B\rangle$ is in general a difficult task. Fortunately there are other tests which are much simpler. A state is separable if and only if the reduced density matrices of its subsystems are pure:

$$|\psi\rangle_{AB} \quad \text{separable} \Leftrightarrow \rho_A = \mathrm{Tr}_B(|\psi\rangle_{AB}\langle\psi|) \quad \text{pure} \Leftrightarrow \mathrm{Tr}(\rho_A^2) = 1 \qquad (2.1.16)$$

where A, B may equally well be interchanged. Given a matrix it is straightforward to calculate the trace, and so this is a good practical test for entanglement.

Defining a good measure of entanglement for mixed states is much harder[7], and presently there is no agreement on any single measure in the literature. Rather a variety of different measures exist. An overview over some of these, with references, may be found in Wei *et al.* [30]. We are not going to need an entanglement measure since in this thesis we will be aiming not just at generating entanglement, but at generating a particular entangled state. What we need then is a notion of closeness of our generated states to this ideal state, and this is provided by the fidelity. Suffice it to say that, whatever measure is adopted, the Bell states are *maximally entangled* and for two-qubit systems all the maximally entangled states are related to the Bell states by single-qubit unitary transformations [5, 30]. Hence when generating entangled states, the best we can hope for is a Bell state.

Entanglement comes about in many ways in nature. For example atoms which interact with light (e.g. through absorption and spontaneous emission) generally become entangled with the light field. Collisions between atoms can also give rise to entangled states. In quantum computing and communication schemes one of the great challenges is to keep the system free of undesirable entanglement with the environment, while preserving controlled entangled states within. To create entanglement it is preferable to use quantum systems which interact strongly with each other, but at the same time we need the interaction with the surroundings to be minimal, hence in any design there must be a trade-off between these two effects. Generating entanglement in a controlled manner is not easy, and naturally the method used must depend on the physical nature of the setup into which it is integrated.

2.1.5 Harmonic Oscillator Systems

To analyse the performance of DLCZ-type repeaters we will model them by harmonic oscillators. In this section we introduce concepts from the theory of harmonic oscillators that we shall find need for. The ideas below are used in our

[7] For pure states one may use the von Neumann entropy.

model of the DLCZ-type repeater, and are applied in the chap. 4 on the generating function as well as in subsequent sections which deal with specific physical systems.

Recall that the state space of the quantum one-dimensional simple harmonic oscillator is spanned by the *number states* $\{|n\rangle\}$, $n = 0, 1, 2, ...$[8]. The annihilation and creation operators $\hat{a}, \hat{a}^\dagger$ have the following properties:

$$[\hat{a}, \hat{a}^\dagger] = 1 \tag{2.1.17}$$
$$\hat{a}|0\rangle = 0, \qquad \hat{a}|n\rangle = \sqrt{n}|n-1\rangle,\ n > 0 \qquad \hat{a}^\dagger|n\rangle = \sqrt{n+1}|n+1\rangle$$

The number states can be expressed in terms of $\hat{a}^\dagger$ as:

$$|n\rangle = \frac{1}{\sqrt{n!}}(\hat{a}^\dagger)^n|0\rangle \tag{2.1.18}$$

The state $|0\rangle$ is sometimes called a vacuum state. In the quantum description, light (or any other bosonic field) is represented by one or more harmonic oscillators, and the vacuum then corresponds to the state where there are no photons in the field.

Since the basis states can be expressed entirely in terms of $\hat{a}^\dagger$ and $|0\rangle$, all other states of the harmonic oscillator may also be expressed in these terms. Two important classes of states are *coherent states* and *squeezed states*.

The coherent states are the right eigenstates of the annihilation operator: for any complex number α there exists a state $|\alpha\rangle$ such that $\hat{a}|\alpha\rangle = \alpha|\alpha\rangle$. The coherent states are not orthogonal but define an overcomplete basis for the state space. In terms of the creation operator the coherent states are:

$$|\alpha\rangle = e^{-\frac{|\alpha|^2}{2}} \sum_{n=0}^{\infty} \frac{\alpha^n}{\sqrt{n!}}(\hat{a}^\dagger)^n|0\rangle = D(\alpha)|0\rangle \tag{2.1.19}$$

where the *displacement operator* D is defined by:

$$D(\alpha) \equiv e^{\alpha\hat{a}^\dagger - \alpha^*\hat{a}} \tag{2.1.20}$$

All properties of the coherent states may be derived from the displacement operator, whose properties may in turn be derived from equations (2.1.17). In the generating function method of sec. 4.1, we make extensive use of displacement operators.

Physically, coherent states are the 'most classical' states of the harmonic oscillator. They represent the opposite wave-like case to the number states, which are the most particle-like states. E.g. in the case of light, the number state $|1\rangle$ represents a single photon while the coherent states give a good description of the output from a laser in which the photon number is not fixed but follows a poissonian distribution [12, 20].

[8] The number states are also called Fock states.

The squeezed states are non-classical. They are states for which the quantum uncertainty of some observable is below the standard limit given by the Heisenberg uncertainty relation. Here we consider quadrature squeezing. The *quadrature operators* are defined by:

$$X = \frac{1}{\sqrt{2}}(\hat{a}^\dagger + \hat{a}) \qquad P = \frac{i}{\sqrt{2}}(\hat{a}^\dagger - \hat{a}) \tag{2.1.21}$$

In the case of light, they correspond to the sine and cosine components of the electric field. For a massive particle in a harmonic oscillator potential, they correspond to position and momentum. They obey the uncertainty relation[9]: $\langle(\Delta X)^2\rangle \langle(\Delta P)^2\rangle \geq \frac{1}{4}$, and a squeezed state is a state for which:

$$\langle(\Delta X)^2\rangle < \frac{1}{2} \qquad \text{or} \qquad \langle(\Delta P)^2\rangle < \frac{1}{2} \tag{2.1.22}$$

In fig. 2.1 this corresponds to a deformation of the disk representing the uncertainty of the state.

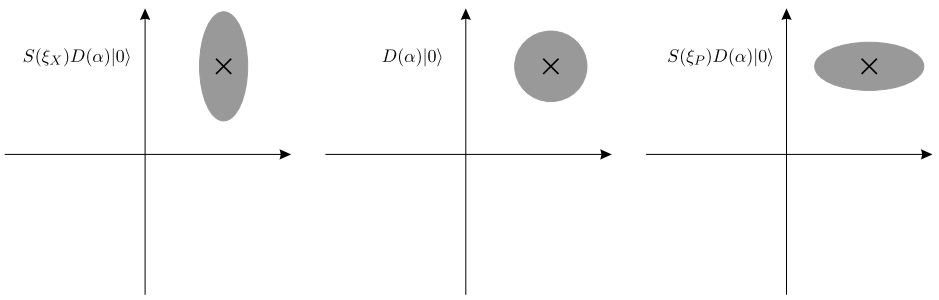

Figure 2.1: Phase-space plot of: **a)** Squeezing in the X-quadrature. **b)** No squeezing. **c)** Squeezing in the P-quadrature. The three pictures illustrate the action the squeezing and displacement operators. The cross indicates the expectation values of X, P, which for the coherent state $|\alpha\rangle$ are $\sqrt{2}\mathrm{Re}(\alpha), \sqrt{2}\mathrm{Im}(\alpha)$ respectively. The coloured area shows the expected spread (variance) around the mean. For no squeezing, the variance is the same in all phase-space directions. When there is squeezing, some directions have reduced variance at the expense of increased variance for the complementary (in the uncertainty relation) directions.

Mathematically, squeezed states can be generated by acting with the *squeezing operator*:

$$S(\xi) \equiv e^{-\frac{1}{2}(\xi\hat{a}^{\dagger 2} - \xi^*\hat{a}^2)} \tag{2.1.23}$$

Here $\xi = re^{i\theta}$ is in general a complex parameter. The magnitude r determines the degree of squeezing and the phase θ determines the axis in phase-space which is squeezed. Squeezing along X, P are obtained for $\theta = 0, \pi$ respectively. If the squeezing is not along one of these, the ellipse in fig. 2.1 will be rotated away from the axes.

[9]From the relation $\langle(\Delta A)^2\rangle \langle(\Delta B)^2\rangle \geq \frac{1}{4}|\langle[A, B]\rangle|^2$, c.f. [27] p. 35.

An important case is the squeezed vacuum state, given by $S(\xi)|0\rangle$. For this state, when $\theta = 0$ we have:

$$\left\langle (\Delta X)^2 \right\rangle = \frac{1}{2} e^{-2r} \qquad \left\langle (\Delta P)^2 \right\rangle = \frac{1}{2} e^{+2r} \tag{2.1.24}$$

This relation also holds for any displacement of the state, as shown in the figure. The squeezed vacuum state will play a role for one of the quantum memories we look at in chap. 6 and the degree of squeezing will be an important parameter.

So far we have considered only a single harmonic oscillator, but what we shall need for our repeater models is a collection of oscillators (or equivalently a higher-dimensional harmonic oscillator). Different oscillators will represent different parts of the physical system, e.g. one describes a field of light while another describes the spin state of atoms. We index the collection of operators by i. Each oscillator is also called a *mode*, and the annihilation and creation operators $\hat{a}_i, \hat{a}_i^\dagger$ are called *mode operators*. The state space of the joint system is spanned by the tensor products of the number states $|n\rangle_i$ for each mode[10]. For N modes we write:

$$|n_1 ... n_N\rangle = \bigotimes_{i=1}^{N} |n_i\rangle_i = \frac{1}{\sqrt{n_1! ... n_N!}} (\hat{a}_1^\dagger)^{n_1} ... (\hat{a}_N^\dagger)^{n_N} |vac\rangle \tag{2.1.25}$$

where $|vac\rangle$ denotes the joint vacuum state, and $\hat{a}_i^\dagger$ acts only on mode i. The commutation relation in (2.1.17) is modified to be:

$$[\hat{a}_i, \hat{a}_j^\dagger] = \delta_{ij} \tag{2.1.26}$$

As for a single oscillator, all states may be described in terms of the mode operators and the vacuum. In particular, the two-mode squeezed vacuum state is given by $S_{ij}(\xi)|vac\rangle$, where:

$$S_{ij}(\xi) = e^{\xi^* \hat{a}_i \hat{a}_j - \xi \hat{a}_i^\dagger \hat{a}_j^\dagger} \tag{2.1.27}$$

which implies:

$$S_{ij}(\xi)|vac\rangle = \operatorname{sech}(r) \sum_{n=0}^{\infty} \left[-e^{i\theta} \tanh r \right]^n |nn\rangle_{ij} \tag{2.1.28}$$

It is easy to see that this state is entangled, since all components have $n_i = n_j$. Two-mode squeezing is important for entanglement generation, and we will see an example in sec. 6.2.

As the last topic in this section, we define *Bogoliubov transformations*. These are transformations on the set of mode operators, which are linear and preserve the commutation relations. Denoting the transformed operators with primes, a general Bogoliubov transformation is given by:

$$\hat{a}_j' = \sum_i b_{ji} \hat{a}_i + c_{ji} \hat{a}_i^\dagger \tag{2.1.29}$$

[10] Since it is the tensor direct product of the Hilbert spaces for each mode.

The b_{ji}, c_{ji} are complex, and the requirement $[\hat{a}'_j, \hat{a}'^{\dagger}_k] = \delta_{jk}$ becomes[11]:

$$\mathbf{b}\mathbf{b}^{\dagger} - \mathbf{c}\mathbf{c}^{\dagger} = \mathbb{1} \tag{2.1.30}$$

where the matrices $\mathbf{b}, \mathbf{c}$ have elements b_{ji}, c_{ji}.

It is sometimes easier to express an operator in terms of the action on the mode operators than in terms of the number states. Many useful operations can be expressed as Bogoliubov transformations, including one- and two-mode squeezing as defined above.

2.2 Basics of Quantum Information

In this section we introduce basic concepts of quantum computing and communication - *quantum information* for short. We do not delve deeply into quantum information theory, but discuss only fundamental ideas that will be needed for the repeater[12]. The section builds primarily on [22] and course materials from courses at DAMTP, Cambridge.

2.2.1 Qubits and Memories

The basic entity of quantum information is the *qubit*. The qubit is the quantum analogue of the classical bit, and it is defined simply as any two-level quantum system. That is any system whose state space is two-dimensional.

There are many examples of physical systems which may serve as qubits. Spin states of spin-$\frac{1}{2}$ particles, polarisation states of photons or two hyperfine energy levels of an atom are but a few. It is one of the great strengths of the mathematical formulation of quantum information theory that it is independent of what system is used for implementation. Thus abstractly a qubit is described by a two-dimensional Hilbert space $\mathcal{H}$. Usually there will be some basis for $\mathcal{H}$ connected in a natural way with the physical system (i.e. a basis in which measurements are carried out naturally). This basis we call *the computational basis* and we denote the elements $\{|0\rangle, |1\rangle\}$. Notice the use of italics to distinguish qubit states from harmonic oscillator number states. The collective state of more qubits is described by the tensor direct product of their Hilbert spaces, and the basis elements of the product space are tensor products of the original basis elements. We adapt a notation similar to (2.1.25), and for e.g. three qubits one computational basis state is $|001\rangle = |0\rangle_1 \otimes |0\rangle_2 \otimes |1\rangle_3$.

When quantum information is transmitted from one location in space to another, it necessarily has to be encoded into qubits which can move (e.g. photons but also other particles). On the other hand, when performing computations it is often the case that not all qubits are operated on simultaneously, and the qubits which are not active then have to be stored in some spatially fixed system. In

[11] From (2.1.26): $[\hat{a}'_j, \hat{a}'^{\dagger}_k] = \sum_{i,\tilde{i}} (b_{ji} b^*_{k\tilde{i}} \delta_{i\tilde{i}} - c_{ji} c^*_{k\tilde{i}} \delta_{i\tilde{i}}) = \sum_i b_{ji} b^*_{ki} - \sum_i c_{ji} c^*_{ki}$

[12] For a thorough introduction to quantum information theory, see [22].

the terminology of quantum information theory we speak of *flying* and *stationary* qubits. An ideal *quantum memory* is a quantum system into which the state of flying qubits can be written and later retrieved unchanged[13]. Naturally for any realistic memory, the retrieved state will not be perfectly identical to the one which was stored, but in any case we strive to keep the output as close to the input as possible (i.e. the fidelity of the retrieved state w.r.t. the input state should be close to 1) and the possible storage times as long as possible. In the context of quantum repeaters, memories are useful because the repeater protocols involve many parallel computations. Some of these will be faster than others and the output qubits then need to be stored while the remaining computations finish. Also a lot of classical communication takes place during the protocols and qubits need to wait for this exchange to be done.

2.2.2 Computation and Communication

Just like the qubit resembles the classical bit by having two levels, the structure of the quantum computer also resembles the structure of ordinary computers. Computation is effected by applying a sequence of gates to a collection of bits and reading out their state. However, the nature of the gates and the readout is very different in the two cases, because qubits allow for superpositions of the levels and their state will in general be disturbed by measurements. Mathematically communication can be viewed as a special case of computation. A communication channel over which quantum information in the form of qubits is transmitted is simply a computation where the input and output are allowed to be separated in space.

On the classical computer, gates are logic operators such as OR or AND. Quantum gates are defined to be linear, unitary transformations on a set of qubits:

$$U : \mathcal{H}^{\otimes n} \rightarrow \mathcal{H}^{\otimes n} \tag{2.2.1}$$

A set of quantum gates is said to be *universal* for quantum computation if any transformation of the form (2.2.1) can be approximated arbitrarily well using only gates from the set. As for the classical computer a small number of different gates is sufficient for a universal set[14].

In general, we distinguish between single-qubit operations, also called *local* operations, and *non-local* operations, which act on more than one qubit and cannot be factored into local operations.

Three single qubit operations, which we shall need below, are the bit flip, phase flip and combined bit and phase flip gates. We denote them X, Z, Y respectively[15]

[13] We can also think about memories outside a qubit description. A quantum memory is simply a system which allows storage and retrieval of the quantum state of some other, usually more volatile, physical system.

[14] It can be proved that single qubit operations and the controlled-NOT gate together form a universal set [22].

[15] In the computational basis, the X, Y, Z-gates are represented by the usual Pauli matrices.

and they act on an arbitrary single qubit state $|\psi\rangle = a|0\rangle + b|1\rangle$ as follows.

$$X|\psi\rangle = a|1\rangle + b|0\rangle \qquad Z|\psi\rangle = a|0\rangle - b|1\rangle \tag{2.2.2}$$
$$Y|\psi\rangle = -ia|1\rangle + ib|0\rangle$$

We note that X interchanges the 0- and 1-components of $|\psi\rangle$ while Z shifts the relative phase by π.

As an example of a non-local operation we look at a two-qubit operation. The controlled-NOT gate (cNOT) is a bit-flip on one qubit conditioned on the state of another. When the state of the control qubit is $|1\rangle$, X is applied to the target qubit. Since cNOT is a quantum gate acting on qubits it is linear and preserves superpositions. For example:

$$\text{cNOT}\left[\frac{|0\rangle + |1\rangle}{\sqrt{2}} \otimes |0\rangle\right] = \frac{|00\rangle + |11\rangle}{\sqrt{2}} \tag{2.2.3}$$

Note in this equation that while the initial state was separable, the final state is a Bell state, i.e. a maximally entangled state. This ability to create entanglement makes cNOT a very powerful gate, and in many proposed implementations of the quantum computer, one of the main challenges is to implement this gate or one which is equivalent to it under local operations [19, 22]. This is a difficult task since the non-local nature of the gate means that the two qubits must interact in a controlled manner.

An important difference between quantum and classical information is that it is impossible to obtain complete knowledge about the state of qubits by measurement, and attempts to do so will destroy the state. If for example we measure an observable with eigenvalues $\{x\}$ and a complete set of associated eigenkets $\{|x\rangle\}$, then the outcome will be one of the x's and the state of the system will be projected to the corresponding eigenket. Hence if the state of the system before the measurement was a superposition:

$$|\psi\rangle = \sum_x c_x |x\rangle \tag{2.2.4}$$

we do not learn anything about the coefficients c_x. In general, to discover the values of these coefficients accurately, we would need to measure on very (infinitely) many copies of the state (2.2.4). But quantum mechanics does not allow us to make copies. The *no-cloning theorem* states that:

> It is impossible to construct a device, which given an unknown quantum state will output two identical, perfect copies of that state [22].

The no-cloning theorem is a major obstacle when designing quantum algorithms and communication protocols. For example we cannot keep backups of quantum information which is sent over a lossy channel, and when we read out the result of a computation, we do not obtain the full state of the qubits. However, even

though complete knowledge of the final state may be inaccessible to us, we can make sure, by designing the algorithms carefully that a single measurement (or a few iterations) does give us information specific to the task the algorithm is performing.

It should be apparent that the discipline of designing quantum algorithms is somewhat more subtle than its classical counterpart. We will not discuss algorithm design much in this thesis. We focus on quantum repeaters and we deal with them partly trough a particular model in terms of harmonic oscillators rather than the qubit formulation. We will need one very important circuit though, namely the quantum teleportation algorithm. It is a remarkable fact that quantum mechanics allows for the transfer of quantum information without any direct quantum channel between the sender and the receiver. By *quantum teleportation* the state of one qubit is transferred unto another, possibly far removed in space from the first, by making use of prior entanglement and classical messages.

2.2.3 Quantum Teleportation

The teleportation circuit is shown in fig. 2.2. Three qubits are involved in the teleportation. The first qubit, initially in the arbitrary state $|\psi\rangle$, is the qubit to be teleported. The second two qubits are prepared in one of the maximally entangled states. Teleportation can be achieved with any maximally entangled state, but for the sake of argument we choose the Bell state $|\Phi^+\rangle$. One may imagine that the qubits of the entangled pair have been separated spatially by a large distance, so that on one location the sender is keeping qubits 1,2 and on another location the receiver is keeping qubit 3.

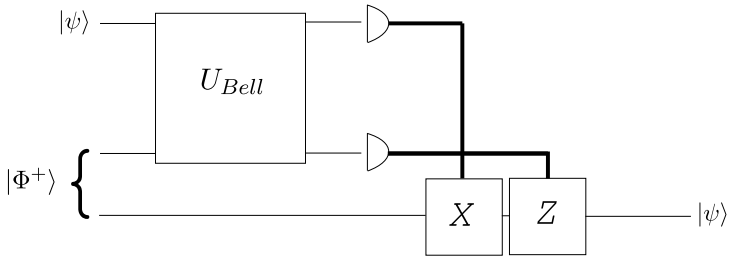

Figure 2.2: Teleportation circuit. Time is running from left to right, and we label the input qubits 1,2,3 from above. The initial state $|\psi\rangle$ of qubit 1 is teleported onto qubit 3. The bold lines carry classical information.

In the first step of the algorithm, a *Bell measurement* is performed on qubits 1 and 2. Since the four Bell states form an orthonormal set, they are a basis for the two-qubit Hilbert space $\mathcal{H}^{\otimes 2}$. A Bell measurement is defined to be a projective measurement onto this basis. Equivalently it is a unitary transformation from the Bell to the computational basis[16] followed by measurement in the computational

[16]Recall that any two bases of a Hilbert space are connected by a unitary transformation.

basis (c.f. sec. 2.2.1). There are four possible outcomes corresponding to the Bell states, and for each of these we list the resulting state of the third qubit:

Measurement outcome	$\|\Phi^+\rangle$	$\|\Phi^-\rangle$	$\|\Psi^+\rangle$	$\|\Psi^-\rangle$
State of qubit 3	$\|\psi\rangle$	$Z\|\psi\rangle$	$X\|\psi\rangle$	$Y\|\psi\rangle$

Table 2.1: Conditional states after the Bell measurement. Z,X,Y are the phase and bit flip gates. The reader is referred to app. A for the details of calculation.

The measurement outcomes have equal probabilities independent of the initial state, and in each case the final state of qubit 3 is a pure state equal to the input state of qubit 1 up to a combination of phase and bit flips conditional on the outcome. Since each of the gates X, Y, Z square to 1, all we have to do to recover $|\psi\rangle$ is to compare our measurement outcome with tab. 2.1 and apply the appropriate gate to qubit 3. This means that the sender must pass a classical message of two bits to the receiver[17].

We have reached a remarkable result: Without any direct interaction and transmitting only a short classical message the full quantum state of qubit 1 has been transferred to qubit 3. What is more, as long as the measurement and gates work perfectly and the prepared entanglement is really maximal, this transfer is perfect, regardless of the separation between qubits 1 and 3. From the point of view of communication this is very promising: If we can manage to distribute entanglement among senders and receivers, then quantum information can be exchanged without any further need for protection from noise. Since the entanglement distribution takes place in advance of the actual signalling it can be allowed to be lossy and imperfect without any risk of losing important messages, as long as the final entangled states are good. The generation and distribution of entanglement is the purpose of the quantum repeater.

Here we adopt the convention that a transformation *from* one basis *to* another actively maps the basis vectors of the first onto the basis vectors of the second. This means that the matrix representation of a state in the new basis is obtained by applying the Hermitean conjugate of the transformation matrix in the old basis to the representation of the state in the old basis ([27] p. 36f).

[17] Note that the need for a classical message prevents faster-than-light signalling. If the receiver does not know the measurement outcomes, his best description of qubit 3 is an equally weighted mixture of the states in tab. 2.1, but that is the state $\rho = \frac{1}{2}\mathbb{1}$ known as a maximally mixed state (c.f. sec. 3.1), corresponding to no information transfer at all.

Chapter 3

Quantum Repeaters

In this chapter we first discuss transmission of quantum information over a noisy channel, which is the problem that quantum repeaters are designed to solve. We then proceed in sec. 3.2 to describe two different quantum repeater protocols, in particular the DLCZ-type repeater which is the main subject for this thesis. We also introduce the model that the analysis and simulations of chap. 5 and chap. 6 are based on.

3.1 The Noise Problem

In any realistic physical system used to implement quantum computation, noise will be present. None of the operations which we perform will be perfect; gates and measurements will have errors and the system will not be perfectly isolated. Hence quantum computation and communication must be implemented fault-tolerantly to function in the presence of these imperfections. Communication across noisy channels is what the quantum repeater is designed to achieve.

To get an idea of what effect noise will have consider a simple model of imperfect operations. A is a single-qubit operation. The qubit system is denoted Q and the environment is E. We take the effect of A on an arbitrary state ρ to be[1] [3]:

$$A\,\rho_{QE} = pA_{ideal}\,\rho_{QE} + (1-p)\frac{\mathbb{1}}{2} \otimes \mathrm{Tr}_Q(\rho_{QE}) \tag{3.1.1}$$

The ideal operator A_{ideal} acts only on the qubit system. p can be understood as the probability for the operation to succeed. With probability $1-p$ the operation fails, in which case we have no knowledge of what happened to the qubit. It is projected to the state $\mathbb{1}/2$. This state is called a *maximally mixed* state, because outcomes of measurements on it are maximally random. For projective measurement onto any orthogonal basis $\{|a\rangle, |b\rangle\}$ we have from (2.1.4): $P(a) = P(b) = \frac{1}{2}$.

[1] In quantum information theory this type of channel is known as a 'depolarising channel' and its transmittance properties, such as capacity, have been studied [22].

The operation is now applied iteratively, and we study the effect of this on the qubit state. Let ρ_i denote the density matrix of the qubit after i iterations of A, and assume the initial state of the qubit to be pure $\rho_0 = |\psi\rangle\langle\psi|$, while the state of the environment is arbitrary. Applying A once to the initial state, we get:

$$\begin{aligned} A\,\rho_0 \otimes \rho_E &= p[A_{ideal}\,\rho_0] \otimes \rho_E + (1-p)\frac{\mathbb{1}}{2} \otimes \rho_E \\ &= \left[pA_{ideal}\,\rho_0 + (1-p)\frac{\mathbb{1}}{2}\right] \otimes \rho_E \\ &= \rho_1 \otimes \rho_E \end{aligned} \tag{3.1.2}$$

where we have used $\mathrm{Tr}_Q(\rho_0 \otimes \rho_E) = \rho_E$ which follows from the unit trace property of the density matrix. Inductively we find after i iterations:

$$\rho_i = p^i A^i_{ideal}\,\rho_0 + \sum_{k=0}^{i-1} p^k (1-p)\frac{A^k_{ideal}\mathbb{1}}{2} \tag{3.1.3}$$

In the case where the qubit is transmitted over a channel, ideal operation corresponds to a perfectly faithful transfer and we simply have $A_{ideal} = \mathbb{1}$. From (3.1.3) it is then easy to compute the fidelity of the transmitted state with respect to the ideal state $|\psi\rangle$. We obtain:

$$\begin{aligned} F(\rho_i, \psi) &= \langle\psi| \left[p^i \rho_0 + \sum_{k=0}^{i-1} p^k (1-p)\frac{\mathbb{1}}{2}\right] |\psi\rangle \\ &= p^i + \sum_{k=0}^{i-1} \frac{p^k(1-p)}{2} \\ &= p^i + \frac{1-p^i}{1-p}\frac{1-p}{2} = \frac{1+p^i}{2} \end{aligned} \tag{3.1.4}$$

where we summed the geometric progression to get the third equality. From this expression we see that whenever the channel is not perfect, i.e. when $p < 1$, the fidelity drops exponentially in the number of iterations, towards $1/2$ which is the fidelity of the maximally mixed state. We may think of a communication channel as made up of many small segments, each with fixed probability of success as in (3.1.1) (or equivalently the channel has a fixed failure rate per unit length). It then follows that the transmission fidelity drops exponentially with the channel length. This feature, exhibited here in our simple noise model, is the general problem which has to be overcome for quantum communication to become viable.

It can be seen (e.g. by computing $\mathrm{Tr}(\rho_i^2)$) that as i increases, ρ_i gradually departs from the initial pure state to become more and more mixed. This loss of purity is called *decoherence*. In a slightly more general noise description it can be seen as the result of entanglement with the surrounding environment: Again we take a single qubit initially in a pure state $|\psi\rangle = a|0\rangle + b|1\rangle$, and the initial state

of the environment may also be taken as pure[2] $|e_{in}\rangle$. The qubit is not perfectly isolated from the environment, but taken together they form a closed system and hence evolve unitarily. Let U denote the transformation when the system evolves for some unspecified, fixed time. The general form of the evolution is then:

$$U|0\rangle \otimes |e_{in}\rangle = |0\rangle|e_{00}\rangle + |1\rangle|e_{01}\rangle \qquad U|1\rangle \otimes |e_{in}\rangle = |0\rangle|e_{10}\rangle + |1\rangle|e_{11}\rangle$$

$$U|\psi\rangle \otimes |e_{in}\rangle = a|0\rangle|e_{00}\rangle + a|1\rangle|e_{01}\rangle + b|0\rangle|e_{10}\rangle + b|1\rangle|e_{11}\rangle \tag{3.1.5}$$

Here the environment states $|e_{jk}\rangle$ need not be mutually orthogonal or normalised. We see that the final state of the qubit is no longer pure. Tracing over the environment gives a mixed reduced density matrix:

$$\begin{aligned}\rho = {} & |0\rangle\langle 0| \left(|a|^2\langle e_{00}|e_{00}\rangle + ab^*\langle e_{00}|e_{01}\rangle + a^*b\langle e_{01}|e_{00}\rangle + |b|^2\langle e_{01}|e_{01}\rangle\right) \\ & + |0\rangle\langle 1| \left(|a|^2\langle e_{01}|e_{00}\rangle + ab^*\langle e_{11}|e_{00}\rangle + a^*b\langle e_{10}|e_{01}\rangle + |b|^2\langle e_{11}|e_{10}\rangle\right) \\ & + |1\rangle\langle 0| \left(|a|^2\langle e_{00}|e_{01}\rangle + ab^*\langle e_{10}|e_{01}\rangle + a^*b\langle e_{00}|e_{11}\rangle + |b|^2\langle e_{10}|e_{11}\rangle\right) \\ & + |1\rangle\langle 1| \left(|a|^2\langle e_{01}|e_{01}\rangle + ab^*\langle e_{11}|e_{01}\rangle + a^*b\langle e_{01}|e_{11}\rangle + |b|^2\langle e_{11}|e_{11}\rangle\right)\end{aligned} \tag{3.1.6}$$

Depending on the environment states (i.e. on the particular U) the final deviation from $|\psi\rangle$ may be large or small. Hence the importance of isolating the qubits well should be apparent.

Starting from models of noise, such as the ones above, it is possible to find general methods for dealing with errors. For example (3.1.5) can be understood as a combination of random bit and phase flips acting on the qubit (see [22] p. 434), and a code can then be designed which will detect and correct these flips. The general idea of the so-called 'error-correcting codes' is to encode one computational qubit redundantly into several physical qubits and use the redundancy to protect the state of the encoded qubit. An important criterion for any scheme of fault-tolerant computing is that the overhead in resources and computation time must not grow exponentially with the size of the computation, since otherwise the scheme quickly becomes obsolete when the circuit size is increased. For quantum computation it turns out that by making use of error-correcting codes any computation can be performed fault-tolerantly, provided that the probability of error for the basic gates in the circuit is below a certain threshold[3] [3, 22].

So in principle the problem of noise is solved. However the threshold is low. Depending on the code, it is typically on the order of 10^{-4} - 10^{-2} for local operations while the tolerable error probability for transmission may be higher [3, 22][4]. This is a very harsh requirement to a practical implementation. Also it should be noted that the error models considered above are not completely general. Physically a qubit may be encoded into a system with more than two levels, and errors

[2] If it is not, we just extend our description of the environment to include whatever other systems it is entangled with.

[3] Also, some physical assumptions must be made about the noise, parallel computing must be possible and ancilla qubits must be provided ([22] chap. 10).

[4] And according to private correspondence with A. S. Sørensen.

could then take the state outside the qubit subsystem, causing the qubit state to become undefined. For example one could imagine encoding the qubit onto a photon which is absorbed.

For these reasons, we are motivated to look for other quantum communication schemes. Fortunately several schemes with less stringent bounds are provided by quantum repeater protocols, which allow efficient transmission of information over an arbitrary distance with error-tolerances at the level of percent[5] [3, 6, 8].

3.2 Quantum Repeaters

As has been stressed several times already, the purpose of the quantum repeater is to create entanglement and distribute it among different parties. In this section we consider the basic structure of the repeater. Several variants of the repeater protocol exist (e.g. [3, 6, 8] and more), and we mention briefly the approach introduced in the original paper [3], where the term *quantum repeater* was also coined[6]. The approach taken in the main work of this thesis was introduced in [8], and we describe it in more detail.

3.2.1 Basic Structure of the Repeater

The basic structure of the repeater is shown in fig. 3.1. Two locations A, B are connected by a noisy quantum channel. Our goal is to establish a maximally entangled pair between A and B. To be specific, say that the state we aim to establish is $|\Psi^+\rangle$. The channel is divided into 2^N segments of length L_0, so that the total channel length is $L = 2^N L_0$. Final entanglement is established in two iterative steps.

Figure 3.1: Quantum repeater. The devision into segments is shown. The meeting point of two segments is called a repeater station or a node. The physical systems underlying different segments and nodes are identical.

Initialisation. To begin with, an entangled pair is created for each L_0-segment. Since the physical qubits must interact to become entangled, entanglement creation has to happen locally. The two qubits of the created pair are stored at either end of the segment. A quantum memory in which qubits may be stored over time and retrieved is an integral part of the repeater and is very

[5] Here it should perhaps be stressed that these schemes achieve only this: *transmission of information*. They do not provide universal quantum computation at the given noise levels.

[6] To the best of my knowledge.

nontrivial to implement; hence in the construction of repeaters much work must be put into finding a good memory. However at this point, we need not worry about the details of how the memory functions. How entanglement is created depends on the physical nature of the qubits, and so also does the form of the created state and the degree of entanglement it possesses. It is crucial that the fidelity F w.r.t. $|\Psi^+\rangle$ is close to unity. Depending on the scheme used, it is possible to find a strict lower limit for the initial fidelity.

Connection When entangled pairs have been established at all segments, they are connected to increase the entanglement distance. The connection is illustrated in fig. 3.2. It consists of a quantum teleportation of one end of a pair onto the far-away end of a neighbouring pair (c.f. sec. 2.2.3). The result is an entangled pair with a new fidelity F' extending over twice the distance, $L_1 = 2L_0$. Performing *entanglement connection*[7] at every second node produces a string of 2^{N-1} segments each of length L_1 and each occupied by pairs of fidelity F'.

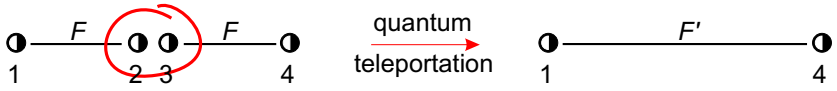

Figure 3.2: Entanglement connection. Solid lines indicate entangled pairs. A Bell measurement is performed on qubits 2 and 3, and the state of 2 is teleported onto 4. Because the initial states are not maximally entangled and the gates and measurements are not perfect, the fidelity is degraded in the process. $F' < F$.

A final entangled state between A and B is established by iterating the connection N times. In each iteration the number of segments is halved and the entanglement distance is doubled by connecting pairs $L_l = 2^l L_0$.

Because of imperfect operations and imperfections in the entangled states, the fidelity decreases in each connection step. For good repeater performance (i.e. better than direct transmission), this decrease must be sub-exponential in the distance. The approach to the repeater [3] and the class of repeaters considered in this thesis are distinguished by how they achieve this.

3.2.2 Repeater with Purification

In the first proposal *entanglement purification* was used to restore a good fidelity after each connection. There are several ways to purify[8] states of low F to states of high F. For example one may distill a nearly maximally entangled state from a collection of low-F states by a sequence of measurements, and selections based on the outcomes. If the initial fidelity of the pairs is above a certain threshold F_{min},

[7] The teleportation process of fig. 3.2 is sometimes called 'entanglement swapping', but in the context of repeaters we prefer the term 'entanglement connection'.

[8] Note that the term purification is also used in the quantum information literature for a mathematical technique to associate a pure state of a composite system with a mixed density operator of a subsystem, e.g. [22].

then the average fidelity of the new collection of pairs after each selection round will be higher. Hence iterating the procedure will drive F towards 1 (or towards an upper limit F_{max}). Fig. 3.3 illustrates the combined connection and purification.

This procedure can be integrated into the repeater by having parallel channels of the type in fig. 3.1. For each L_0-segment then, we create a collection of low-F pairs from which a smaller number of nearly maximally entangled states are distilled. These high-F pairs are then connected and the process is iterated.

The imperfections in gates and measurements determine F_{max}, F_{min} and the drop in fidelity by connection, and so the condition $F' > F_{min}$ fix the error bounds above which the repeater becomes inoperable. With an error model of the type (3.1.1), Briegel *et al.* show that error probabilities on the percent-level can be tolerated. They also demonstrate that the resources required for operation (i.e. the number of parallel channels) and the time needed to establish entanglement between A and B grow at worst polynomially with the distance. Hence the repeater is in principle operable over long distances and in the presence of noise [3].

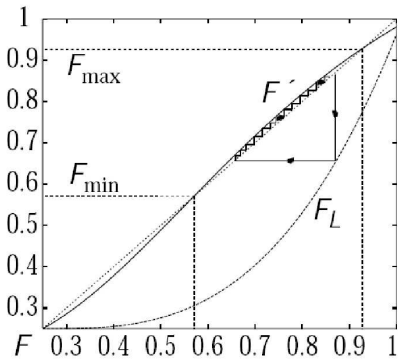

Figure 3.3: Iteration loop. The figure is taken from [3]. The upper and lower curve show the fidelity after one purification or entanglement connection step respectively as functions of the fidelity before the step.

A few other purification schemes [2, 7] were considered already in [3], and it was demonstrated that the need for many parallel channels can be eliminated. In [6] it is shown that purification can be achieved with just two qubits at each node.

The lowest possible value of the threshold for purification F_{min} is $1/2$ [7], and this provides us with a benchmark for the fidelity of the entangled states generated by the quantum repeater. $1/2$ is the maximal average fidelity that may be reached by means of classical communication. This may be realised in the following way. If it was possible by classical communication alone to establish qubit pairs with an average fidelity above $1/2$, then by purification of a collection of such pairs it is also possible to establish a (nearly) maximally entangled pair. Thus maximal entanglement would be established between distant systems without *any* quantum interaction between those systems whatsoever. We will refer to the $1/2$ classical limit on several occasions later in the thesis.

3.2.3 DLCZ-type Repeater

In [8] Duan, Lukin, Cirac and Zoller have proposed a repeater protocol which has no separate purification step. Instead the entanglement connection is probabilistic. Although a specific implementation were considered in [8], in this thesis the term *DLCZ-type repeater* refers to any repeater protocol with this structure: i.e.

probabilistic connections and no separate purification. The DLCZ-type repeater is illustrated in fig. 3.4.

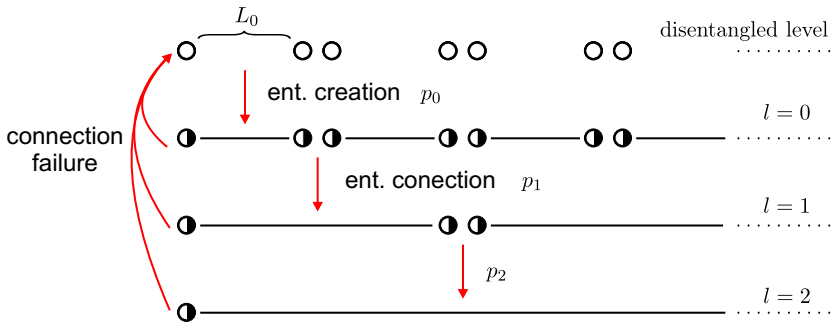

Figure 3.4: DLCZ-type repeater. l denotes distance levels. At the l'th level, after l connections, each of the entangled pairs span a distance $L_l = 2^l L_0$. p_l is the probability of success for stepping from level $l-1$ to level l by entanglement connection (or creation).

At each entanglement connection, success is conditioned on the outcome from some measurement. The probability p_l of obtaining the required outcome may depend on the level[9]. The purpose of the conditioning is to project the created L_l-pair to a state which minimises the drop in fidelity from one level to the next and in this way ensure that the decrease in fidelity as the entanglement distance increases is sub-exponential in the distance. A low drop in fidelity per connection step may be thought of as being paid for by a high probability for the connection to fail: $1 - p_l$. As a general rule, the lower the required drop in F, the lower p_l must be. Since for the unaided, noisy channel fidelity of transmittance drops exponentially (c.f. sec. 3.1), we can think of the DLCZ-type repeater as having some built-in purification in the entanglement connection [8]. It should be noted that, in contrast to the first approach, there is no need for any non-local operation to be involved in the connection step. In particular it is not necessary to perform Bell measurements or to implement the cNOT gate (no Bell measurement is needed for probabilistic teleportation in fig. 3.2). This is good because implementing non-local operations is generally hard.

From fig. 3.4 it should be clear that a good quantum memory is important for operation of a DLCZ-type repeater. Since all entanglement connection and generation steps are probabilistic, connection or generation for neighbouring segments cannot be expected to succeed simultaneously. Therefore entangled states need to be stored while corresponding entangled pairs are established for neighbouring segments. Only then can the states be retrieved and connection can be attempted.

As for the earlier proposal, the DLCZ-type repeater can be made to have sub-exponential overhead in resource use and communication time. Since all the nodes are identical systems, we see that the resource use is linear in the channel length.

[9] the purification procedure described in sec. 3.2.2 also had a probabilistic element, because it used conditioning on measurement outcomes, but here we associate a probability with the entire step from one level to the next

To estimate the communication time we consider entanglement connection between pairs of length L_{l-1}. When the connection fails, entanglement is lost on the whole L_l-segment involved, as illustrated in fig. 3.4, and the repeater protocol has to be restarted from the initial entanglement generation on this segment. The average number of attempts before connection succeeds is $1/p_l$. We let τ denote the time spent on a single entanglement connection or creation attempt[10], and t_l denote the average time needed to establish an entangled L_l-pair. If we approximate the time needed to generate (in parallel) two neighbouring L_{l-1}-pairs by the average time for generating one such pair[11], we obtain a recurrence relation for t_l:

$$t_l = \frac{1}{p_l}(\tau + t_{l-1}) \tag{3.2.1}$$

which has the solution:

$$t_l = \tau(\frac{1}{p_l} + \cdots + \frac{1}{p_l \cdots p_0}) = \frac{\tau}{p_l \cdots p_0}\left(1 + \sum_{i=0}^{l-1}\prod_{j=0}^{i} p_j\right) \tag{3.2.2}$$

Putting l equal to $N = \log_2(L/L_0)$ in this expression gives the total time needed to establish entanglement between A and B as a function of the channel length. The behaviour of t_N depends on the specific implementation through the p_l. We see that for t_N to have sub-exponential dependence of the channel length, the p_l must not drop off exponentialy with l. This has to balance with the complementarity between low drop in F and low p_l; there is a trade-off between low communication time and a high final state fidelity. A scheme which achieves such balance was demonstrated by Duan *et al.* in [8][12].

As a last remark of this section, we mention another purpose of the measurements in the entanglement connection step. In addition to minimising the fidelity drop, they are also used to control the form of the final entangled states generated by the repeater. If the form of the final states is known, it may be possible to design (probabilistic) quantum communication schemes which can operate even when the fidelity of the states is not high. For example, the entangled states might take the form:

$$\rho = c|vac\rangle\langle vac| + (1-c)|\Psi^-\rangle\langle\Psi^-| \tag{3.2.3}$$

where we imagine the underlying physical system to be photonic modes. If we make a joint measurement with another state and condition on the presence of a photon, the vacuum component in this expression cannot contribute to the successful outcomes. This way it is possible to construct a probabilistic teleportation

[10] the time spent on classical communication between the nodes may also be included in τ.

[11] This is an underestimation. The average time for two pairs to succeed is higher than for a single pair. The error in the final communication time due to this approximation is found when we compute communication rates for specific repeaters in chap. 6. It is approximately a factor 2.5.

[12] Note that in [8] the authors consider only the dominant term of (3.2.2). This is in addition to the approximation made in obtaining that formula.

protocol which works with almost perfect fidelity [8]. The probability for the protocol to succeed is determined by the coefficient c. We return briefly to this in sec. 5.4.

3.2.4 Modelling

A major part of the work presented in this thesis has been to analyse the performance of different DLCZ-type repeaters. To do this we need a specific model for the physical systems which make up the repeater, i.e. the quantum memories, the manner of entanglement creation, etc. As our model we choose a set of harmonic oscillators.

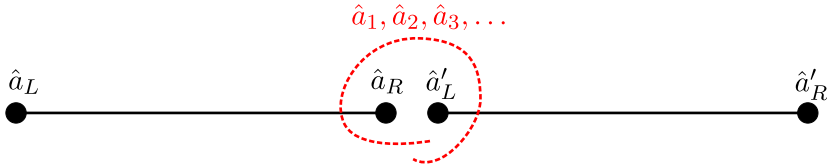

Figure 3.5: Harmonic oscillator model. Two oscillator modes are associated with each repeater segment. Additional modes may be involved in write-in and read-out from memories and in entanglement generation and connection. Modes involved in connection are indicated by red.

For a given segment, we associate a mode with either end. All operations which are part of the repeater protocol are assumed to be described by Bogoliubov transformations of the mode operators for these and auxiliary modes, and by projective measurements in the the number state basis (2.1.18).

With this model, the computational basis for our qubits is given by the two lowest number states:

$$|0\rangle_{qubit} = |0\rangle \qquad |1\rangle_{qubit} = |1\rangle \tag{3.2.4}$$

This kind of qubits is usually considered not to be a very good encoding, because some single-qubit operation, such as the bit flip gate X, are difficult to do. With this encoding X requires a change of the excitation number (e.g. photon number for light), that is, an active transformation. It is prefferable to encoded a qubit into two modes with a fixed excitation number in a so called dual-rail encoding. However, as demonstrated in [8] , entangled states of the form (3.2.5) below may be used to teleport dual-rail encoded qubits and they can also be used in quantum cryptography applications.

If we denote the mode operators for a segment by $\hat{a}_L, \hat{a}_R$, then a maximally entangled state across that segment is given by:

$$|\Psi^+\rangle = \frac{1}{\sqrt{2}}(|01\rangle + |10\rangle) = \frac{1}{\sqrt{2}}(\hat{a}_L^\dagger + \hat{a}_R^\dagger)|vac\rangle \tag{3.2.5}$$

The entanglement creation step aims to generate states that are close to this expression. The process is a Bogoliubov transformation of $\hat{a}_L, \hat{a}_R$ along with axillary

modes followed by measurements - for example entanglement may be generated for photonic modes which are then loaded into atomic memory modes. Similarly, entanglement connection is a Bogoliubov transformation of e.g. $\hat{a}_L$ and $\hat{a}'_R$ from the neighbouring segment complemented by auxiliary modes (see fig. 3.5). In this case the memories may be read out into the extra modes, which are then manipulated and measured. The result is an entangled state stored in modes $\hat{a}'_L, \hat{a}_R$ which form the modes of the new segment (c.f. fig. 3.2). The modes $\hat{a}_L, \hat{a}_R$ can be storage modes of quantum memories located at the nodes of the repeater, but they do not have to be. Alternatively one can view the complete state transfer (write-in + read-out) formally as part of the entanglement connection.

Each entanglement connection - no matter the distance level - is supposed to be performed in the same manner; that is, the form of the auxiliary states involved and the Bogoliubov transformation are always the same. Likewise the entanglement creation procedure is also the same on all segments of the channel. In principle, when the Bogoliubov transformations and measurements of the protocol are fixed, it is enough to specify the input state for the entanglement creation. The state of entangled pairs at any higher level can then be calculated (conditional on connections to succeed).

Although at first glance the choice of harmonic oscillators as a model may seem restrictive, it is in fact quite general. Many quantum systems may be described by or approximated by harmonic oscillators. For example we shall consider light interacting with spin states of atomic ensembles. Other examples might include electrons in potential wells or vibrational modes of trapped ions - systems which are considered for implementation of quantum computation. The Bogoliubov transformation also has wide applicability. It includes, but is not restricted to: all linear optical transformations (e.g. beam splitters), generation of squeezed states, and light-atom interactions. However it cannot generally be used to treat evolution under Hamiltonians that are not quadratic in the mode operators. One example of a phenomenon our model is insufficient to treat is the optical Kerr effect, which is a photon number dependent phase shift experienced by an optical mode passing through a non-linear medium. The phase shift can produce an effective photon-photon interaction, and it has been proposed to use this for implementation of non-local quantum gates. The Hamiltonian relevant for the Kerr effect is fourth order in the mode operators for the light field [12, 14].

Our strategy for analysing repeaters will be to develop numerical and analytical tools for dealing with general Bogoliubov transformations and projective measurements. We shall want to monitor the density matrix for the entangled states at each distance level, to study it's dependence on the parameters of the Bogoliubov transformation, the probabilities for measurement conditions to be fulfilled, and the fidelity w.r.t. maximally entangled states. Having such tools at our disposal, we can then insert the appropriate parameters for various specific, physical implementations of the repeater and obtain results for their performance. For example we can investigate the distance over which a high fidelity can be maintained and the dependence of this on memory parameters. To get as realistic models as pos-

sible, we should make sure that the tools developed allow for errors such as loss of excitation in a mode (e.g. photon loss) or imperfect detectors.

Chapter 4

Methods for Analysis

At the end of the preceding chapter we introduced a model for single-step repeaters based on harmonic oscillators. In the present chapter we develop a mathematical tool for doing calculations on such a system — a generating function for Bogoliubov transformations. We then proceed to explain how the generating function is used to analyse the performance of repeaters, and sketch how it is implemented in *Mathematica* notebook programs. To the best of my knowledge, the idea of the generating function described below is due to A. S. Sørensen, K. Mølmer and J. Sherson.

4.1 The Generating Function

Our basic problem is the following: For interaction processes interesting to us, e.g. interaction between light and atoms, we are often able to solve the equations of motion in the Heisenberg picture, and hence find a Bogoliubov transformation which describes the evolution of the mode operators. However we would like to find also the evolution of the state density matrix in the Schrödinger picture. The generating function is a tool to do this.

Generally, given an arbitrary Bogoliubov transformation on a set of modes we can define a generating function from which the contribution to any element of the output density matrix from any element of the input density matrix can be calculated by differentiation. The generating function method is employed both in our numerical simulations and in deriving analytical expressions for the evolution of the density operator (c.f. chap. 5).

We assume that our system S can be described by a set of harmonic oscillator modes $\{a_i\}$. To construct the generating function, we begin by noting:

$$|n\rangle_i = \frac{1}{\sqrt{n!}}(\hat{a}_i^\dagger)^n|vac\rangle = \left[\frac{1}{\sqrt{n!}}\frac{\partial^n}{\partial\alpha^n}e^{\alpha\hat{a}_i^\dagger}|vac\rangle\right]_{\alpha=0} \tag{4.1.1}$$

where the parameter α is arbitrary (and thus can be chosen real). Now we also

have[1]:

$$\begin{aligned} e^{\alpha\hat{a}_i^\dagger}|vac\rangle &= e^{\alpha\hat{a}_i^\dagger}e^{-\alpha^*\hat{a}_i}|vac\rangle = e^{\alpha\hat{a}_i^\dagger-\alpha^*\hat{a}_i}e^{\frac{1}{2}[\alpha\hat{a}_i^\dagger,-\alpha^*\hat{a}_i]}|vac\rangle \\ &= e^{\frac{1}{2}|\alpha|^2}D_i(\alpha)|vac\rangle \end{aligned} \tag{4.1.2}$$

thus

$$|n\rangle_i = \left[\frac{1}{\sqrt{n!}}\frac{\partial^n}{\partial\alpha^n}e^{\frac{1}{2}|\alpha|^2}D_i(\alpha)|vac\rangle\right]_{\alpha=0} \tag{4.1.3}$$

This is a useful result because it allows us to evaluate contributions from the input to the output density matrix simply as vacuum expectation values of displacement operators, as we will see below.

We let O denote the subsystem for which we are interested in the output state, and R denote the remaining modes $S = OR$. Furthermore we assume that a Bogoliubov transformation U on S is known. The reduced density matrix for the output modes is then:

$$\rho_O^{out} = \mathrm{Tr}_R(U\rho_S^{in}U^\dagger) \tag{4.1.4}$$

In the following we assume for simplicity that S consists of just two modes, and that we are interested in the output state of mode 2 (think for example of one light mode interacting with one atomic mode). In app. B we give general expressions valid for arbitrary mode numbers. The contribution from the $|nm\rangle_{12}\langle n'm'|$ element of the input state to the $|l\rangle_2\langle l'|$ element of the output state is:

$$(\rho_S^{in})_{nmn'm'} \cdot {}_2\langle l|\mathrm{Tr}_1\left[U|nm\rangle_{12}\langle n'm'|U^\dagger\right]|l'\rangle_2 \tag{4.1.5}$$

Defining a generating function:

$$\begin{aligned} &F(\alpha_1,\alpha_2,\beta_1,\beta_2,\gamma_2,\delta_2) \\ &= \mathrm{Tr}_1\left[{}_2\langle 0|e^{\delta_2\hat{a}_2}Ue^{\beta_1\hat{a}_1^\dagger}e^{\beta_2\hat{a}_2^\dagger}|vac\rangle\langle vac|e^{\alpha_1\hat{a}_1}e^{\alpha_2\hat{a}_2}U^\dagger e^{\gamma_2\hat{a}_2^\dagger}|0\rangle_2\right] \end{aligned} \tag{4.1.6}$$

the weight factor can be written:

$$\begin{aligned} &{}_2\langle l|\mathrm{Tr}_1\left[U|nm\rangle_{12}\langle n'm'|U^\dagger\right]|l'\rangle_2 \\ &= \left[\frac{1}{\sqrt{n'!m'!n!m!l'!l!}}\frac{\partial^{n'}}{\partial\alpha_1^{n'}}\frac{\partial^{m'}}{\partial\alpha_2^{m'}}\frac{\partial^n}{\partial\beta_1^n}\frac{\partial^m}{\partial\beta_2^m}\frac{\partial^{l'}}{\partial\gamma_2^{l'}}\frac{\partial^l}{\partial\delta_2^l}F(\alpha_1,\alpha_2,\beta_1,\beta_2,\gamma_2,\delta_2)\right]_{\text{all zero}} \end{aligned} \tag{4.1.7}$$

The parameters α_i, β_i select the input matrix element while γ_2, δ_2 select elements of the output matrix; all zero means that the bracket should be evaluated at $\alpha_1, \alpha_2, \beta_1, \beta_2, \gamma_2, \delta_2 = 0$. We see that if the function F is known we can compute the output state for any given input state. It is in this sense that F generates the Bogoliubov transformation U.

[1] We get this by using the *disentangling theorem*: If $[A,[A,B]] = [B,[A,B]] = 0$ for a pair of operators A, B, then $e^{A+B} = e^Ae^Be^{-\frac{1}{2}[A,B]}$ ([12] p. 49).

As it stands the generating function (4.1.6) cannot be directly evaluated, since most often we know only the transformation of the mode operators $\hat{a}_i$ but not the matrix representation[2] of U. Therefore we rewrite F in a more useful form.

First, by making use of (4.1.2) and the definition of the trace we, have:

$$\begin{aligned} & F(\alpha_1,\alpha_2,\beta_1,\beta_2,\gamma_2,\delta_2) \qquad (4.1.8)\\ & = \langle vac|e^{\alpha_1\hat{a}_1}e^{\alpha_2\hat{a}_2}U^\dagger e^{\gamma_2\hat{a}_2^\dagger}|0\rangle_2 \left[\sum_{i=0}^{\infty}|i\rangle_1\langle i|\right] {}_2\langle 0|e^{\delta_2\hat{a}_2}Ue^{\beta_1\hat{a}_1^\dagger}e^{\beta_2\hat{a}_2^\dagger}|vac\rangle \\ & = e^{\frac{1}{2}(\alpha_1^2+\alpha_2^2+\beta_1^2+\beta_2^2+\gamma_2^2+\delta_2^2)} \\ & \quad \times \langle vac|D_1(-\alpha_1)D_2(-\alpha_2)U^\dagger D_2(\gamma_2)|0\rangle_2\langle 0|D_2(-\delta_2)UD_1(\beta_1)D_2(\beta_2)|vac\rangle \end{aligned}$$

where we have taken the parameters of F to be real.

Next, in app. B we prove that the projection operator in the middle of the above expression can be written:

$$|0\rangle_2\langle 0| = \int \frac{dpdx}{2\pi} e^{-(x^2+p^2)/4} D_2(\frac{x+ip}{\sqrt{2}}) \qquad (4.1.9)$$

Inserting this into (4.1.8) and pulling out the integration, we get:

$$\begin{aligned} & F(\alpha_1,\alpha_2,\beta_1,\beta_2,\gamma_2,\delta_2) \qquad (4.1.10)\\ & = e^{\frac{1}{2}(\alpha_1^2+\alpha_2^2+\beta_1^2+\beta_2^2+\gamma_2^2+\delta_2^2)} \\ & \quad \times \int \frac{dpdx}{2\pi} e^{-(x^2+p^2)/4} \\ & \qquad \times \langle vac|D_1(-\alpha_1)D_2(-\alpha_2)U^\dagger D_2(\gamma_2)D_2(\frac{x+ip}{\sqrt{2}})D_2(-\delta_2)UD_1(\beta_1)D_2(\beta_2)|vac\rangle \end{aligned}$$

The general many-mode expression corresponding to this is given in (B.7). Under a Bogoliubov transformation a displacement operator transforms into a product of displacement operators, and so (4.1.10) expresses F as an integral over the vacuum expectation value of a product of displacement operators. For any given U a final expression for F is obtained in three steps:

1) The transformed displacement operators are calculated. Explicitly, under the general Bogoliubov transformation:

$$U^\dagger \hat{a}_j U = \sum_i b_{ji}\,\hat{a}_i + c_{ji}\,\hat{a}_i^\dagger \qquad (4.1.11)$$

[2]The generating function method is one way to obtain this representation.

the density operator $D_j(\beta)$ transforms to:

$$\begin{aligned} U^\dagger D_j(\beta) U &= \mathrm{Exp}\left[\beta \sum_i (b_{ji}^* \hat{a}_i^\dagger + c_{ji}^* \hat{a}_i) - \beta^* \sum_i (b_{ji} \hat{a}_i + c_{ji} \hat{a}_i^\dagger)\right] \\ &= \prod_i \mathrm{Exp}\left[(\beta b_{ji}^* - \beta^* c_{ji}) \hat{a}_i^\dagger + (\beta c_{ji}^* - \beta^* b_{ji}) \hat{a}_i\right] \\ &= \prod_i D_i(\beta b_{ji}^* - \beta^* c_{ji}) \end{aligned} \tag{4.1.12}$$

2) The vacuum expectation of the displacement operators is evaluated. This is done first by reducing the product to a single operator for each mode via the identity ([12] p. 50):

$$D(\alpha) D(\beta) = e^{i\mathrm{Im}(\alpha\beta^*)} D(\alpha + \beta) \tag{4.1.13}$$

and second by taking the expectation values of these operators:

$$\langle vac | D(\alpha) | vac \rangle = e^{-\frac{1}{2}|\alpha|^2} \tag{4.1.14}$$

3) The resulting expression, which is a quadratic expression in the output mode integration variables x, p, is integrated along with the prefactors present in (4.1.10). After integration we have an analytic expression for F which involves only the $\alpha, \beta, \gamma, \delta$-variables and the parameters of U.

From the F obtained by going through steps (1)–(3) above we can calculate the transformation of any input state ρ_S^{in} under U. However, when analysing physical setups we shall also want to include the effect of measurements, which cannot be described by a unitary transformation. In particular, we want to compute the state of the output modes O conditioned on a certain outcome from a measurement on some of the remaining modes R. Fortunately the generating function can be extended to allow for this.

We consider the measurement to take place after the transformation U. From (2.1.4) the unnormalised conditional output state is seen to be:

$$\rho_O^{out} = \mathrm{Tr}_R(P U \rho_S^{in} U^\dagger P^\dagger) \tag{4.1.15}$$

where the projection operator P acts on the subset of modes R which is measured. This expression replaces (4.1.4) and the formulae deriving from it must be modified accordingly. In the two-mode example above we can take $P = P_1$ to act on mode 1 (e.g. we measure the light mode after interaction and find the conditional state of the atoms). Then, using $P^\dagger P = P^2 = P$ (since P is a projection operator) we find that the last term in (4.1.8) is replaced by:

$$\langle vac | D_1(-\alpha_1) D_2(-\alpha_2) U^\dagger D_2(\gamma_2) | 0 \rangle_2 \langle 0 | P_1 D_2(-\delta_2) U D_1(\beta_1) D_2(\beta_2) | vac \rangle \tag{4.1.16}$$

We are interested in cases where the measured modes are photonic, and the required outcomes are either one or no clicks in a photodetector. For detectors which

are perfect but do not resolve the number of photons (i.e. they distinguish only between presence and absence of light), the possible projection operators are:

$$P_{dark} = |0\rangle\langle 0| \qquad P_{light} = \mathbb{1} - |0\rangle\langle 0| \tag{4.1.17}$$

From (4.1.9) both of these may be written in terms of displacement operators, and so the new generating function now including measurements is again expressed as vacuum expectation values of displacement operators. The many-mode generating function including measurements is given in (B.9).

Having established that the generating function is general enough to suit our purposes, we mention two additional useful features of this formulation.

Firstly, note that because the state (4.1.15) is not normalised, the trace $\mathrm{Tr}(\rho_O^{out})$ equals the probability of obtaining the measurement outcome corresponding to P. Hence by defining the generating function as above we obtain both the conditional output states and their probabilities in one calculation.

Secondly, we see that squeezing of input states may be treated easily. Recall that the squeezed vacuum state is $S(\xi)|0\rangle$ with the squeezing operator given by (2.1.23). This state in principle contains finite contributions from all the even number states ([12] p. 161). But if we were to specify the corresponding input density matrix in (4.1.15), we would have to make a cutoff since we cannot take arbitrarily high derivatives in our programs (or sum arbitrarily many terms). However we can avoid this necessity by incorporating $S(\xi)$ into the Bogoliubov transformation U and thus into the generating function. U is replaced by $US(\xi)$ and the input state for the squeezed mode is vacuum. The three steps to obtain F are unchanged; in (1) the displacement operators transform first under U and then under $S(\xi)$ using[3]:

$$\begin{aligned} &S^\dagger(\xi)D(\beta)S(\xi) \\ &= \mathrm{Exp}\left[\beta\left(\cosh(r)\hat{a}^\dagger - \sinh(r)\hat{a}\right) - \beta^*\left(\cosh(r)\hat{a} - \sinh(r)\hat{a}^\dagger\right)\right] \\ &= D(\beta\cosh(r) + \beta^*\sinh(r)) = D(\mathrm{Re}(\beta)e^r + i\mathrm{Im}(\beta)e^{-r}) \end{aligned} \tag{4.1.18}$$

where the squeezing is in the X-quadrature. Multi-mode squeezing can be treated in similar fashion.

4.2 Using the Generating Function

When investigating the performance of various DLCZ-type repeaters we focus on two crucial properties, namely the fidelity which can be maintained over a given distance, and the communication rate which can be achieved. There is a simple strategy to access these properties, using the generating function:

[3]Since we have: $S^\dagger(\xi)\hat{a}S(\xi) = \cosh(r)\hat{a} - \sinh(r)\hat{a}^\dagger$ (e.g. [12] p.153).

1) First one should consider the entanglement generation step. In some cases this step is simply assumed to be perfect and the generated states are perfect Bell states. In other cases we can obtain an appropriate Bogoliubov transformation for the generation, and then use the generating function to compute the output state of this transformation starting from a disentangled input. Note that successful entanglement generation for any segment of the repeater results in the same density matrix, and hence we need only perform the computation once.

2) Next the entanglement connection step is considered. From the Bogoliubov transformation for connection the corresponding generating function is computed, and using the entangled states from the generation step as input, the state after successful connection is found. Referring to fig. 3.4, this gives us the entangled state at the $l = 1$ level. The states at subsequent distance levels are found by iterating this procedure using the output states from one connection as input to the next.

3) Finally, from the list of density matrices found in (2), we can get the fidelity and the probability of successful entanglement connection at each level. The fidelity w.r.t. the Bell state (3.2.5) is easily computed using the definition (2.1.9). The probability for entanglement connection to succeed is simply the trace of the computed unnormalised output state, as mentioned in sec. 4.1. Knowing p_l at each level, we can find the average time spent on creating one final entangled pair and hence the communication rate, either from the approximate expression (3.2.2) or by numerical simulation.

The strategy may be used both for numerical simulation and for obtaining analytical results. This is simply a question of whether we specify numerical values for the parameters of the Bogoliubov transformations. In the analytical case, the computer-generated expressions for the density matrix and the fidelity can be very complex, and it is then necessary to make some approximation to simplify them, e.g. by expanding in small parameters.

Chapter 5

A Perturbative Approach

This and the following chapter contain the main results of the work behind this thesis. In the present chapter we derive general analytical expressions, which will apply to any DLCZ-type repeater using the same entanglement connection setup as the original proposal [8] and fulfilling a few additional assumptions. In the following chapter we analyse three particular repeater systems, comparing analytical predictions with numerical simulation.

5.1 Starting Point for the Perturbation

Consider the most general Bogoliubov transformation describing a complete state transfer (i.e. write-in and subsequent read-out) for a quantum memory[1]:

$$\hat{a}_1' = b_1 \hat{a}_1 + c_1 \hat{a}_1^\dagger + \sum_i \tilde{b}_i \hat{\tilde{a}}_i + \tilde{c}_i \hat{\tilde{a}}_i^\dagger \tag{5.1.1}$$

Here $\hat{a}_1$ is the mode operator for the input mode containing the state to be stored in the memory, and $\hat{a}_1'$ is the output mode into which the state is read out. The remaining operators describe auxiliary modes involved in the write-in and read-out processes. The b and c coefficients are in general complex.

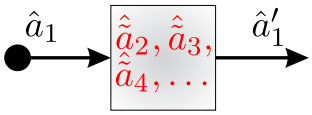

Figure 5.1: Complete state transfer. The state of mode a_1 is stored in the quantum memory and later retrieved into the mode a_1'.

Starting from this equation we will derive analytical results for the behaviour of DLCZ-type repeaters using a particular entanglement connection scheme and *any* quantum memory. We do this by perturbation in the parameters of the memory Bogoliubov transformation away from the case of perfect state transfer. The entanglement connection scheme is illustrated in fig. 5.2

[1] For readers who are worried that the discrete sum is not the most general form, the mode reduction of the next section can be applied also when the sum is replaced by an integral over a continuous index.

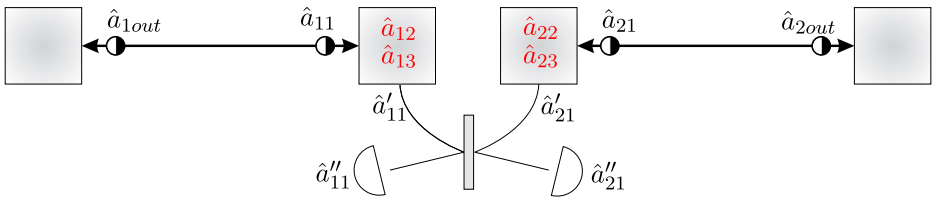

Figure 5.2: Conditional entanglement connection. Two entangled pairs, stored in modes $\hat{a}_{1out}, \hat{a}_{11}$ and $\hat{a}_{2out}, \hat{a}_{21}$ are connected. The modes $\hat{a}_{11}$ and $\hat{a}_{21}$ are written into and then read out from two quantum memories. The output modes are mixed on a 50-50 beam splitter and measured. The auxiliary modes $\hat{a}_{12}, \hat{a}_{13}, \hat{a}_{22}, \hat{a}_{23}$ involved in the state transfer will be explained in the next section.

Although the figure depicts mixing on a beam splitter as for light modes, we keep in mind that beam splitter interactions can be realised also for other physical systems and hence the connection does not have to operate on light [21, 24].

Successful connection is conditioned on a single click in one detector only. The procedure can be understood intuitively as follows: Each of the two entangled pairs which are being connected is of the form (3.2.5) and contains one excitation. In the case of ideal memories and detectors, there are three possibilities for the read-out: none, one or both of the excitations are read out. If no excitation is read out, there can be no click and the connection fails. If both excitations are read out, there will be two clicks and the connection fails. If just one excitation is read out, the beam splitter will erase any information about which pair it originated from, and hence the system is left in a superposition of excitation in modes $\hat{a}_{1out}$ or $\hat{a}_{2out}$ which is exactly the desired state.

The intuitive explanation can be made rigorous by considering the effect of the beam splitter on the state $|\Psi^+_{1out,11'}\rangle \otimes |\Psi^+_{2out,21'}\rangle$ and subsequent projective measurements. The details are referred to app. C. When the memories and detectors are not perfect, or the input state is not maximally entangled, the fidelity will begin to degrade on connection and the goal of the following analysis is to tell how much and in what manner this happens.

Referring back to fig. 3.4, our aim is to find an expression for the density matrix of the entangled pairs at each distance level. The number of modes in (5.1.1) is not fixed and may in principle be large. The first step towards this end will therefore be to reduce the mode number, to the convenient size of three.

5.2 Mode Reduction

It is always possible to define new, independent mode operators $\hat{a}_2, \hat{a}_3$ by:

$$b_2\hat{a}_2 \equiv \sum_i \tilde{b}_i\hat{\tilde{a}}_i \qquad c_2\hat{a}_2^\dagger + c_3\hat{a}_3^\dagger \equiv \sum_i \tilde{c}_i\hat{\tilde{a}}_i^\dagger \tag{5.2.1}$$

where b_2, c_2, c_3 are complex coefficients. We can then rewrite (5.1.1):

$$\hat{a}_1' = b_1\hat{a}_1 + c_1\hat{a}_1^\dagger + b_2\hat{a}_2 + c_2\hat{a}_2^\dagger + c_3\hat{a}_3^\dagger \tag{5.2.2}$$

This is our new Bogoliubov transformation, which now involves only three modes. The modes $\hat{a}_2, \hat{a}_3$ are exactly the auxiliary modes of fig. 5.2. In the figure, the first index refers to the pair (left or right), while the second index corresponds to the index in (5.2.2). The b, c coefficients should be obtained from (5.1.1) and there is some freedom in the choice of phases.

The overall phase of the output mode is not important[2] and therefore we may always assume that b_1 is real and nonnegative. From the expression for $b_2\hat{a}_2$ we see that a possible complex phase on b_2 can be absorbed into the definition of the mode operator $\hat{a}_2$ and so we can also assume that b_2 is real[3]. Likewise the phase of c_3 can be absorbed in $\hat{a}_3$. For this mode we have:

$$c_3^*\hat{a}_3 = \sum_i \tilde{c}_i^*\hat{\tilde{a}}_i - \frac{c_2^*}{b_2}\tilde{b}_i\hat{\tilde{a}}_i \tag{5.2.3}$$

and so we choose c_3 real. Hence in general we have:

$$b_1, b_2, c_3 \in \mathbb{R} \qquad 0 \leq b_1 \qquad c_1, c_2 \in \mathbb{C} \tag{5.2.4}$$

The values of b_1, c_1 are given from (5.1.1). For the remaining coefficients we have:

$$|b_2|^2 = [b_2\hat{a}_2, b_2^*\hat{a}_2^\dagger] = \sum_i |\tilde{b}_i|^2 \tag{5.2.5a}$$

$$c_2 = [\hat{a}_2, c_2\hat{a}_2^\dagger + c_3\hat{a}_3^\dagger] = \sum_i \frac{\tilde{b}_i\tilde{c}_i}{b_2} \tag{5.2.5b}$$

$$|c_3|^2 = [c_2^*\hat{a}_2 + c_3^*\hat{a}_3, c_2\hat{a}_2^\dagger + c_3\hat{a}_3^\dagger] - |c_2|^2 = \sum_i |\tilde{c}_i|^2 - |c_2|^2 \tag{5.2.5c}$$

And because $\hat{a}'$ must preserve the canonical commutation relations:

$$b_1^2 + b_2^2 - |c_1|^2 - |c_2|^2 - |c_3|^2 = 1 \tag{5.2.6}$$

Now, with the above expressions for the memory Bogoliubov transformation and the coefficients involved, we are ready to consider repeater operation perturbatively.

5.3 Perturbation

To compute the generating function for entanglement connection, we need to know the corresponding transformation on the modes which are measured, and on the

[2] We can choose any value for it, by a phase shift on the output mode.

[3] We may also take b_2 to be nonnegative but this assumption is not necessary.

modes which contain the interesting output state — i.e. modes $\hat{a}_{1out}$, $\hat{a}_{2out}$ in fig. 5.2. We need not know the transformation on the auxiliary modes which are traced out (see sec. 4.1 and (B.9)). Since the two output modes are not involved in the connection procedure, the transformation on these modes is simply the identity. From fig. 5.2 we obtain for the measured modes:

$$\hat{a}''_{11} = \frac{1}{\sqrt{2}}\left(\hat{a}'_{11} + \hat{a}'_{21}\right) \qquad \hat{a}''_{21} = \frac{1}{\sqrt{2}}\left(\hat{a}'_{11} - \hat{a}'_{21}\right) \tag{5.3.1}$$

with primed operators given by (5.2.2). In addition to the mode transformation, we also need the measurement operators corresponding to the desired outcomes for successful connection. Because efficient photon-resolving detectors are very difficult to implement in practice, we choose to work solely with detectors that do not count the number of excitations. For non-counting detectors, the measurement operators are given by (4.1.17).

Having computed the generating function according to the three steps of sec. 4.1, we can find the output density matrix of modes $\hat{a}_{1out}$ and $\hat{a}_{2out}$ for any input entangled state. Since all segments of the repeater are identical, the input states of the right and left pair are the same.

We now derive an expression for the density matrix of the entangled pairs as a function of the distance level. In the ideal case of a perfect quantum memory, $b_1 = 1$ in (5.2.2) while the remaining coefficients vanish. We do perturbation away from this case in each of the coefficients separately, keeping the others at zero. We will perform the derivation in the best-case scenario of a perfect entanglement generation step, i.e. the input state to the first entanglement connection is maximally entangled. This means that our derivation gives the best possible performance for a repeater using a quantum memory described by (5.1.1) and the conditioning scheme of fig. 5.2.

The strategy we use is to parametrise the density matrix on a form which is preserved by connection to lowest order in the perturbation. By performing connection with this parametrised matrix as, input we obtain coupled recurrence relations for the parameters in the matrix, and solving these we find an expression for the matrix as a function of the number of entanglement connections or equivalently as a function of the distance level. We present here the derivation for perturbation in b_2. Perturbation in the other coefficients is treated similarly and the recurrence relations and expressions for the density matrix can be found in app. D.

We start by computing the generating function for the connection, from the Bogoliubov transformation (5.3.1). We assume the initial input state to be $|\Psi^+\rangle$, i.e. in the first step we connect two Bell states. The input state of all auxiliary modes is supposed to be vacuum. Inserting this input and the generating function for the connection into our *Mathematica*-program, we obtain an expression for the output density matrix, which we may expand in b_2, assuming that $b_2 \ll 1$. We

make the following substitutions:

$$b_1 \to \sqrt{1-b_2^2} \qquad c_1, c_2, c_3 \to 0 \tag{5.3.2}$$

where we have used (5.2.6). Expanding each entry of the matrix to lowest order then gives (in the number state basis):

$$\rho_1 = \begin{pmatrix} 1/3 + 2\,b_2^2/9 & 0 & 0 & 0 \\ 0 & 1/3 - b_2^2/9 & 1/3 - b_2^2/9 & 0 \\ 0 & 1/3 - b_2^2/9 & 1/3 - b_2^2/9 & 0 \\ 0 & 0 & 0 & 0 \end{pmatrix} \tag{5.3.3}$$

Repeating the procedure a few times with the new density matrix as input motivates us to try the following parametrisation:

$$\rho_l = \begin{pmatrix} 1 - 2f_l + 2g_l b_2^2 & 0 & 0 & 0 \\ 0 & f_l - g_l b_2^2 & f_l - g_l b_2^2 & 0 \\ 0 & f_l - g_l b_2^2 & f_l - g_l b_2^2 & 0 \\ 0 & 0 & 0 & 0 \end{pmatrix} \tag{5.3.4}$$

where f_l, g_l are functions of l. We now perform the entanglement connection with the parametrised ρ_l as input and after some simplification we find that the output takes the form:

$$\rho_{l+1} = \begin{pmatrix} 1 - 2\frac{f_l}{2-f_l} + 2\frac{f_l^2+2g_l}{(f_l-2)^2}\,b_2^2 & 0 & 0 & 0 \\ 0 & \frac{f_l}{2-f_l} - \frac{f_l^2+2g_l}{(f_l-2)^2}b_2^2 & \frac{f_l}{2-f_l} - \frac{f_l^2+2g_l}{(f_l-2)^2}b_2^2 & 0 \\ 0 & \frac{f_l}{2-f_l} - \frac{f_l^2+2g_l}{(f_l-2)^2}b_2^2 & \frac{f_l}{2-f_l} - \frac{f_l^2+2g_l}{(f_l-2)^2}b_2^2 & 0 \\ 0 & 0 & 0 & 0 \end{pmatrix} \tag{5.3.5}$$

We note that the form of the matrix is preserved if we set:

$$f_{l+1} = \frac{f_l}{2-f_l} \qquad \text{and} \qquad g_{l+1} = \frac{f_l^2 + 2g_l}{(f_l-2)^2} \tag{5.3.6}$$

This confirms our choice of parametrisation, if these recurrence relations have a unique solution. We will see that they do, and we can obtain the functional form of ρ_l by solving them.

To solve the recurrence for f_l, we define a new variable $\tilde{f}_l \equiv f_l^{-1}$, and the recurrence relation becomes:

$$\tilde{f}_{l+1} = 2\tilde{f}_l - 1 \tag{5.3.7}$$

This is a linear inhomogeneous difference equation with constant coefficients, and has a unique solution. From (5.3.3) the initial condition is $\tilde{f}_1 = f_1^{-1} = 3$. It is easy to check that $\tilde{f}_l = 2^l + 1$ is a solution, and hence we have $f_l = 1/(2^l + 1)$. Now

f_l can be eliminated from the recurrence relation for g_l by inserting the solution. We get:

$$g_{l+1} = \frac{2(2^l+1)^2 g_l + 1}{(2^{l+1}+1)^2} \tag{5.3.8}$$

Again this equation may be simplified by a change of variable. With $\tilde{g}_l \equiv (2^l+1)^2 g_l$ we find:

$$\tilde{g}_{l+1} = 2\tilde{g}_l + 1 \tag{5.3.9}$$

The initial condition is $\tilde{g}_1 = 9g_1 = 1$ and the solution is seen to be $\tilde{g}_l = 2^l - 1$. Thus the relations (5.3.6) with initial conditions given by (5.3.3) are solved by:

$$f_l = \frac{1}{2^l+1} \qquad \text{and} \qquad g_l = \frac{2^l-1}{(2^l+1)^2} \tag{5.3.10}$$

Note that the solution is valid also for $l = 0$, and that the approximation (5.3.4) to the density matrix is valid as long as the term $g_l b_2^2$ is small.

Together (5.3.4) and (5.3.10) determine the density matrix for entangled pairs at any distance level of the repeater for which the approximation is valid, and enable us to compute physically interesting quantities. In the next section we look at the fidelity.

In app. D we give the density matrices, recurrence relations and solutions for perturbation in the other coefficients c_1, c_2, c_3. The solution when more than one of the coefficients are nonzero is obtained simply by adding each perturbation separately to the solution for perfect state transfer (as given by (5.3.4) and (5.3.10) when $b_2 = 0$). For this to be valid the perturbative expansion must not contain any cross terms of the same order as the lowest order term for any single coefficient. We have checked this by performing the expansion in all coefficients simultaneously in *Mathematica* and eliminating higher order terms.

5.4 Conditional Fidelity

To lowest order in b_2 the fidelity of ρ_l w.r.t. $|\Psi^+\rangle$ is:

$$F_l = F(\rho_l, \Psi^+) = \frac{2}{2^l+1} - 2\frac{2^l-1}{(2^l+1)^2} b_2^2 \tag{5.4.1}$$

The first thing we notice from this expression is that even in the ideal case of $b_2 = 0$ the fidelity is decreasing very fast. After only two connection steps $F = 2/5$ which is below the classical $1/2$-limit. The decrease is sub-exponential in $L_l/L_0 = 2^l$, but if the fidelity is below $1/2$ after two connections even for an ideal memory, this is not of much encouragement. It looks like something is wrong with our scheme; however we should check exactly what the problem might be.

In fact an exponential decrease in l should not come as a great surprise. It is due to the fact that we are using non-counting detectors. Recall that in the conditional entanglement connection of fig. 5.2 we can think intuitively of three

possibilities: read out of none, one or both of the excitations contained in the two entangled pairs. None lead to no click, and one leads to a single click and successful connection. In the case where two excitations are read out, the event should be rejected as a failed connection. However because of bunching at the beam splitter[4], both excitations will enter the same detector, and when the detectors are non-counting this will produce only a single click. Hence this event will be accepted as a successful connection, but the conditional state of the output modes is vacuum. This vacuum can propagate to subsequent distance levels of the repeater, since connection of a vacuum state with an entangled state can also lead to a detector click and a vacuum output. From (5.3.4) we see that the the vacuum component of the density matrix at the l'th level deviates from 1 by $2f_l$, and from the solution (5.3.10) this deviation decreases exponentially. It is the growing vacuum component which leads to the decay of the fidelity.

Is it then a hopeless task to build the repeater using non-counting detectors? No, we have found that the problem is with the vacuum component of the states, and in this case there is a workaround. In the original proposal [8] by DLCZ a teleportation protocol for qubits in dual rail encoding was described, in which the vacuum components of the entangled states used do not contribute to the fidelity of teleportation. The protocol is not straightforward to implement; it is probabilistic and involves a posterior confirmation of successful operation after the conditioning step. But this has no influence on the operation of the repeater, which simply delivers final entangled pairs that are used in the teleportation protocol for quantum communication. In quantum cryptography entangled states with a large vacuum component are also potentially useful. The Ekert protocol for sharing a secret key between two parties require the parties to share a large number of entangled pairs of qubits. Both qubits of each pair is measured, and the presence of an excitation will thus be automatically confirmed [11]. Hence pairs with a vacuum component might well be used in such a protocol. Since the quality of the secret key or the fidelity of teleportation using the DLCZ proposal is not influenced by the vacuum component of the generated entangled states, we need a new figure of merit for the quality of these states. Instead of the fidelity, we will use the *conditional fidelity* defined as:

$$\tilde{F}_l \equiv F(\tilde{\rho}_l/\mathrm{Tr}(\tilde{\rho}_l), \Psi^+) \qquad \text{where} \qquad \tilde{\rho}_l \equiv \rho_l - |vac\rangle\langle vac|\rho_l|vac\rangle\langle vac| \tag{5.4.2}$$

The conditional fidelity is simply the fidelity when the vacuum component of the density matrix is set to zero. The teleportation proposed by DLCZ works perfect when the conditional fidelity of the entangled states used is 1.

Now we can review the perturbation in b_2. From (5.3.4) it is not hard to find that:

$$\tilde{F}_l = 1 \tag{5.4.3}$$

[4]When two photons enter a 50-50 beam splitter from opposite sides, they will always exit on the same side. This derives from the postulate that the wave-function of bosonic particles must always be symmetric. The effect is called 'bunching'.

Apart from a growing vacuum component, the entangled pairs of the repeater are perfect when $c_1, c_2, c_3 = 0$. This is because the transformation (5.2.2) is passive in this case, i.e. it contains only annihilation operators, and therefore no extra excitations can arise during the state transfer in and out of the memory. All that can happen is loss of excitations into the auxiliary mode $\hat{a}_2$, which can lead either to connection failure or vacuum output. For perturbation in c_1, c_2, c_3 the transformation is not passive, and consequently the conditional fidelity decreases with increasing distance level.

In the following sections, we will consider three particular physical repeater systems. We will compare the results of numerical simulation for the conditional fidelity with analytical predictions from the perturbative approach, and we shall see that there is very good agreement within the range of validity of the perturbation.

Chapter 6

Three Repeater Systems

In this chapter we employ the generating function method to find the performance of three different proposals for repeater systems, obtaining for each of them the fidelity which can be maintained over a given number of connection steps and the corresponding communication rate. Each repeater is described in detail and the results from numerical simulation are presented and compared with the analytical prediction.

6.1 Common features

All three repeaters are based on atomic ensemble quantum memories interacting with light. Such a memory consists of an ensemble of atoms contained within a cell which allows access by light beams, e.g. for the memory of sec. 6.4 paraffin-coated glass cells are used. By passing a light pulse through the cell, it is possible to transfer the quantum state of a light mode to the internal state of the atoms, and later to retrieve it by another pulse. The light-atom interaction is not the same for the three setups, but it is common to all of them that it is the collective atomic mode which is used for storage. Individual atoms are not addressed. The three setups also use the same entanglement connection scheme, namely the one given in fig. 5.2. This choice was motivated by its simplicity and by the initial idea of this project: to insert the one-pass memory (see sec. 6.4) into the original DLCZ-repeater protocol [8] and find the performance.

Chronologically, the DLCZ-repeater is the oldest proposal (2001) followed by the one-pass memory (2004) and the two-pass larmor precessing memory (2005). We treat the last two systems in opposite order, because this makes for an easier read.

6.2 The DLCZ-repeater

The first repeater protocol we look at is the original DLCZ-protocol[1] presented in [8]. In the first section below we describe the physical setup and give the Bogoliubov transformations applicable to entanglement generation and connection, which is what we need to know to apply the generating function. In the following section we present the results of our simulation of the protocol.

6.2.1 Setup

The level structure of the atoms relevant for the light-matter interaction to be used is shown in fig. 6.1a. The atoms are assumed to be described by a true λ-system[2]. The two lower states may f.x. correspond to hyperfine sublevels of an alkali metal [8]. All atoms are initially prepared in the ground state $|1\rangle$ and excitations can then be stored by inducing transitions $|1\rangle \rightarrow |2\rangle$. Read-out can be achieved by the inverse transition. We now introduce quantum operators to give a formal description of the system of light and atoms.

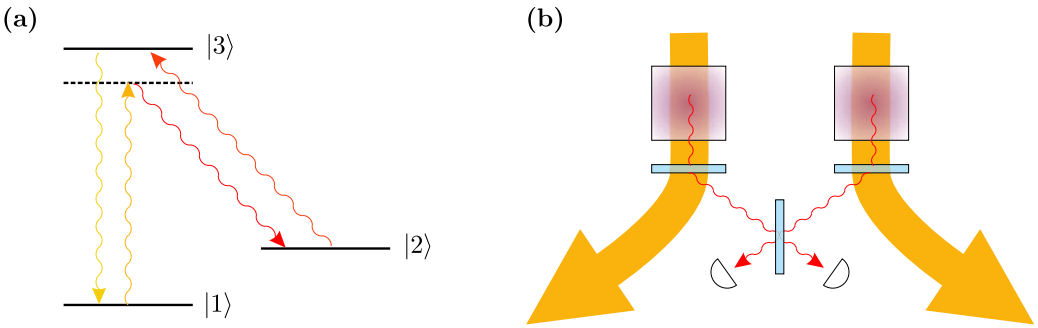

Figure 6.1: Elements of DLCZ. **a)** Each of the quantum memories consists of an ensemble of atoms with the level structure shown. The transitions involved in entanglement generation and connection are displayed. **b)** Successful entanglement generation requires a click in one detector only. The incoming beams are filtered away, and the Stokes light associated with atomic excitations is measured.

The light fields are naturally described by mode operators $\hat{a}_L$, where different modes are distinguished spatially or by polarisation or wavelength. We can make a similar description for the atoms. We define the collective ground (or 'vacuum') state for an atomic ensemble to be $\bigotimes_j |1\rangle_j$ with j running over all the atoms. The

[1] Do not mistake the terms 'DLCZ-repeater' and 'DLCZ-type repeater'. The first refers only to the original proposal [8] while the second refers to a broader class of protocols (c.f. sec. 3.2.3)

[2] For any real atom the actual level structure is more complicated that this, and it is an approximation to use the λ-system description. According to private correspondance with A. S. Sørensen good experimental approximations to the λ-system can be obtained, although it is not easy.

ensemble is then described by a harmonic oscillator with creation operator:

$$\hat{a}_A^\dagger = \frac{1}{\sqrt{N_A}} \sum_j |2\rangle_j\langle 1| \tag{6.2.1}$$

where N_A is the number of atoms. The light pulses of the scheme are designed such that the excited level $|3\rangle$ always has vanishing population, and it does not enter our description. The mode given by $\hat{a}_A$ is called a symmetric, collective mode. It should be noted at this point that since there is a finite number of atoms, only a finite number of excitations are allowed for the mode $\hat{a}_A$. However the ground state population will always be dominant, and the collective mode behaves just like a harmonic oscillator mode.

The setup for entanglement generation is shown in fig. 6.1b. Entanglement is generated between two cells directly; we do not generate entangled light and store it subsequently. In fact the DLCZ-protocol 'as is' does not use a full quantum memory. Write-in for arbitrary states of the light mode is not implemented. However, this is not necessary for repeater operation, as long as entanglement between nodes can be established. To create entanglement a weak coherent pulse of light with a detuning from the $|1\rangle \rightarrow |3\rangle$ transition is passed through each of the cells. With a small probability the symmetric collective mode of the ensemble will then be excited, and an associated Stokes photon will be emitted[3]. The scattered Stokes light is filtered from the input light, mixed on a beam splitter and measured. A single click in one detector only is required for successful connection.

The interaction between the light and atoms can be understood effectively as a two-mode squeezing acting on the collective mode $\hat{a}_A$ and the measured mode $\hat{a}_L$ of the Stokes light. The details of the derivation may be found in [9][4]. This means that the state after passage of the input light is a squeezed state of the form (2.1.28) which exhibits perfect correlation between atomic excitations and output Stokes photons. Now we can see that our entanglement generation is very reminiscent of the connection shown in fig. 5.2. The two atomic cells play the roles of output modes and each of them is entangled with a Stokes light mode. Measuring the light modes leads to an entangled state of the atomic cells. The mathematical details are given in app. C.

To be able to simulate the generation step, we need the Bogoliubov transformation for modes $\hat{a}_A$ and $\hat{a}_L$. From the results given in [9], we can find the expression:

$$\hat{a}'_L = \hat{a}_L\sqrt{\frac{1}{1-p_c}} + \hat{a}_A^\dagger\sqrt{\frac{p_c}{1-p_c}} \qquad \hat{a}'_A = \hat{a}_A\sqrt{\frac{1}{1-p_c}} + \hat{a}_L^\dagger\sqrt{\frac{p_c}{1-p_c}} \tag{6.2.2}$$

[3] One may think of this as one atom making a transition $|1\rangle \rightarrow |2\rangle$, the identity of the particular atom being unknown to us. But quantum mechanically the state of the ensemble after emission of the Stokes photon is the *coherent* superposition of excitation of individual atoms.

[4] The essential steps are adiabatic elimination of the excited level $|3\rangle$ to find the interaction Hamiltonian and then solution of the Heisenberg equations of motion for the interesting modes.

where primes denote the operators after the interaction and p_c determines the probability to create an atomic excitation. More precisely, the probability of creating at least one excitation[5] is $(p_c+p_c^2)/(1-p_c)$, which reduces to p_c when $p_c \ll 1$. In terms of experimentally controllable parameters, p_c is given by:

$$p_c = 1 - e^{-\kappa^2} \tag{6.2.3}$$

where κ is the effective coupling strength for the light-atom interaction, with κ^2 proportional to the number of atoms and the number of photons in the input pulse [9, 10, 28].

From the calculation in app. C it is found that the probability for entanglement connection to succeed is p_c and that the deviation of the created states from $|\Psi^+\rangle$ is also of order $O(p_c)$. Hence there is a trade-off between these two effects. A high fidelity requires low p_c, but this will decrease the communication rate.

Denoting the output operators by double primes, the full transformation for entanglement generation including the beam splitter becomes:

$$\begin{aligned} \hat{a}''_{L1} &= \frac{1}{\sqrt{2}}\left(\hat{a}'_{L1} + \hat{a}'_{L2}\right) \qquad \hat{a}''_{L2} = \frac{1}{\sqrt{2}}\left(\hat{a}'_{L1} - \hat{a}'_{L2}\right) \\ \hat{a}''_{A1} &= \hat{a}'_{A1} \qquad \hat{a}''_{A2} = \hat{a}'_{A2} \end{aligned} \tag{6.2.4}$$

with primed operators given by (6.2.2).

The setup for entanglement connection is similar to fig. 6.1b, except that the incoming light pulse is now a strong coherent pulse resonant on the $|2\rangle \rightarrow |3\rangle$ transition. This pulse converts the excitations stored in the atoms into light on the $|3\rangle \rightarrow |1\rangle$ transition and leaves the atoms in the collective ground state. The efficiency of this conversion can be made very close to 1 [8], and the corresponding Bogoliubov transformation is therefore:

$$\hat{a}''_{L1} = \frac{1}{\sqrt{2}}\left(\hat{a}_{A1} + \hat{a}_{A2}\right) \qquad \hat{a}''_{L2} = \frac{1}{\sqrt{2}}\left(\hat{a}_{A1} - \hat{a}_{A2}\right) \tag{6.2.5}$$

The two transformation equations (6.2.4) and (6.2.5) are all that we need to know to apply the generating function method. From the transformation for entanglement generation we compute the initial entangled state of the atomic storage modes (i.e. the state at the 0th level of the repeater). To find the states at higher levels it is then sufficient to know the Bogoliubov transformation for read-out. In fig. 5.2 we are allowed to think of modes $\hat{a}_{1out}, \hat{a}_{11}, \hat{a}_{21}, \hat{a}_{2out}$ as storage modes, rather than input modes for the memories. Two of these modes are read out and measured, and the resulting state of the remaining two modes, which is at the next level of the repeater, is computed. The difference between this way of calculation, and the one implied by fig. 5.2 is of no importance. It is simply a question of whether the final entangled state generated by the repeater will be contained in the atomic storage modes or in some other (light) mode.

[5] From [9], the joint state of the modes after interaction is: $\sqrt{1-p_c}\sum_n \frac{p_c^{n/2}}{n!}(\hat{a}_L^\dagger \hat{a}_A^\dagger)^n|vac\rangle$ and it follows that the probability of excitation is $(p_c+p_c^2)(1-p_c^{N_a})/(1-p_c)$ where N_a is the number of atoms. This gives the expression in the text, except when p_c is very close to 1.

6.2.2 Results

Using the Bogoliubov transformations obtained in the previous section we have simulated the DLCZ-repeater for varying values of the parameter p_c and we have found the fidelity at each distance level. For a certain value of p_c we have also obtained the communication rate. In the model of the DLCZ-repeater protocol presented in the previous section, the entanglement connection step is essentially assumed to be perfect[6], while the p_c-dependence enters in the entanglement generation step. The analytical model of sec. 5 was based on the opposite assumption and does therefore not apply in the present case. However some analytical predictions for the communication rate were given already in [8]. Only very rough estimates of the fidelity were given there, and we present accurate values from numerical simulation and suggest an explanation for the observed behaviour. We begin by studying the fidelity and subsequently look at the communication rate.

Note that except for the communication rate which is found by a stochastic method, we do not indicate any uncertainties in our numerical results. The errors in the numerical output from *Mathematica* were $\sim 10^{-16}$ (i.e. 15 digits precision), which is at least 10 orders of magnitude less than the smallest numbers in our results, corresponding to a relative error of $\sim 10^{-10}$.

We have simulated the repeater using non-counting photodetectors, and as predicted in sec. 5.4 the fidelity drops hyperbolically with the communication distance L_l (this prediction applies also when entanglement connection is perfect, and of course having an imperfect generation step does not help). An example is plotted in fig. 6.2

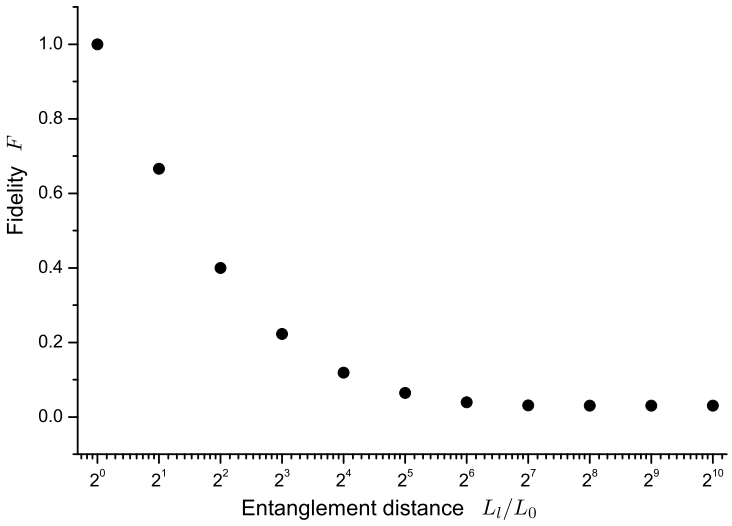

Figure 6.2: Simulated fidelity. The DLCZ-repeater was simulated at $p_c = 10^{-3}$. Note that the values follow the first term of (5.4.1) very nicely.

[6]The read-out has unit efficiency. It is possible to introduce a finite efficiency for this process. We will come back to this when we discuss sources of error.

We note that already after two connection steps the fidelity has dropped below the classically obtainable value of 1/2. Recall from sec. 5.4 that the drop is a consequence of an increasing vacuum component.

However, if we consider distribution of entanglement for cryptography or teleportation via the protocol suggested in [8], then the figure of interest is the conditional fidelity. In fig. 6.3[7] we show the conditional fidelity obtained from simulation of the DLCZ-repeater for five different values of p_c.

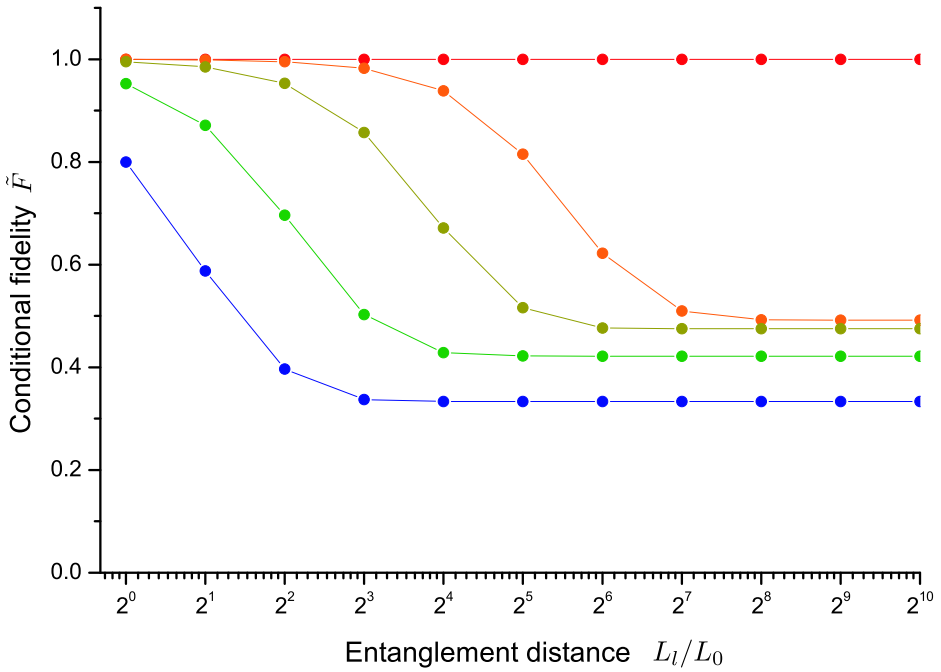

Figure 6.3: Simulated conditional fidelity. Starting from the top, the values of p_c for the five plots are 10^{-10} (red), 10^{-3} (orange), 10^{-2} (olive), 10^{-1} (green), ~ 0.5 (blue)

As expected the highest fidelities are obtained when p_c is small and higher order effects such as double excitations are suppressed. We note that the plots are s-shaped: $\tilde{F}$ remains almost constant for a few steps before dropping abruptly below the classical limit 1/2.

It then saturates to a constant value. Focusing on the first part of the plots, the plateau and drop, this can be seen on closer inspection (e.g. by plotting it on a linear scale) to have the shape of a function of the form $1 - \beta(L_l/L_0)^\alpha$. We can understand this in the following manner.

We know (c.f. app. C) that errors of order $O(p_c)$ in form of double excitations enter the generated entangled states. In fact the coefficient of the double excitation term of the generated state is $p_c/2$ and the conditional fidelity of the state is $\tilde{F} = 1 - p_c/2$. Now, if a pair containing two excitations is connected with $\Psi^+\rangle$ using

[7] Apologies in advance to any red/green colourblind readers. The figure should be readable from the legend, even if colours cannot be distinguished.

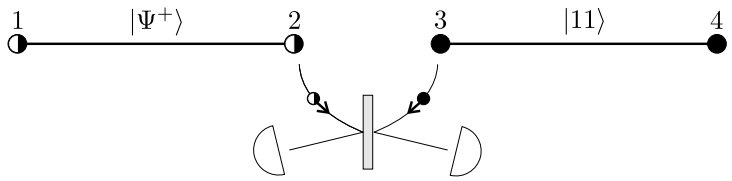

Figure 6.4: Connecting a doubly excited pair. In the RHS pair both samples are excited. Since read-out is perfect the excitation in mode 3 is always read out. If the detectors count photons the read-out from mode 2 must therefore be vacuum for successful connection and modes 1,4 are then in the state $|11\rangle$. If photons are not counted, read-out of the LHS excitation also contributes to successful connection and the output is $(|01\rangle\langle 01| + |11\rangle\langle 11|)/2$.

photon counting detectors, then the state conditioned on successful connection again has two excitations (see fig. 6.4). This means that this type of error will propagate to higher distance levels of the repeater. The effect persists also for non-counting detectors, with a coefficient $1/\sqrt{2}$ for the double excitation term of the output. Since the number of initial entangled pairs which contribute to an entangled pair at level l is 2^l and the error probabilities for all of them are equal, we expect the double-excitation error in the entangled state, and hence in $\tilde{F}$, to increase exponentially with l: $\tilde{F} \approx 1 - \beta a^l$, where β should be of order p_c. Now $l = \log_2(L_l/L_0)$ and so:

$$\tilde{F} \approx 1 - \beta a^{\log_2(L_l/L_0)} = 1 - \beta(L_l/L_0)^{\log_2(a)} = 1 - \beta(L_l/L_0)^{\alpha} \qquad (6.2.6)$$

This type of function does in fact fit the simulated results for $\tilde{F}$ quite well[8]. Fig. 6.5 shows a fit to the plot for $p_c = 10^{-3}$. For the plots of fig. 6.3 we find α in the range 1 to 2 and $\beta \sim 0.5p_c$.

Since we find good agreement between the simple model (6.2.6) and the simulations, it is reasonable to suppose that it is double-excitations in the generated entangled pairs which cause the conditional fidelity to fall off. The DLCZ-repeater performs well in terms of $\tilde{F}$, as long as no double-excitations enter the system, but as soon as a double excitation are present, $\tilde{F}$ drops. The scheme breaks down whenever there is 'a photon too much' somewhere. The probability of an extra photon grows linearly with the number of repeater segments, i.e. with the distance L_l, and this leads to a polynomial scaling for the error in $\tilde{F}$. The value of α is not exactly 1 because the errors from the initial states do not simply add. Successful connection events coming from connection of two Bell states have a vacuum component and are therefore partially suppressed in the conditional fidelity. But the output from connection of a double-excitation with a Bell state has no vacuum component and is not suppressed.

Note that a polynomial - or at least sub-exponential - scaling for the (conditional) fidelity is one of the essential requirements for a repeater system to beat

[8]In [8] the error in $\tilde{F}$ was assumed to be linear, and hence our model is a slight improvement over this.

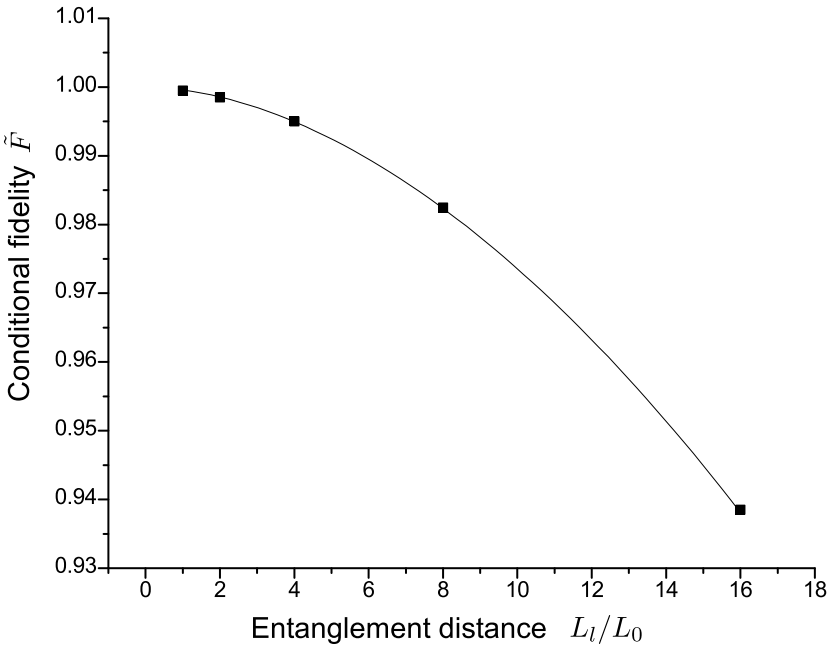

Figure 6.5: Fit of the function (6.2.6) to $\tilde{F}$ obtained from simulation with $p_c = 10^{-3}$. The fit has $\alpha = 1.8$ and $\beta = 0.4p_c$.

the classical channel, and we have seen that the DLCZ-repeater does in fact meet this demand.

Now for the communication rate. When we simulate the repeater we obtain at each level l the unnormalised density matrix, and by taking the trace of this we find the success probability p_l for the entanglement connection leading to this level. From the list of probabilities we can simulate the communication rate. The algorithm that we use to find the communication rate is explained in chap. 8 in the context of channel mixing repeaters. It is based on stochastic processes (i.e. it is a kind of Monte-Carlo simulation), because measurements in quantum mechanics are inherently random. Due to the nature of the algorithm the runtime complexity is $O(2(L/L_0)) = O(2^{N+1})$, where N is the number of connection steps required to generate a final entangled pair and L is the total length of the repeater. The number of runs necessary for good statistics also increases linearly with the time t_N required to generate a final entangled pair. From the estimate (3.2.2) we can see that this is at least exponential in N $(= p_0)$, since $p_l < p_c$ for all higher levels. The algorithm was written in *Mathematica*, which is not a great tool for numerics, and is rather slow. Therefore the distance levels and values of p_c that we can reach within moderate runtimes are considerably restricted. On our hardware, by running in parallel ~20 copies of the program it is possible to obtain overnight a good estimate for the rate with reasonable statistics when $N = 3$ and $p_c = 10^{-3}$. As a consequence of the limitations, it has not been possible to simulate the communication rate for many different values of p_c. The simulations that we

have performed are summarised in tab. 6.1 below, together with the corresponding analytical values from (3.2.2).

In all cases $N = 3$	$p_c = 10^{-3}$	$p_c = 10^{-2}$	$p_c = 10^{-1}$
Simulated rate $[10^{-5} \cdot \tau^{-1}]$	6.6 ± 0.6	73 ± 2	880 ± 8
Analytical rate $[10^{-5} \cdot \tau^{-1}]$	15	150	1700
Final conditional fidelity $\tilde{F}$	0.98	0.86	0.50

Table 6.1: Communication rate for the DLCZ-repeater. The final values of $\tilde{F}$ which may be read off fig. 6.3 are also given.

The rates are given in units of $10^{-5}\tau^{-1}$, where τ is the time spent on a single entanglement generation or connection attempt. That is τ is the light-atom interaction time plus the time spent on measurements and classical communication between different segments of the repeater.

We note that the analytical expression (3.2.2) overestimates the rate by a factor of approximately 2.5. This is due to the approximations made in the derivation of the expression, as given in sec. 3.2.3. As a tool for order-of-magnitude estimates, our numerical simulations confirm the validity of (3.2.2) and hence also of the corresponding expression used in [8], which is simply the dominant term of (3.2.2). The dominant term is larger than the sum of all the other terms by a factor of at least $O(p_0) = O(p_c)$.

The rates obtained here are not directly comparable with the communication times which were found by DLCZ in [8], because they consider only photon counting detectors and compensate by including an inefficiency for the entanglement connection step. In the paper [8] it is claimed that introducing an inefficiency for the connection step is equivalent to using non-counting detectors, and analytical expressions for the communication time are derived on this basis. However we have checked that the expressions given there for the connection probabilities (which lead to the expression for the time) actually imply photon counting. For a channel length $L \approx 2^4 L_0$ and an efficiency 2/3 for the entanglement connection DLCZ predict a rate of $O(10^{-6}\tau^{-1})$, which is within one order of magnitude from the lowest rate in tab. 6.1.

The rates given in tab. 6.1 are low from the viewpoint of practical quantum communication. To get a feeling for the numbers, we can take $\tau \approx 1$ms. The pulses used in the experiments with the one-pass memory have this order of magnitude [18], and we can use it to get an idea of the rate. With $\tau = 1$ms the lowest rate of tab. 6.1 becomes $O(10\text{ms}^{-1})$ corresponding to about 0.5 qubits/minute. For comparison, in a quantum key distribution experiment performed in Vienna in 2004, the key size was $\sim 80,000$bits [23], and so, with the DLCZ-repeater rate, the key would take about 4 month to send. If τ can be reduced to a nanosecond however, the key may be sent in $\sim$15 minutes, which might be sufficient for experimental verification of the protocol. For the DLCZ-system it may be possible to use short

pulses[9].

Even though the rates for the DLCZ-repeater are low, they are substantially higher than for direct communication between sender and receiver. We can view direct communication as a situation in which the nodes of the repeater are connected sequentially from one end of the channel towards the other, instead of in parallel. I.e. entanglement connection is performed first at node 2, then at node 3 etc. until the last node is reached. Entanglement generation is performed not in parallel, but one segment ahead of the connection. The communication time increases exponentially with the channel length L/L_0. If we let $p_c = 10^{-3}$ and use the same success probability for entanglement connection as was used in obtaining tab. 6.1, then the rate for direct communication over a channel of length $L = 2^3 L_0$ is $\sim 10^{-26}\tau^{-1}$. This is 10^{21} times less than the repeater rate.

In summary, we have found that the DLCZ-repeater outperforms direct communication both in terms of fidelity and communication rate. We have found that it is double excitations which cause the conditional fidelity to degrade. We have also found that for ms pulses the communication rate is too low for practical application of the repeater, and that for experiments to be viable the connection time τ needs to be reduced to substantially below this order of magnitude, e.g. to the ns level. Many sources of noise present in a realistic system have been ignored in our treatment, and the cost of classical communication has been completely neglected. These error sources will be discussed in the outlook sec. 7.2.

6.3 Repeater with Two-pass Larmor Precessing Memory

In this section we consider a repeater based on the quantum memory proposed in [21]. Christine Muschik of the Max-Planck-Institut für Quantenoptik, Germany has kindly shared her results and provided the Bogoliubov transformation for a full state transfer into and out of the memory, including noise terms from atomic decoherence and reflection losses. This means that of the three systems we treat in this thesis, the results for this repeater are likely to give the most realistic picture of actual performance.

6.3.1 Setup

In contrast to the memory used in the DLCZ-repeater, the proposal [21] is a full-fleshed quantum memory with both write-in and read-out. Fig. 6.6b shows the procedure which is the same for storage and retrieval. A strong coherent light beam polarised along x makes two passes through the atomic ensemble. States to be written into the memory are encoded in a weak y-polarised field superposed on the coherent beam, and they can be stored in and retrieved from the collective atomic spin, which is also assumed to be strongly polarised along x. The states

[9] Since a high fidelity requires κ to be small, while for the one-pass memory a high κ is desirable (recall that κ is proportional to the total photon number).

are retrieved in y-polarisation. For completeness we mention that if one chooses a direction for the second pass of the light pulse opposite to the one shown in fig. 6.6b (bottom to top), then one obtains the same type of two-mode squeezing interaction between atoms and light as in the entanglement generation of the DLCZ-scheme (sec. 6.2.1). Here however, we are concerned with a repeater using the shown memory protocol for which the interaction takes a new form.

The atomic level structure relevant for the interaction involves four sublevels as shown in fig. 6.6a. We quantise the system along x and the quantum number m refers to the x-component of the total angular momentum of an atom. The population of the ground state $|1\rangle$ is dominant, so that the collective spin is polarised along x[10]. The x-polarised coherent pulses are detuned from the transition from ground to excited level and couples to transitions between sublevels of equal m while the y-polarised field couples to transitions which change m.

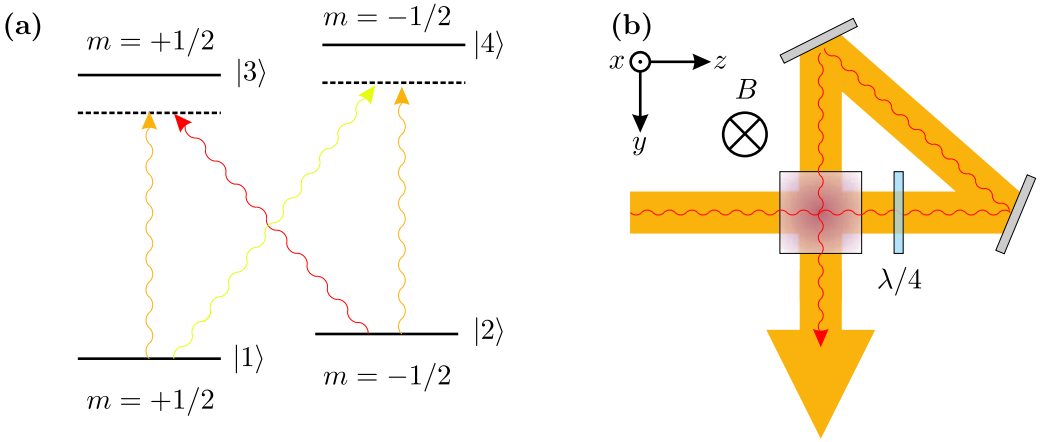

Figure 6.6: Two-pass larmor precessing memory. **a)** Level structure of the atoms in the external magnetic field. The collective atomic spin is assumed to be polarised with a dominant population of the $m = 1/2$ ground state. **b)** Setup for write-in or read-out. The length of the light pulse is assumed to be much longer than the path length from first entry to second exit of the ensemble, and two parts of the pulse therefore interact with the atoms simultaneously.

For light quantum information is encoded in small deviations of the total polarisation from the x-direction, and similarly for atoms it is encoded in deviations of the angular momentum from the x-direction. Hence the relevant quantum variables for describing the memory are those of polarisation and angular momentum. Due to the strong x-polarisation it is possible to make a two-dimensional description which will look the same for light and atoms [18, 21, 25, 28].

Fig. 6.7 illustrates this for light. The Cartesian axes correspond to components of the light Stokes vector (see below), and every point on the surface of the sphere represents a possible Stokes vector of polarised light[11]. For a strongly x-polarised

[10] Such a state of the ensemble is sometimes called a coherent spin state (CSS) [17, 18].
[11] Points inside the sphere corresponds to light with an unpolarised component.

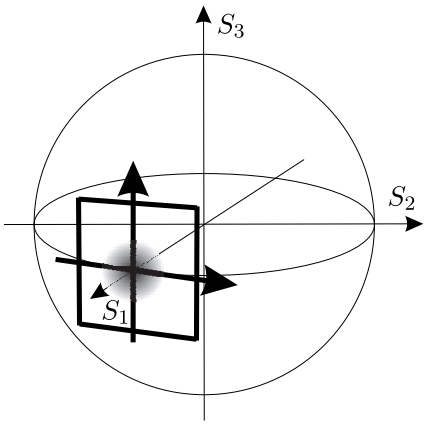

Figure 6.7: Holstein-Primakoff approximation. This figure was inspired by [25].

beam the states are localised closely around the S_1-pole, and the magnitude of any deviation from the pole is much smaller than the mean of S_1. In a tight region around the pole the spherical geometry may be replaced by a two-dimensional planar one.

Starting with the light, recall from classical optics that the polarisation of a light beam is determined by three Stokes parameters which are the differences of intensities between polarisation along orthogonal axes x,y, between axes rotated $+45°$ and $-45°$ from x and between right- and left-circular light (see e.g. [16]). The quantum analogues, called *Stokes operators*, are defined by:

$$\begin{aligned} S_1 &\equiv \frac{1}{2}(\hat{a}_x^\dagger \hat{a}_x - \hat{a}_y^\dagger \hat{a}_y) \\ S_2 &\equiv \frac{1}{2}(\hat{a}_{+45}^\dagger \hat{a}_{+45} - \hat{a}_{-45}^\dagger \hat{a}_{-45}) = \frac{1}{2}(\hat{a}_x^\dagger \hat{a}_y + \hat{a}_y^\dagger \hat{a}_x) \\ S_3 &\equiv \frac{1}{2}(\hat{a}_l^\dagger \hat{a}_l - \hat{a}_r^\dagger \hat{a}_r) = \frac{1}{2i}(\hat{a}_x^\dagger \hat{a}_y - \hat{a}_y^\dagger \hat{a}_x) \end{aligned} \tag{6.3.1}$$

The Stokes operators obey the angular momentum commutation relation:

$$[S_\alpha, S_\beta] = i\epsilon_{\alpha\beta\gamma} S_\gamma \tag{6.3.2}$$

In the case where one polarisation is dominant, this relation can be replaced by a Heisenberg-Weyl (position-momentum) commutator. This is exactly the situation for the write-in and read-out light: since $\langle \hat{a}_x^\dagger \hat{a}_x \rangle \gg \langle \hat{a}_y^\dagger \hat{a}_y \rangle$ the possible outcomes of measurement of S_1 are concentrated tightly around some fixed value $s_1 = \langle S_1 \rangle$, as illustrated in fig. 6.7. Therefore we can replace the operator S_1 by $s_1 \mathbb{1}$, and define new variables:

$$X_L \equiv \frac{S_2}{\sqrt{s_1}} \qquad P_L \equiv \frac{S_3}{\sqrt{s_1}} \qquad [X_L, P_L] = i \tag{6.3.3}$$

where the subscript L is for 'light'. The polarisation of the light is now completely described by a harmonic oscillator with creation operator $\hat{a}_L^\dagger = (X_L - iP_L)/\sqrt{2}$ (which is effectively $\hat{a}_y^\dagger$)[12].

We can obtain a similar description for the atomic angular momentum. The collective angular momentum operators for the ensemble are defined similar to (6.2.1):

$$J_\alpha = \frac{1}{\sqrt{N_A}} \sum_i j_{\alpha,i} \qquad \alpha = x, y, z \tag{6.3.4}$$

where $j_{\alpha,i}$ is the operator for the i'th atom. The angular momentum operators obey the commutation relation (6.3.2), i.e. $[J_\alpha, J_\beta] = i\epsilon_{\alpha\beta\gamma}$ and when J_x is dominant, the angular momentum may be described by operators X_A, P_A, analogous to X_L, P_L for the light:

$$X_A = \frac{J_2}{\sqrt{\langle J_1 \rangle}} \qquad P_A = \frac{J_3}{\sqrt{\langle J_1 \rangle}} \tag{6.3.5}$$

With these variables everything we need to know about the dynamics of the light-atom interaction can be expressed.

The derivation of the Bogoliubov transformation for write-in and read-out of the memory can be found in [21], and we will not reproduce it here. We simply outline the ingredients in the scheme.

The interaction Hamiltonian for light passing through an atomic sample like the one used here was derived in [17], and has the form $X_L X_A$ or $P_L P_A$ depending on geometry. Each of these interactions alone do not lead to a memory protocol. Something more is needed, and in the present case it is provided by the second passage of the light (in sec. 6.4.1 we shall see another approach). The interaction during the first passage is $P_L P_A$. The quarter-wave plate, shown in fig. 6.6b, interchanges circular and linear polarisation and hence interchanges X_L and P_L and at the same time the geometry of the second passage implies that the atomic variables are also interchanged. The interaction in the second passage is therefore $X_L X_A$. The combination of these two interactions does lead to a memory protocol. This was shown in [28]. However the protocol presented there is not symmetric in X and P due to the asymmetry of the setup fig. 6.6b. The last ingredient of the present scheme, the magnetic field, is introduced to compensate this asymmetry. In the presence of an external magnetic field along the x-axis, the y,z-components of the atomic angular momentum will experience Larmor precession. Let τ be the pulse length and t the time of one passage through the loop of fig. 6.6b. When the Larmor frequency Ω is fixed such that $t \ll \Omega^{-1} \ll \tau$, i.e. such that the angular momentum is frozen during interaction with one slice of the light pulse

[12] The procedure we have described here for approximating the angular momentum algebra by the Heisenberg-Weyl algebra, although not quite rigorous, is well established in the literature [10, 17, 18, 21, 28]. It is sometimes called the Holstein-Primakoff approximation. Some caution should be taken with this approach, as demonstrated in the more mathematically careful treatment of [25].

but rotates over the total pulse, then the asymmetry is washed out. As a result the Bogoliubov transformation describing the memory is completely symmetric, and in the absence of noise the efficiency of a state transfer depends only on the strength of the interaction between atoms and light.

The transformation for the full state transfer in the absence of noise is, from [21]:

$$X'_L = -(1-e^{-\kappa^2})X_L - e^{-\kappa^2/2}\sqrt{1-e^{-\kappa^2}}X_A + e^{-\kappa^2/2}\tilde{X}_L \tag{6.3.6a}$$

$$P'_L = -(1-e^{-\kappa^2})P_L - e^{-\kappa^2/2}\sqrt{1-e^{-\kappa^2}}P_A + e^{-\kappa^2/2}\tilde{P}_L \tag{6.3.6b}$$

Here primes denote the output light, X_L, P_L apply to the write-in pulse, while $\tilde{X}_L, \tilde{P}_L$ are the input operators for the retrieval pulse. κ is the coupling strength and is assumed to be the same for write-in and read-out. κ^2 is proportional to the number of atoms and photons [10, 28][13]. To compute the generating function, we prefer to rewrite the equations as a Bogoliubov transformation of the mode operators. This is easy, since they are symmetric in X and P:

$$\hat{a}'_L = -(1-e^{-\kappa^2})\hat{a}_L - e^{-\kappa^2/2}\sqrt{1-e^{-\kappa^2}}\hat{a}_A + e^{-\kappa^2/2}\hat{\tilde{a}}_L \tag{6.3.7}$$

Note that the memory is perfect, when $\kappa \gg 1$.

In our simulation we do not actually use the noiseless transformation (6.3.7). We take into account reflection losses when the light passes through the cell with the atoms, and decoherence of the atomic spin state by spontaneous emission. Decoherence of the atomic angular momentum happens when the atoms scatter photons into other modes than the forward mode. The angular momentum of the atoms is changed by the scattering. We consider only transverse decoherence, where the y- and z-components of J change, but neglect longitudinal decoherence, in which J_x is changed.

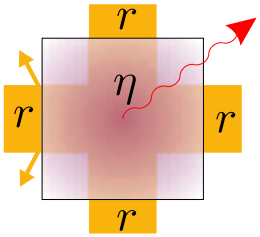

Figure 6.8: Losses.

The Bogoliubov transformation including noise contains 22 independent modes, and will be omitted here[14]. When we compute the generating function for entanglement connection we first apply the mode reduction of sec. 5.2. The parameters of the transformation are κ, the reflection coefficient r (the same for all cell walls) and the atomic decoherence rate η/τ. They are indicated on fig. 6.8. When $r \to 0$ and $\eta \to 0$ the noisy transformation reduces to (6.3.7). Note that other sources of photon loss between the two passes or before detection can also be included in r.

[13]The coupling constant kappa here is not the same as for the DLCZ-repeater. However, they are both proportional to photon and atom numbers.

[14]We omit is also because Christine Muschik has kindly shared her unpublished results, and hence it would not be fitting to reproduce them.

Referring to fig. 5.2 the full transformation for entanglement connection becomes:

$$\hat{a}''_{L1} = \frac{1}{\sqrt{2}}\left(\hat{a}'_{L1} + \hat{a}'_{L2}\right) \qquad \hat{a}''_{L2} = \frac{1}{\sqrt{2}}\left(\hat{a}'_{L1} - \hat{a}'_{L2}\right) \tag{6.3.8}$$

with primed operators given by (6.3.7) (or the corresponding noisy transformation).

So far we have said nothing about entanglement generation. Since the present repeater is using quantum memories for light, the way to generate entanglement would be to create entangled states of light and store them subsequently. This can be achieved f.x. by parametric down conversion: in a non-linear crystal one photon can be converted into two photons of lower frequency, and the output light is then in a two-mode squeezed state (2.1.28), i.e. it is entangled. If we condition on a single click in the setup shown in fig. 6.9, the two such states can be used to generate $|\Psi^+\rangle$. It is possible to include such entanglement generation in our simulations (the squeezing operator may be included in a generating function). However, we will assume simply a perfect entanglement generation step. This is a good starting point to examine the behaviour of the repeater for varying values of the memory parameters.

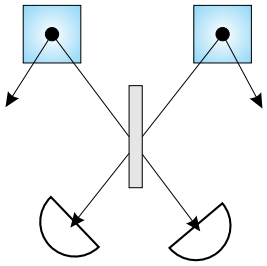

Figure 6.9: Entanglement generation.

Summing up, for simulation we use the Bogoliubov transformation for the full state transfer including noise, and we assume the initial state of the input modes to be perfectly entangled pairs $|\Psi^+\rangle$. The initial state of all other modes is assumed to be vacuum.

6.3.2 Results

We have performed numerical simulation of the two-pass protocol described above and found the conditional fidelity and communication rate. For this repeater protocol all the results of chap. 5 apply. Below we compare the analytical predictions from perturbation theory with the results of the numerical simulation.

There are three parameters, κ ,r, η, in our memory model. Of these κ and η turn out not to be crucial for the conditional fidelity, while r limits the number of connection steps for which a good fidelity can be maintained. κ is important for the success probability of the entanglement connection and hence for the communication rate. This also depends on r, although weaker. The value of η is not crucial for the performance of the protocol, and for a realistic value $\eta \approx 0.1$ it performs essentially the same as for $\eta \approx 0$. Fig. 6.10 shows the dependence of the conditional fidelity on κ and η.

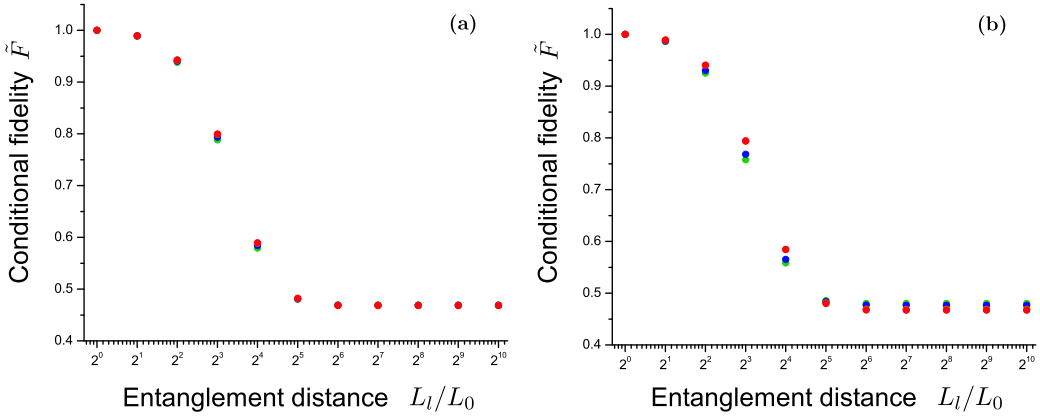

Figure 6.10: Simulated conditional fidelity. **a)** Dependence on η. The plots show $\tilde{F}$ plotted for $\eta = 0$ (red), $\eta = 0.01$, $\eta = 0.1$, $\eta = 0.2$ (green). **b)** Dependence on κ. $\tilde{F}$ is plotted for $\kappa = 0.1$, $\kappa = 1.0$ (red), $\kappa = 2.0$, $\kappa = 3.0$ (green). For both (a) and (b) $r = 0.01$. Not all plots are visible due to overlap.

In fig. 6.11 we display $\tilde{F}$ for varying values of the reflection coefficient. We get the same s-shaped plots as for the DLCZ-repeater, indicating that the mechanism causing the fidelity to drop may be similar. $\tilde{F}$ is plotted for $\kappa = 2$ and $\eta = 0.1$. According to private correspondence with C.A. Muschik and J. Sherson these are realistic numbers close to the limit of what can be achieved experimentally at present.

Note that the conditional fidelity depends strongly on r. It is desireable to keep r as low as possible, whence one should be very careful about the cells that are used in experiment. The strong dependece on r might motivate us to dispence with cells, and use potential-trapped atomic clouds instead, although other problems may be envisaged in such systems.

We would like to compare the simulation results with the analytical model of chap. 5. Therefore we have applied mode reduction as described in sec. 5.2 to

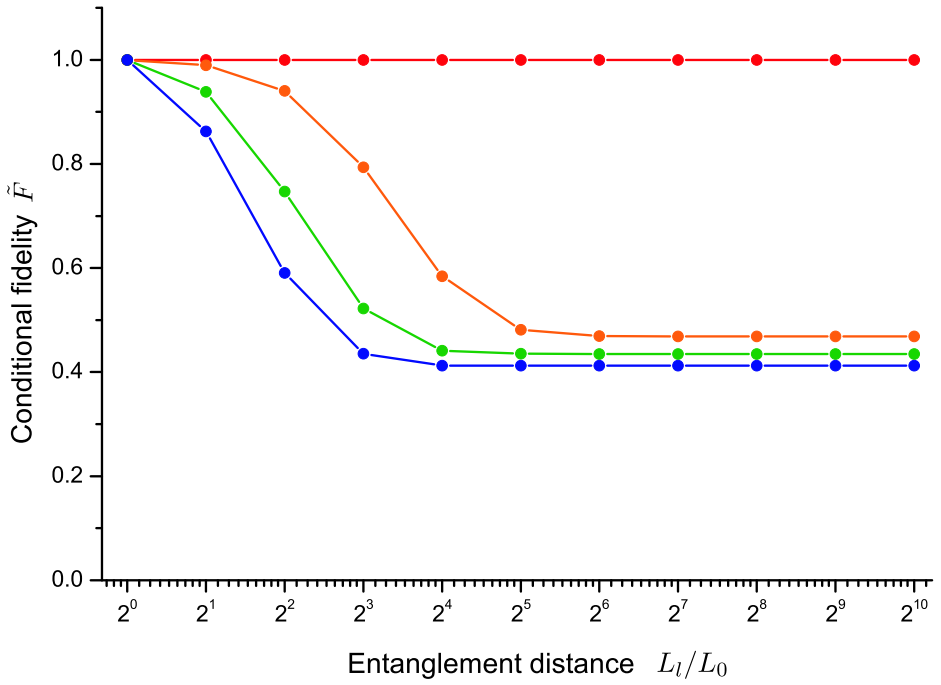

Figure 6.11: Simulated conditional fidelity. For all plots $\kappa = 2$ and $\eta = 0.1$ except the top for which $\eta = 0$. From top to bottom the values r are: $r = 0$ (red), $r = 0.01$ (orange), $r = 0.05$ (green), $r = 0.1$ (blue).

the full state transfer Bogoliubov transformation. This transformation contains 22 independent modes (i.e. i in (5.1.1) runs from 1 to 21) and the coefficients of the mode operators are complicated expressions in κ, r and η, but nevertheless there are some nice features: First the coefficient $c_1 = 0$. Second, for all modes either $\tilde{b}_i = 0$ or $\tilde{c}_i = 0$, which implies that $c_2 = 0$. Third, the remaining coefficients turn out to be real. Hence we need only do perturbation in b_2 and c_3 and we need not worry about the phases. Recall that there are no cross terms and that we obtain the simultaneous perturbation in b_2, c_3 simply by adding the separate solutions. From the expressions in sec. 5.3 and app. D one may find the density matrix ρ_l for the entangled pairs at the l'th level of the repeater, and from ρ_l we can compute F and $\tilde{F}$. We find:

$$F = \frac{2}{2^l+1} - 2\frac{2^l-1}{(2^l+1)^2}b_2^2 + \frac{1}{3}\frac{(2^l-1)(2^l-6)}{2^l+1}c_3^2 \tag{6.3.9}$$

and to lowest order in b_2 and c_3:

$$\tilde{F} = 1 - \frac{1}{2}2^l(2^l-1)c_3^2 \tag{6.3.10}$$

Note that only c_3 appears in the conditional fidelity. We can understand this in the following way. Referring back to (5.2.2) for the reduced Bogoliubov transformation

of the state transfer it is seen, that a non-zero c_3 changes the transformation from passive to active. Non-zero b_2 cannot add any extra excitations into the system, but non-zero c_3 leads to double excitations, and, as we have seen, these lead to a decrease of $\tilde{F}$. The presence of double excitations, when c_3 is non-zero can be seen directly from the expression for the density matrix given in app. D. From (D.4) we have:

$$\mathrm{Tr}(|11\rangle\langle 11|\rho_l) = 2\frac{2^l - 1}{2^l + 1}c_3^2 \tag{6.3.11}$$

which implies that the probability for a double excitation to occur is directly proportional to c_3^2 and approaches c_3^2 with increasing level.

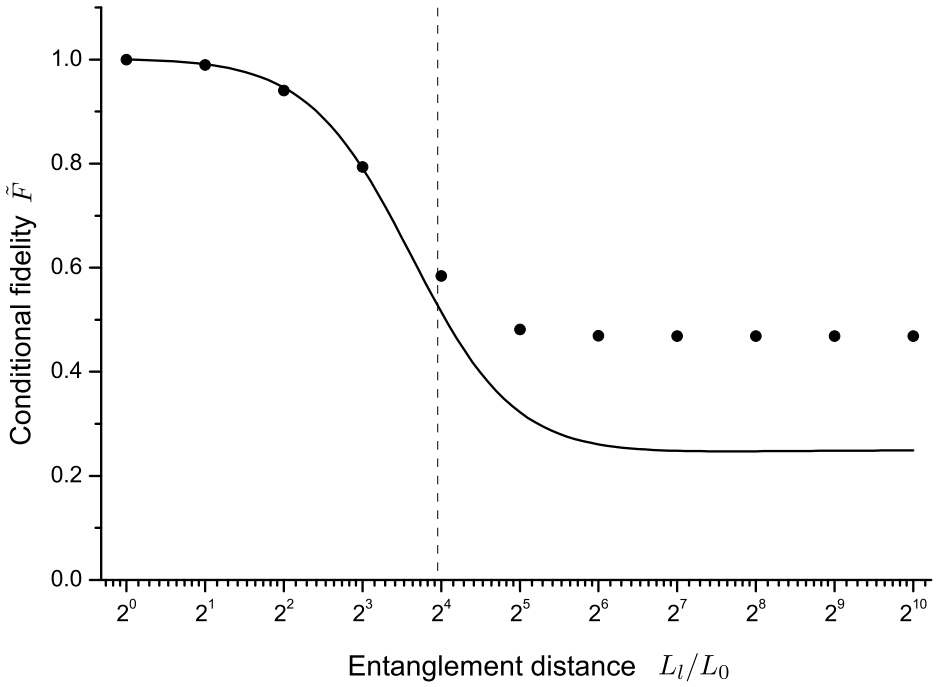

Figure 6.12: Analytic (curve) and simulated (dots) conditional fidelity. The parameter values are $\kappa = 2$, $r = 0.01$, $\eta = 0.1$. The dashed vertical line indicates the predicted level at which $\tilde{F}$ drops away from 1.

In fig. 6.12 we plot $\tilde{F}$ obtained from the pertubative approach, and the corresponding values from simulation for the orange curve of fig. 6.11. Note that (6.3.10) is the lowest order approximation to the full expression obtained in the pertubation, and hence agrees witht the plot only for small l. We see that there is good agreement until the deviation of $\tilde{F}$ from 1 becomes large, i.e. until the error in $\tilde{F}$ becomes significant. Similar agreement is found for other values of the parameters; further plots can be found in app. E. We can use (6.3.10) to give a rough estimate of the level at which the error in conditional fidelity becomes significant, or equivalently the level at which good repeater performance breaks down. The

breakdown occurs when the magnitude of the c_3-term approaches 1, i.e. when:

$$\frac{1}{2}2^l(2^l-1) = c_3^{-2} \tag{6.3.12}$$

For any choice of parameters κ, r, η the value of c_3 is computed and this equation is solved to find the value of l where $\tilde{F}$ drops[15]. We have indicated the estimated breakdown on fig. 6.12 and we note that there is good agreement with the numerical simulation (see also app. E). The values for the location of the breakdown obtained from (6.3.12) should only be taken as rough estimates since, when the c_3-term approaches 1, the perturbation to first order in c_3 which lead to (6.3.10) ceases to be valid and the drop is also not a well located entity. The breakdown of repeater performance and the breakdown of the perturbative approach coincide.

We should note that the expression (6.3.10) resembles the simple model of (6.2.6) but is not identical to it. In sec. 6.2.2 we did not have any exact analytical model for the evolution of errors and we simply allowed the power α of $L_l/L_0 = 2^l$ to deviate from 1 because we observed that some contributions to $\tilde{F}$ containing errors are suppressed less than others. In the present case we have a more accurate description of the density matrix and the form of the errors. It may well be that the actual form of $\tilde{F}$ for the DLCZ-repeater also involves several terms of different powers in L_l/L_0, and by fitting we can find that the model (6.2.6) is in fact a good approximation to (6.3.10) for low levels. However the essential feature is the same in both cases: the error in conditional fidelity grows polynomially in the communication distance $L_l/L_0 = 2^l$. Both repeater schemes outperform direct communication (via a noisy channel) as required.

For the communication rate obtained by simulation we have only single number. This is again due to the restrictions imposed by the runtime of our algorithm. We obtain the communication rate for the orange curve of fig. 6.11 when $N = 3$. Three connection steps is about the highest we can go with moderate runtimes and we choose the orange curve because a fidelity well above the classical 1/2 limit is maintained. By increasing κ one may also increase the rate, but $\kappa = 2$ is already pushing the experimental limits and so we do not go above this value. Since in the simulation of the repeater which led to the fidelities fig. 6.11 we assumed perfect generation of entanglement, i.e. $|\Psi^+\rangle$, we do not have a success probability for the generation step. Therefore we have to make a choice. To ease comparison with the DLCZ-repeater results, we choose $p_0 = 10^{-3}$. We find:

Again we see that the analytically calculated rate is too high by a factor of about 2.5, but is accurate within the order of magnitude. The rate for direct communication is $\sim 10^{-27}\tau^{-1}$, i.e. 10^{22} times less.

From the simulated rates the performance of the DLCZ-repeater is slightly better than for the system of this section: The rates agree within two standard deviations, but the final conditional fidelity for the DLCZ-repeater is 19% higher.

[15] The solution can be found either numerically or by solving $x(x-1) = 2c_3^{-2}$. Putting $x = 2^l$ yields $l = \log_2(1 + \sqrt{1 + 8c_3^{-2}}) - 1$ where we chose the positive root since $l \geq 0$.

$N = 3$	Simulated rate $[10^{-5} \cdot \tau^{-1}]$	Analytical rate $[10^{-5} \cdot \tau^{-1}]$	Final $\tilde{F}$
$\kappa = 2$ $\eta = 0.1$ $r = 0.01$	5.3 ± 0.7	12	0.79

Table 6.2: Communication rate for repeater with two-pass larmor rotating memory and final conditional fidelity. τ is the time for a single connection or generation attempt.

However, in the simulation of the DLCZ-repeater we did not consider any noise sources, while here we have taken into account realistic reflection losses and atomic decoherence. Hence we cannot say anything conclusive about which protocol performs better. It might be interesting to examine the communication rate in the case of no noise, $r = \eta = 0$.

Further sources of noise which were not included in our simulations will be discussed in the outlook sec. 7.2.

6.4 Repeater with One-pass Memory

The third and last repeater we shall look at is based on the quantum memory realised experimentally by the quantum optics group at the Niels Bohr Institute (part of QUANTOP[16]). Their results were reported in [18]. Only the write-in step has been demonstrated in experiment and in simulations we assume a perfect read-out. We also consider a read-out in terms of sequential passes of a light pulse, which leads to transformation equations similar to those of write-in.

6.4.1 Setup

The setup for write-in to this memory shown in fig. 6.13 is very similar to that of sec. 6.3.1, and the level structure of the atoms is the same. As for the two-pass scheme, the interesting quantum states are encoded in a weak y-polarised field superposed on a strong x-polarised coherent beam, and they are written into the atomic angular momentum. The system is quantised along x and the population of the ground level (with $m = \pm 1/2$) is assumed to be dominant, so that the angular momentum is strongly polarised in the x-direction. Hence the Holstein-Primakoff approximation (fig. 6.7) applies again, and the light and atoms are described by harmonic oscillator quadrature operators X_L, P_L, X_A, P_A. As mentioned previously a single pass through the cell is not enough to make a quantum memory. For the two-pass scheme the second pass was introduced to obtain the desired storage of states. In the present scheme measurement and feedback is used. As indicated on the figure, the operator X_L for the light is measured after passage through the cell, and the outcome of the measurement is fed back onto the atomic

[16]Danish National Research Foundation Center for Quantum Optics, http://www.quantop.nbi.dk/

operator P_A using a magnetic pulse. With this feedback the write-in equations for the quadrature operators become [17, 18]:

$$X'_A = X_A + \kappa P_L \tag{6.4.1a}$$
$$P'_A = (1 - \kappa g)P_A - gX_L \tag{6.4.1b}$$

where primes denote operators after the interaction and feedback. κ is the coupling strength and g is the feedback gain. Note that the equations are *not* symmetric in X and P because the geometry of the setup is not symmetric in y and z and because of the absence of any external magnetic field.

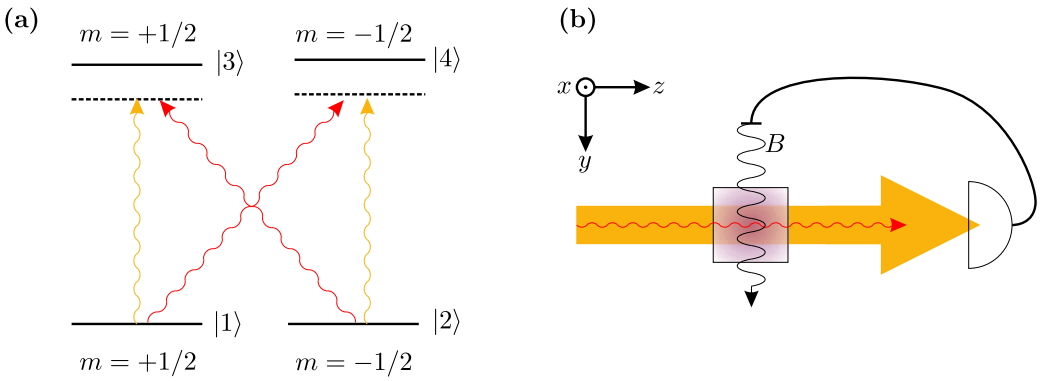

Figure 6.13: One-pass memory. **a)** Level structure of the atoms in the ensemble. The collective atomic spin is assumed to be polarised with a dominant population of atoms in an even superposition of the $m = \pm 1/2$ ground states. **b)** Setup for write-in. A magnetic pulse conditioned on measurement outcome feeds X_L back onto the atoms.

Write-in described by (6.4.1) has been demonstrated in experiment with a fidelity of stored states up to ∼70% as reported in [18]. However no read-out from the cells has been demonstrated, and in our simulations we will assume that the read-out used in the entanglement connection step is simply perfect. It would of course be preferable to have a more realistic model for the read-out, but as none has been demonstrated and there is no obvious, experimentally feasible protocol (see below) we take this approach. Using a perfect read-out means that our simulations will give an upper bound on the performance of a repeater based on the connection scheme fig. 5.2 and the one-pass memory. Any such repeater with a realistic read-out is bound to perform worse than our ideal case. With this choice for the read-out, the full state transfer into and out of the memory is given by:

$$X'_L = X'_A = X_A + \kappa P_L \tag{6.4.2a}$$
$$P'_L = P'_A = (1 - \kappa g)P_A - gX_L \tag{6.4.2b}$$

which in terms of the mode operators takes the form:

$$\hat{a}'_L = (1 - \frac{\kappa g}{2})\hat{a}_A + \frac{\kappa g}{2}\hat{a}^\dagger_A - \frac{i}{2}(\kappa + g)\hat{a}_L + \frac{i}{2}(\kappa - g)\hat{a}^\dagger_L \tag{6.4.3}$$

We note that in this equation, there is no choice of the parameters κ, g for which the transfer is perfect. Two terms drop out when $\kappa = g = 1$, and the transfer would be perfect, up to a phase shift, if the $\hat{a}_A^\dagger$-term was not there. The phase $(-i)$ on $\hat{a}_L$ we can eliminate simply by a $\pi/2$ phase shift on the incoming light. To suppress the $\hat{a}_A^\dagger$ contribution to the output requires the initial atomic state to be squeezed.

Recall from sec. 2.1.5 that a squeezed state is a state for which the uncertainty (variance) of one of the quadrature operators is below the limit in the Heisenberg uncertainty relation at the expense of a larger uncertainty in the conjugate operator. We can generate squeezed states by acting with the squeezing operator (2.1.23), and as discussed at the end of sec. 4.1, this operator can be included into the Bogoliubov transformation used to compute the generating function. This means that we should replace the input atomic operator $\hat{a}_A$ by (see [12] p. 153):

$$S^\dagger(\xi)\hat{a}_A S(\xi) = \cosh(r)\hat{a}_A - e^{i\theta}\sinh(r)\hat{a}_A^\dagger \tag{6.4.4}$$

From (6.4.2) we see that it is the X_A-quadrature that we need to squeeze. Hence we set $\theta = 0$. For convenience we also define a new parameter s which from (2.1.24) is the factor of squeezing in the quadratures:

$$s \equiv e^{2r} \qquad \cosh(r) = \frac{s+1}{2\sqrt{2}} \qquad \sinh(r) = \frac{s-1}{2\sqrt{2}} \tag{6.4.5}$$

Applying the squeezing to the input atomic operators and a phase shift to the input light, we find that the Bogoliubov transformation for the state transfer becomes:

$$\hat{a}'_L = \frac{s(1-\kappa g)+1}{2\sqrt{s}}\hat{a}_A + \frac{s(\kappa g - 1)+1}{2\sqrt{s}}\hat{a}_A^\dagger + \frac{1}{2}(\kappa + g)\hat{a}_L - \frac{1}{2}(\kappa - g)\hat{a}_L^\dagger \tag{6.4.6}$$

We immediately see that the state transfer is perfect in the limit $\kappa = g = 1$ and $s \gg 1$.

To simulate the repeater using the generating function method, we need the transformation for the entanglement connection fig. 5.2, including the beam splitter. The Bogoliubov transformation used in the simulations is:

$$\hat{a}''_{L1} = \frac{1}{\sqrt{2}}\left(\hat{a}'_{L1} + \hat{a}'_{L2}\right) \qquad \hat{a}''_{L2} = \frac{1}{\sqrt{2}}\left(\hat{a}'_{L1} - \hat{a}'_{L2}\right) \tag{6.4.7}$$

with primed variables given by (6.4.6). With equation (6.4.7) we have included the squeezing operator, which generates the squeezed input states, into the state transfer Bogoliubov transformation, and the input state of the atomic modes should therefore be taken to be vacuum. The states of the input light are supposed to be perfect Bell states $|\Psi^+\rangle$ coming from an ideal entanglement generation step. Any realistic entanglement generation, such as parametric down conversion, will lead to a worse performance of the repeater.

Above we stated that there is not an obvious experimentally feasible protocol for read-out of the one-pass memory. We can however suggest a scheme which

leads to equations of the same form as (6.4.1). Fig. 6.14 shows the proposed setup. The entire read-out pulse makes two sequential passes through the cell (this is in contrast to the setup fig. 6.1 where the pulse meets itself in the sample). The transformation equations in this case are:

$$X'_L = X_L + \kappa_2 P'_A \tag{6.4.8a}$$
$$P'_L = (1 - \kappa_1\kappa_2)P_L - \kappa_1 X'_A \tag{6.4.8b}$$

Here κ_1, κ_2 are the coupling strengths in the first and second pass respectively. We see that κ_1 corresponds with the feedback gain for write-in while κ_2 corresponds to the coupling strength. The primes on the atomic operators indicate that a light state has already been stored in them during write-in.

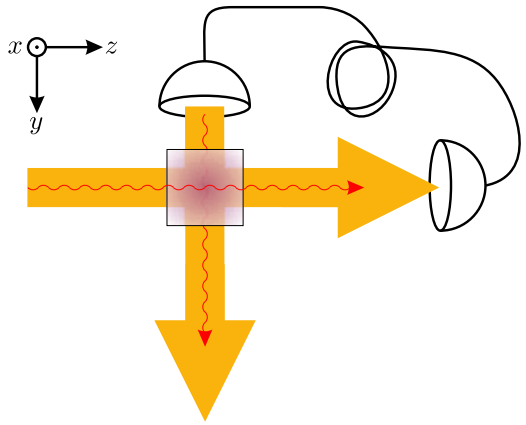

Figure 6.14: Read-out from one-pass memory. After the first passage, the entire light pulse is coupled into a delay line (it is not measured) and then makes a second passage through the cell.

The setup fig. 6.14 is not very realistic with current experimental technology. Sequential passes require a delay line, as illustrated, with an optical length greater than the read-out pulse length. In [18] the duration of write-in pulses is on the order of ms which means above 10km of delay line. At the current experimental stage this is impossible[17]. However we should not exclude the possibility that future experiments might be constructed with shorter pulse lengths or otherwise, to allow a delay line, and that the dynamics of (6.4.8) might be realised[18].

The primary reason that we have mentioned the read-out scheme above is that the simulations we have performed can be understood alternatively as simulations of a repeater using this read-out scheme together with a perfect write-in step ,(as opposed to perfect read-out and write-in described by (6.4.1)). With perfect write-

[17] According to private correspondence with J. Sherson.

[18] An obvious alternative to sequential passes is feedback onto the light in complete analogy with the write-in. However this is at least as difficult to realise experimentally.

in, the transformation for the state transfer becomes:

$$X_L' = X_L + \kappa_2 P_A' = X_L + \kappa_2 P_L^{in} \tag{6.4.9a}$$

$$P_L' = (1 - \kappa_1\kappa_2)P_L - \kappa_1 X_A' = (1 - \kappa_1\kappa_2)P_L - \kappa_1 X_L^{in} \tag{6.4.9b}$$

where X_L^{in}, P_L^{in} apply to the input light which is stored in the atoms and X_L, P_L apply to the read-out pulse before interaction. The form of (6.4.9) and (6.4.2) is exactly the same except that the noisy terms to be squeezed now come from the read-out light pulse and not from the initial atomic state. Hence our simulation results apply equally well to a repeater with the read-out fig. 6.14. The symmetry between the two models comes from the fact that the identity transformation — which describes the perfect step in both protocols — commutes with any other transformation.

6.4.2 Results

We will proceed along the same lines as in sec. 6.3.2. Numerical simulations of the one-pass memory repeater are compared with analytical results from the perturbative approach in chap. 5, and we also find the communication rate for a specific choice of parameters.

In our model of the one-pass memory there are three parameters κ, g and s, and no sources of decoherence have been included. We have noted already in the description of our model that the squeezing s is crucial for the quality of a state transfer into and out of the memory and hence for repeater performance. In fig. 6.15 we have plotted the conditional fidelity found from simulation for five different values of s. The values of κ, g are chosen to be optimal with the given squeezing. Using the generating function we have performed the first entanglement connection analytically in *Mathematica* and obtained an expression in s, κ, g for the fidelity after connection. For fixed values of s this expression was optimised w.r.t. κ and g and the resulting values were then used in numerical simulation of the remaining connection steps[19]. The values are given in the figure caption and we note that they are always close to 1, which is the optimal choice when $s \gg 1$. The curves again take an s-shape, as with both systems previously analysed.

Mode reduction of the Bogoliubov transformation (6.4.6) for the state transfer is easy, since it is already on the reduced form (5.2.2), and we can simply read off the coefficients:

$$b_1 = \frac{1}{2}(\kappa + g) \qquad b_2 = \frac{s(1 - \kappa g) + 1}{2\sqrt{s}} \tag{6.4.10}$$

$$c_1 = \frac{1}{2}(\kappa - g) \qquad c_2 = \frac{s(\kappa g - 1) + 1}{2\sqrt{s}} \qquad c_3 = 0$$

[19]It is not possible simply to obtain an exact analytic expression for the density matrix at each level via the generating function, because the complexity of the expressions generated by *Mathematica* increase explosively with the level and so does the time it takes to generate the expressions.

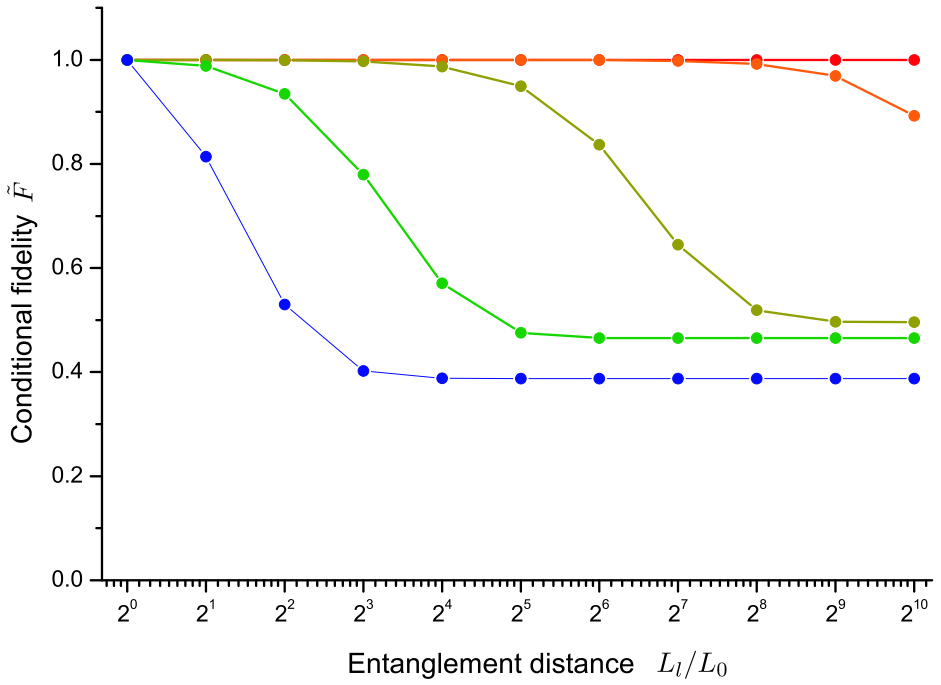

Figure 6.15: Simulated conditional fidelity. From top to bottom the values of $[s, \kappa, g]$ are $[10^9, 1.00, 1.00]$ (red), $[10^6, 1.00, 1.00]$ (orange), $[10^3, 1.00, 1.00]$ (olive), $[10, 1.01, 0.96]$ (green), $[1, 1.17, 0.83]$ (blue).

Adding the solutions for perturbation in b_2, c_1, c_2 from sec. 5.3 and app. D we obtain the density matrix ρ_l in the perturbative approximation and the corresponding fidelity and conditional fidelity:

$$F = \frac{2}{2^l+1} - 2\frac{2^l-1}{(2^l+1)^2}b_2^2 + \frac{1}{3}\frac{2\cdot 2^{3l} - 6\cdot 2^{2l} - 5\cdot 2^l + 9}{(2^l+1)^2}c_1^2 + \frac{1}{3}\frac{(2^l-1)(2^l-6)}{2^l+1}c_2^2 \tag{6.4.11}$$

and

$$\tilde{F} = 1 - \frac{1}{2}(2^l-1)c_1^2 - \frac{1}{2}2^l(2^l-1)c_2^2 \tag{6.4.12}$$

Note that the coefficient of c_2 in (6.4.12) is the same as the c_3-coefficient in (6.3.10). This is because perturbation in c_2 and c_3 lead to the same parametrisation of the density matrix (see app. D).

Again, c_1, c_2 constitute the active elements of the state transformation, while b_2 does not contribute to the conditional fidelity. From (D.1) and (D.4) the probability for a double excitation in ρ_l is:

$$\mathrm{Tr}(|11\rangle\langle 11|\rho_l) = (1 - \frac{2}{2^l+1})c_1^2 + 2\frac{2^l-1}{2^l+1}c_2^2 \tag{6.4.13}$$

And from (6.4.12) we may estimate the level at which repeater performance breaks

down by solving the equation[20]:

$$\frac{1}{2}(2^l - 1)c_1^2 + \frac{1}{2}2^l(2^l - 1)c_2^2 = 1 \tag{6.4.14}$$

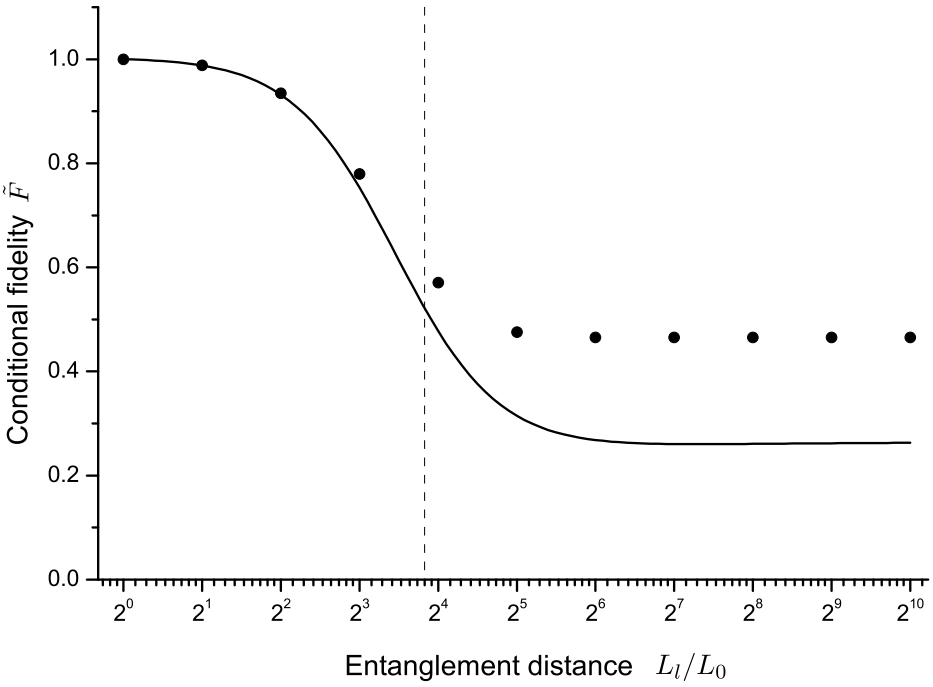

Figure 6.16: Analytic and simulated conditional fidelity. The parameter values are $s = 10$, $\kappa = 1.01$, $g = 0.96$. The dashed vertical line indicates the predicted level at which $\tilde{F}$ drops away from 1.

The locations of breakdown obtained this way are indicated on fig. 6.16 and the figures in app. E. As for the repeater of sec. 6.3 we find good agreement with numerical simulation.

Note that the expression (6.4.12) is polynomial in the communication distance $L_l/L_0 = 2^l$, as for both of the repeater schemes studied previously.

As for the repeater with the two-pass larmor rotating memory, we have just a single number for the communication rate of the repeater using the one-pass memory. We have computed the rate for three connection steps of the green curve in fig. 6.15. We choose this curve, since $N = 3$ is the highest number of steps we can simulate with moderate runtimes and, according to private correspondence with J. Sherson and others, a squeezing of $s = 10$ is the maximum which can be achieved with present technology[21]. For the entanglement generation, which was assumed to be perfect, we choose a success probability of $p_0 = 10^{-3}$. For these parameters, we have found:

[20] We have solved the equation numerically.

[21] In more conventional experimentalist terms: a squeezing of 10db

$N = 3$	Simulated rate $[10^{-5} \cdot \tau^{-1}]$	Analytical rate $[10^{-5} \cdot \tau^{-1}]$	Final $\hat{F}$
$s = 10$ $\kappa = 1.01$ $g = 0.96$	6.8 ± 0.7	15	0.78

Table 6.3: Communication rate for repeater with one-pass memory and final conditional fidelity. τ is the time for a single connection or generation attempt.

Also for this system the analytical rate is off by a factor of ca. 2.5 but agrees with the simulated rate on the order of magnitude, and the direct communication rate is $\sim 10^{-26}\tau^{-1}$. Within a few standard deviations the rate agrees with both the DLCZ-repeater and the repeater with a two-pass larmor rotating memory, and we can give no conclusion as to which protocol performs better. We note, though, that no errors sources were included in simulations of the present scheme and even under these ideal conditions a high squeezing is required for repeater operation.

Chapter 7

Conclusion and Outlook

In this chapter we summarise and conclude the results which have been presented and discussed in chap. 5 and 6. We also outline future work: extending simulations to include noise and photon counting.

7.1 Conclusion

Three DLCZ-type repeaters have been studied in this thesis. Each of them use a different atomic quantum memory, but all use the entanglement connection scheme of the original DLCZ proposal (fig. 5.2) with non-counting photodetectors. Very idealised models have been considered for the memories. In all three cases either write-in or read-out was assumed to be perfect, and only for the two-pass memory of sec. 6.3 was noise during memory operation considered.

To make the simulations possible all memories were treated as harmonic oscillator systems, and a range of *Mathematica* programs were developed, based on the generating function method of chap. 4. These programs themselves constitute a substantial part of the output from the master thesis project. They allow simulation of any DLCZ-type repeater using a memory which may be described by harmonic oscillators. Indeed they allow us to compute the output state from any Bogoliubov transformation, given the input. They can be used to obtain both numerical and analytical results, although some numerical tasks are solved rather inefficiently, due to the fact that *Mathematica* is not a very fast language for numerics. The slow numerical algorithms should be portable to faster languages. Based on the harmonic oscillator model and the generating function, we also developed a perturbative model of a DLCZ-type repeater using a general parametrised quantum memory and perfect entanglement generation. This model was applicable to two out of the three systems studied.

For the three repeaters which were studied the relevant measure of the quality of generated entanglement was found to be the conditional fidelity $\tilde{F}$, because non-counting detectors lead to a rapidly increasing vacuum component of the generated states. States with good conditional fidelity may be used for quantum key

distribution or in probabilistic teleportation with posterior confirmation of excitations, as explained in [8]. The conditional fidelity decreases polynomially with the communication distance for all three systems, as required to beat direct communication, and within the validity range of the perturbation there is good agreement between $\tilde{F}$ computed from numerical simulation and $\tilde{F}$ computed from our analytical model. The model gives good estimates of the level (i.e. the number of connection steps) after which $\tilde{F}$ departs from 1, as this coincides with the level where the perturbation breaks down.

It was seen that the observed decrease in fidelity can be explained by the occurrence of extra excitations created during light-atom interaction. The double excitations can cause decrease fast-than-linear in the communication length L, and we believe this is because states without excitations are suppressed more in $\tilde{F}$. Our analytical model provides expressions for the probability of double-excitations to occur in terms of the perturbation parameters.

For realistic settings of the memory parameters, the communication distances for which a good conditional fidelity can be maintained are rather low. The system of sec. 6.3, a reflection coefficient of $r = 0.01$ is straining the current experimental limits. With this value a conditional fidelity well above the classical $1/2$ limit is maintained only for three connection steps. Similarly, with a high squeezing $s = 10$ for the system of sec. 6.4 we can do three connections before $\tilde{F}$ drops below $1/2$. For the DLCZ-repeater the important parameter is the excitation probability p_c, and high fidelities are obtained when $p_c \ll 1$ which may be achieved by using light pulses of low photon number (i.e. weak pulses). For this system about six steps can be reached with good $\tilde{F}$ with a p_c equal to the entanglement generation success probability for the other two systems. However $\tilde{F}$ is likely to drop faster if reflection losses and other noise sources are included. Judging from recent experiments with entangled photons, the segment length L_0 of the repeaters may be of order 1-100km [8, 23, 26]. Three connection steps then corresponds to a total communication length of at most $L = 2^3 L_0 = 800$km. Hence we find that even within our idealised models, the inter-country communication implied by the city names in fig. 3.1 is far from a realistic scenario for the systems considered. It cannot be excluded that one of them may be used for experimental verification of the repeater protocol.

Communication rates were obtained for three parameter settings of the DLCZ-repeater and for only one parameter setting for each of the remaining repeaters. The rates confirm that the repeaters outperform direct communication significantly: when the communication distance $L = 2^3 L_0$ and the success probability for entanglement generation $p_0 = 10^{-3}$, all three repeaters give rates[1] of order $10^{-5}\tau^{-1}$, while the rate for direct communication is $\sim 10^{-26}$. Here τ is the time spent on a single connection or generation attempt. Taking $\tau = 1$ms, which from

[1] One might worry that the fact that the communication rates are close to equal is an artifact of the runtime limitations on our simulation. However, this is not so. We have chosen realistic values of the memory parameters, and found the rates for those settings. We have not adjusted the parameters to maximise the rate.

[18] is a realistic value, the bit-rate becomes $\sim$0.5 qubits/minute. Again this is much too low for practical applications such as quantum key distribution, but may also be insufficient for experimental verification of the protocols, since in experiment good statistics is required for conclusive results.

Because our models are very idealised it is difficult to say anything about which repeater would be easier to implement in an experimental setting, or which repeater will perform better under realistic conditions. All three systems that have been studied exhibit the important features of a quantum repeater: sub-exponential scaling of the (conditional) fidelity and communication rates well above the rate for direct transmission. Hence each of them may in principle be used in experimental verification of DLCZ-type quantum repeaters. The DLCZ-repeater seems to maintain better fidelity at a communication rate of the same order of magnitude as those found for the other two protocols, but this picture may change when reflection losses and other error sources are included. For the repeater of sec. 6.3, reflection losses at the sides of the cell containing the atomic sample was the major source of noise, and the important parameter for the conditional fidelity was the reflection coefficient r. Because the memories used in the two other protocols only require one pass of the light pulse, we do not expect reflection losses to be as severe for these systems, but they are still likely to play a role. For the repeater using the one-pass memory a high squeezing is required for performance comparable to that of sec. 6.3 under ideal conditions, and if the fidelity is further degraded by reflection losses and other noise this repeater will not perform well. Hence we suggest that it is more expedient to implement either the DLCZ-repeater or the repeater using the two-pass memory in experiment.

7.2 Outlook

The work presented in this thesis is very open ended in the sense that much can be done to improve and extend the results.

First, it is desirable simply to perform more simulations than we have done, since some aspects of the repeaters were not studied very thoroughly due to lack of time to perform the required program runs. Particularly for the communication rates it could be interesting to obtain more data to find e.g. how the rate depends on the communication distance L and the coupling parameter κ. As a part of this, it might be advantageous to port the algorithm used to simulate the rate to a language which handles numerics fast than *Mathematica*. For example *C++*. From the pertubative model we may also obtain analytical expressions for the success probabilities for entanglement connection, and from these probability we may get an analytical expression for the communication rate, which could then be compared with simulation.

Second, in all our work we have considered only non-counting photodetectors, because efficient photon counting detectors are very difficult to construct experimentally. However, it cannot be excluded that a photon counting detector suitable

for the repeater schemes studied here could be developed and it is interesting to examine how the protocols would perform with such a detector. Photon counting may easily be treated with the generating function method and in fact during the work on this project, we have already implemented photon counting partially. Programs computing the generating function for entanglement connection using photon counting detectors have been written for all three memories, and the perturbation in chap. 5 has been partially solved for a repeater using this connection procedure. Simulations leading to values of the fidelity and communication rate still remain to be carried out.

Third, and most important, a lot of error sources have been neglected in the simulations that have been done so far. The most important of these errors are *dark counts*. For a photodetector it may happen that the detector clicks even though no photon is present. Such an event is called a dark count. Dark counts are a serious type of error because they can lead to double excitations in the entangled states of the repeater, and we have seen that double excitations caused the observed decrease in conditional fidelity. If a dark count occurs at the time of connection of two entangled states, we may get the situation shown in fig. 7.1. None of the excitations in the two entangled pairs are read out, but the detector clicks and hence connection is assumed to be successful. The resulting state of mode 1 and 4 is a double excitation.

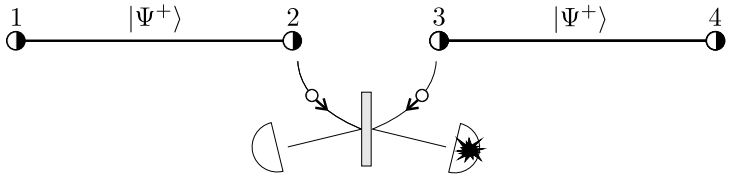

Figure 7.1: A dark count error leading to a double excitation.

A low dark count rate is 10Hz to 100Hz[2], which for an entanglement connection time of $\tau = 1$ms corresponds to a dark count probability during connection of 1 to 10%. This probability is not negligible, and hence dark counts must be expected to have significant impact on repeater performance. It is possible to treat dark counts within the generating function method by considering separately the two situations: 1) no dark count occurs, 2) a dark count occurs. For each situation the generating function can be computed (recall that measurements are included in the generating function), and at each timestep of the repeater we can then compute the state after entanglement connection as

$$\rho = (1 - p_{dc})\rho_1 + p_{dc}\rho_2 \tag{7.2.1}$$

where ρ_1, ρ_2 come from entanglement connection with the two generating functions corresponding to (1) and (2). Inclusion of dark count in the simulations is of high priority in future work.

[2]See e.g. http://www.edinst.com/detectors.htm

In addition to dark counts there are other physical sources of error present: Reflection losses and atomic decoherence were considered for the repeater of sec. 6.4 and should also be considered for the two other systems. Detector inefficiency is equivalent to photon loss and can be included by an increase of reflection coefficient. Background photons hitting the detectors have the same effect as dark counts and should be isolated against.

Fourth and last, as in the original DLCZ proposal [8], the cost of classical communication has been completely neglected in our simulations of the communication rate. It is not obvious that the time spent on classical information exchange is negligible compared to the time needed for entanglement generation and connection attempts, and a thorough analysis of the exact amount of classical communication needed for repeater operation would be desirable.

In summary, much can still be done in terms of noise inclusion to improve our picture of the performance of the three repeater systems considered in this thesis. The tools needed to do so are largely in place in our *Mathematica* implementation of the generating function method. Most important are dark counts, which may be included by a slight modification of the programs we have developed.

Chapter 8

Parallel Channel Mixing

In this chapter we report on investigation of an idea to improve the performance of parallel DLCZ-type repeaters by a modification of the repeater protocol on the abstract level, i.e. independent of the physical implementation, namely channel mixing. After unsuccessful attempts at an analytical solution, an algorithm for numerical simulation was implemented in *Mathematica* to find the communication rate. The idea for modification and the method used for simulation are presented in the sections below.

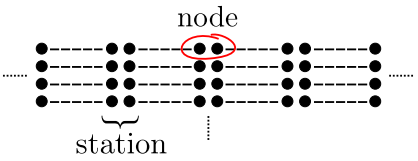

Figure 8.1: Parallel DLCZ-type repeater channels. The terms node and station have different meanings as illustrated.

Unfortunately time has not allowed a thorough numerical analysis of what communication rates can be achieved with the modified protocol. For an accurate analysis good statistics are required, demanding many runs of our algorithm for each parameter setting. Although we have been careful about the complexity of the algorithm it has a runtime on the order of 10 hours on our machines[1] for moderate communication distances and realistic values of the connection probabilities. As mentioned in the previous chapter, it would have been preferable to use a numerically fast programming language such as *C++* or perhaps *MATLAB*. We have used the algorithm to obtain the communication rates given in chap. 6 and have also made a few simulations of parallel channel mixing for the systems discussed there.

8.1 Idea

Recall that the communication rate for a quantum repeater is the number of final entangled states established per unit time. If m identical repeaters are operated independently in parallel, then the combined communication rate will be m times

[1] The IMB pentium 4 machines in the NBI computer room.

the rate for a single repeater. We want to investigate, how much the combined rate can be improved for parallel DLCZ-type repeaters by mixing channels.

Recall from sec. 3.2.3 that entanglement between nodes of separation L_0 is initially created and then extended over increasing distances by successive connection at every second node. We consider a system of m parallel DLCZ-type repeaters, and we suppose that nodes in different repeaters which are at the same distance from the endpoints are located close to each other spatially in stations as shown in fig. 8.1. Following the DLCZ-type repeater protocol, each entanglement connection is a probabilistic event which fails with a probability depending on the distance level (c.f. fig. 3.4). In the case of failure entanglement is lost on the whole segment involved in the connection. If connection was successful for the neighbouring segments on the same level, these pairs will then be idle until a new attempt succeeds. With parallel repeater channels, it may therefore happen that we have the situation shown in fig. 8.2 (a).

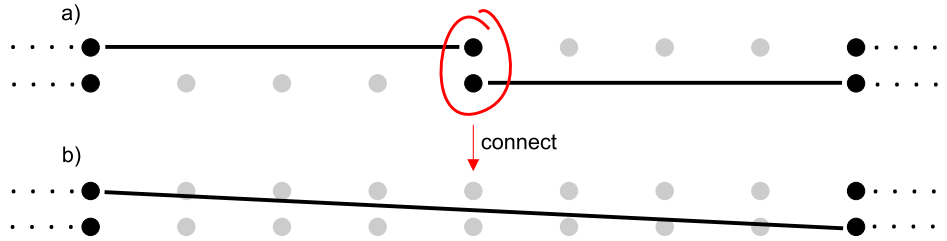

Figure 8.2: Mixing of channels. **a)** A situation where entanglement connections on corresponding segments have failed in one channel and succeeded in the other. **b)** The encircled nodes are located on the same spatial location. We can therefore connect the entangled pairs in each channel, to create a new pair of double length.

Instead of leaving the segments for which connection has succeeded idle, we can combine pairs from parallel channels as illustrated in fig. 8.2 (b). This way the communication rate may be improved.

It is not clear a priory how large the improvement in the communication rate will be. On the one hand the number of possible 'routes' that lead to a final entangled pair - i.e. the number of combinations of nodes which are connected to create the pair - increases dramatically with the number of parallel channels for large L. If we take account of the fact that fixing one route excludes all other routes which have entanglement connections on nodes shared with the first one at any level, then the number of different ways to prepare in parallel m final entangled pairs is $\sim (m!)^{2L/L_0}$. On the other hand, the probability for any one of these routes to occur must depend on the connection probabilities p_l, and it is apparent that in the case where $p_l = 1$ for all levels l, there will be no improvement over the independent parallel scheme because there is never need for any entangled pair to be idle. When the p_l depart from 1 we expect the improvement to increase.

To be able to make a quantitative analysis of channel mixing we need to specify the details of the repeater system we look at. The features we choose for our system

are as follows:

- There are m parallel channels of length $L = 2^N L_0$.
- At each timestep the maximal number of entanglement connections are attempted at each distance level in parallel.
- Inner nodes are freed for reuse after successful connections.
- Connections are always at every second station on a given level. What end of a pair to connect is fixed.
- The nodes of final entangled pairs are freed for reuse after one timestep.

We assume the repeater to operate in discrete timesteps of duration τ which may be taken as the time spent on a single entanglement creation or connection attempt. At each timestep and each distance level[2] we check for entangled pairs in neighbouring segments which may be connected, and all possible connections are attempted, if necessary by mixing channels as in fig. 8.2. This means that an entangled pair in a given segment will never be idle, unless the neighbouring segment has fewer or no pairs to connect with.

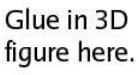

Figure 8.3: Channel mixing repeater. At some fixed timestep the figures show each distance level for a possible state of a simple channel mixing repeater with $N = 3$ and hence $L = 2^3 L_0$.

Fig. 8.3 shows a possible state of a repeater with channel mixing. At each level the entangled pairs and the connections that will be attempted are indicated. Note that the repeater operates in parallel on all levels; 0-level segments of a channel which are 'free' - i.e. for which the nodes are not part of any entangled pair - will immediately be used for new entanglement creation. In particular, whenever a connection attempt succeeds on a level higher than 1, the 0-level segments ending on the nodes involved in that connection (i.e. those encircled in fig. 8.2 (a)) are freed. Nodes at the channel ends which form a final entangled pair, are assumed to be used for communication in the timestep following their creation. They are then freed for reuse.

At a fixed level the stations along the repeater where entanglement connection may be performed are fixed to be every second station on that level. One might imagine a situation where an entangled pair could be extended by connecting it at the end which is not at one of these stations, but in that case we choose rather to leave the pair idle. The reason for not allowing this type of connection is, mainly that it would imply a significant complication of the simulation algorithm - and also of the repeater protocol itself.

[2] I.e at each level in fig. 3.4

8.2 Algorithm

Now, having decided on the particulars of the repeater to work with, we are ready for simulation. Here we outline the basic structure of the algorithm used. The actual code is not included in the thesis. It can be found online, refer to app. F for the reference. Note that because the entanglement creation and connections are probabilistic events, the simulation is necessarily a stochastic process, i.e. a Monte Carlo simulation. The inputs to the algorithm are m, N, a list of the success probabilities p_i for entanglement connection and generation and the number of timesteps for which the repeater should be run, given by T/τ.

In the most direct approach an algorithm can keep track of every single node in the repeater, storing information about whether the node is entangled and with what other node. It can then loop through all nodes to check whether entanglement connection or creation can be attempted and perform the attempts where possible. Such an approach would need to allocate an array of length $m2^N$ (the total number of nodes) and the runtime complexity for a single timestep would be at least $O(m2^N)$. We can do somewhat better than this with a less direct approach. The algorithm we use is outlined in fig. 8.5.

Instead of keeping track of individual nodes, we store the population of entangled pairs for each segment of the repeater at each level. On level l there are 2^{N-l} segments - the disentangled level has 2^N - and so we need to store an array of

$$2^N + \sum_{l=0}^{N} 2^{N-l} = 2^{N+1} + 2^N - 1 = 3 \cdot 2^N - 1 \tag{8.2.1}$$

integers. This is $O(3 \cdot 2^N)$ independent of m and is an improvement over the approach above when $m > 3$. For each timestep on each level $N > l \geq 0$ we then loop through all pairs of segments between which connection is allowed. There are 2^{N-l-1} segment pairs on level l. Thus, including 2^N iterations for entanglement creation on the disentangled level and one iteration for freeing end-point pairs, the total runtime complexity per timestep becomes

$$2^N + 1 + \sum_{l=0}^{N-1} 2^{N-l-1} = 2^N + 1 + 2^N - 1 = 2^{N+1} \tag{8.2.2}$$

which is $O(2 \cdot 2^N)$. Again this is independent of m and is an improvement over the direct approach when $m > 2$.

The purpose of the loop over segment pairs is to perform entanglement connections. This is done as follows. We start by finding the lowest population number n in the two segments. This is the number of connections which can be attempted. If it is nonzero, we draw a number at random according to a binomial distribution $b(n, p_{l+1})$, where p_{l+1} is the probability for connection of two level l pairs to succeed. This random number is the number of successful connection attempts; the rest fail. The successful connections add to the population of the corresponding

segment on level $l+1$. The ones which fail add to the free pairs on the disentangled level. Finally n is subtracted from the populations of the two segments in the pair.

After running the algorithm for the specified number of timesteps we find the rate in units of τ^{-1} by dividing the total number of entangled state generated on level N by the number of timesteps T/τ.

8.3 Preliminary Results

To analyse the effect of channel mixing, we should run the algorithm for various settings of the parameters in the model, i.e. the channel length determined by N, the number m of parallel channels, and the connection and creation probabilities p_l. The communication rates obtained this way should then be compared with the corresponding rates for independent channels which can be found by scaling the rate found when $m = 1$ with m.

We have used the algorithm, with $m = 1$, to compute the communication rates given in sections 6.2.2, 6.3.2 and 6.4.2. We have also made one simulation of the m-dependence of the rate with and without channel mixing. The result is shown in fig. 8.4. The plot was obtained with connection probabilities of half the value of those corresponding to the rate for the repeater with two-pass larmor rotating memory (tab. 6.2).

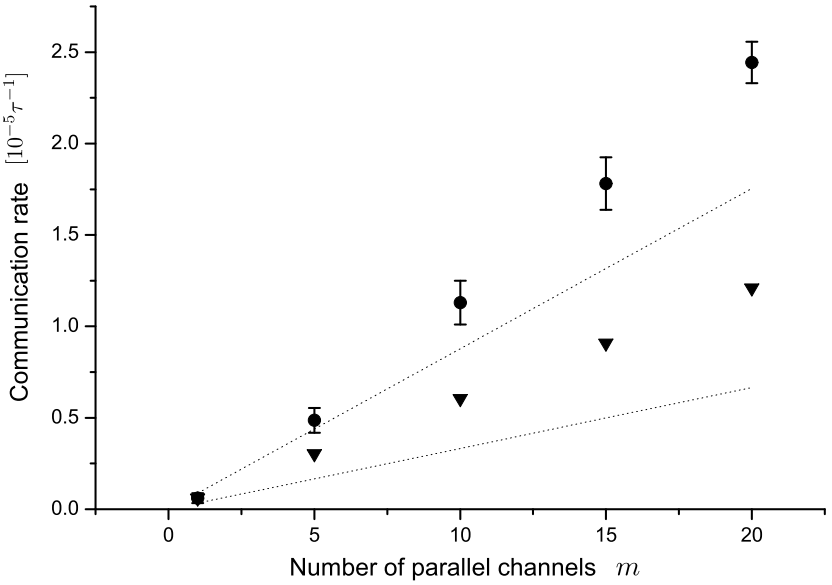

Figure 8.4: Rates with and without channel mixing. Circles show the rate with mixing, triangles without mixing. Dotted lines bound the error in linear extrapolation from the simulated $m = 1$ rate.

We observe an increase in communication rate of about a factor two for each $m > 1$. The rate with mixing appears to have a slightly superlinear scaling with

m, but the deviation is not significantly outside the errors. To test for such a deviation the rate should be plotted for a larger range of m-values. Whether or not the rate with channel mixing is really superlinear, the improvement over independent parallel channels is not big. In our calculations we have completely neglected the increase in classical communication which is necessary for channel mixing. For a single channel each node need only communicate with two other nodes at each timestep. With channel mixing each node needs to communicate with $2m$ other nodes. Hence the amount of classical information exchange needed for channel mixing scales linearly in m, and if the improvement in rate over independent channels is close to constant (as suggested by fig. 8.4) then the gain in rate by mixing might well be cancelled by the time spent on classical communication[3]. A more thorough analysis of the effect of classical communication on the rate is needed to determine how much, if anything, can be gained by parallel channel mixing.

As a conclusion on the preliminary results above, we make two hypotheses:

1) When mixing channels according to the model described in sec. 8.1 the scaling of the communication rate with m is superlinear.

2) With a moderate number of parallel channels $m \sim O(10)$ no significant gain in communication rate is obtained by channel mixing.

[3]Note though that a linear increase in the total number of classical messages sent does not necessarily imply a linear increase in communication time.

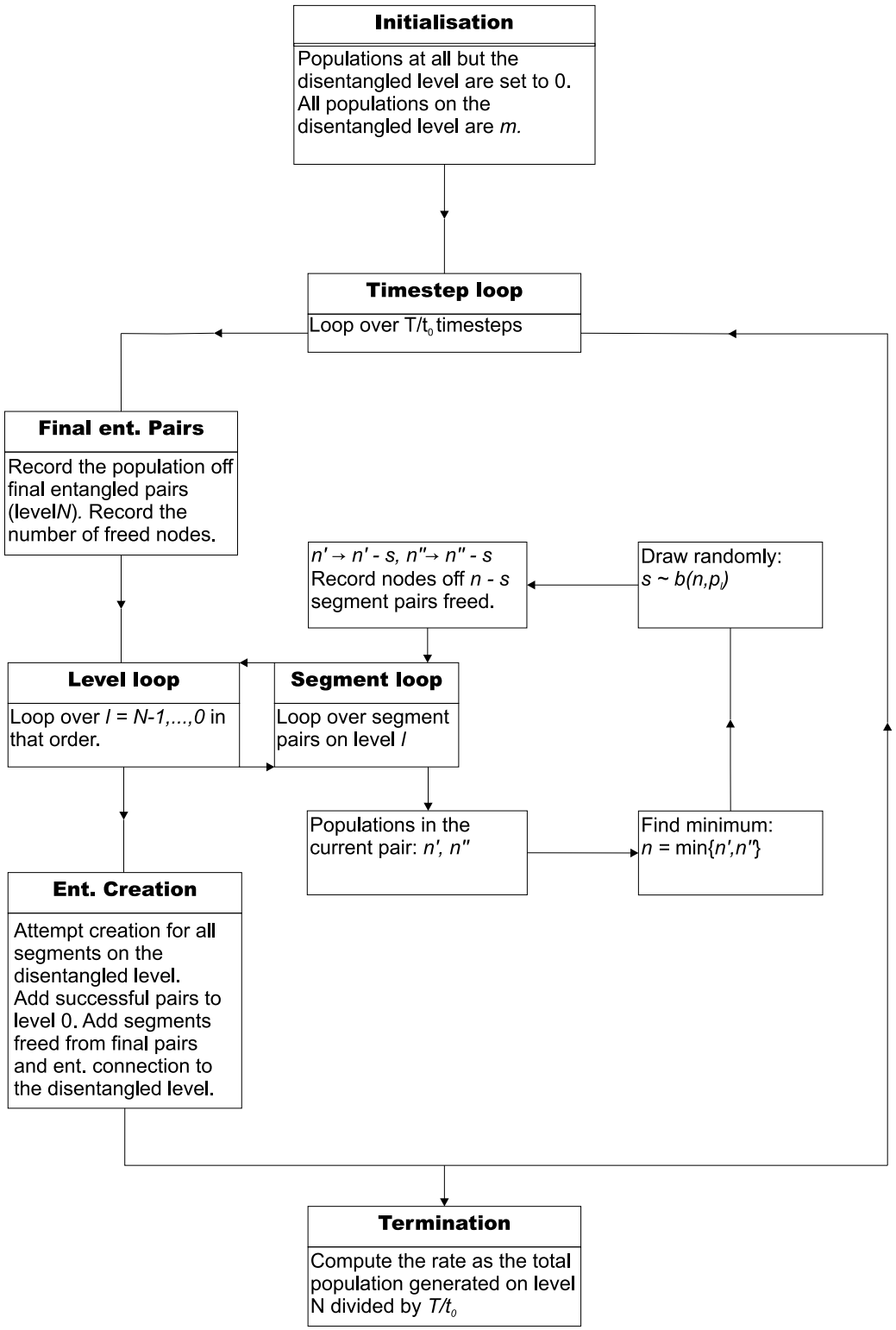

Figure 8.5: Layout of algorithm for simulation of a channel mixing repeater.

Appendix A

Quantum Teleportation

In this appendix we justify the results shown in tab. 2.1. Please refer to sec. 2.2.3 for the setup.

Let the initial state of qubit 1 be given by $|\psi\rangle = a|0\rangle + b|1\rangle$ where $a, b \in \mathbb{C}$ and $|a|^2 + |b|^2 = 1$. The joint initial state is $|\psi\rangle_1 \otimes |\Phi^+\rangle_{23}$. To find the state of the qubits after the measurement we have to act on this state with U_{Bell} followed by one of the projection operators

$$|00\rangle_{12}\langle 00| \quad |01\rangle_{12}\langle 01| \quad |10\rangle_{12}\langle 10| \quad |11\rangle_{12}\langle 11| \tag{A.1}$$

We will do the calculation for the second of these, corresponding to the measurement outcome 01.

Since U_{Bell} is the transformation from the Bell to the computational basis, acting to the left it turns computational basis states into Bell states. Hence we find:

$$\begin{aligned}
& \Big[|01\rangle_{12}\langle 01|\Big] U_{Bell} \Big[|\psi\rangle_1 \otimes |\Phi^+\rangle_{23}\Big] \qquad (A.2)\\
= \; & \Big[|01\rangle_{12}\langle \Phi^-|\Big]\Big[|\psi\rangle_1 \otimes |\Phi^+\rangle_{23}\Big] \\
= \; & \frac{|00\rangle_{12}\langle 00| - |00\rangle_{12}\langle 11|}{\sqrt{2}} \left[\frac{a|00\rangle_{12} + b|10\rangle_{12}}{\sqrt{2}} \otimes |0\rangle_3 + \frac{a|01\rangle_{12} + b|11\rangle_{12}}{\sqrt{2}} \otimes |1\rangle_3\right] \\
= \; & \frac{1}{2}|00\rangle_{12} \otimes \big[a|0\rangle_3 - b|1\rangle_3\big]
\end{aligned}$$

From this output we see that the probability of obtaining the measurement outcome 00 is $\frac{1}{4}$ independent of the coefficients a, b since this is the square of the normalisation factor for the state (we could also have found this by the standard route of taking the trace of the projection operator with the reduced density matrix for the measured system).

What is more, we see that the final state of qubit 3 is precisely $Z|\psi\rangle$ as claimed in tab. 2.1. The calculations for the three other measurement outcomes are similar.

Appendix B

Many-mode Generating Function

In this appendix we state expressions for the generating function of a Bogoliubov transformation on an arbitrary (countable) number of modes. We have built on and extended an idea due to A. S. Sørensen. Before we proceed, we prove the following

Lemma

$$|vac\rangle\langle vac| = \int \frac{dpdx}{2\pi} e^{-(x^2+p^2)/4} D(\frac{x+ip}{\sqrt{2}}) \tag{B.1}$$

where $|vac\rangle$ is the vacuum state for the mode on which D acts.

Proof

The quadrature operators are defined by $X = (\hat{a}^\dagger + \hat{a})/\sqrt{2}$ and $P = i(\hat{a}^\dagger - \hat{a})/\sqrt{2}$. The eigenstates of X form a complete set and are denoted by $|x\rangle$, where $x \in \mathbb{R}$ (up to a factor, X is the position operator of the simple harmonic oscillator). Since the commutator is $[X, P] = i$, the translation operator for the X-eigenstates is given by $e^{-iP\Delta x}$ (see e.g. [27] p. 44ff). We may therefore write:

$$|x\rangle\langle x'| = |x\rangle\langle x| e^{iP(x'-x)} = |x\rangle\langle x| e^{-(\hat{a}^\dagger - \hat{a})\frac{x'-x}{\sqrt{2}}} = |x\rangle\langle x| D(\frac{x-x'}{\sqrt{2}}) \tag{B.2}$$

Now for any $x' \in \mathbb{R}$ we have:

$$\begin{aligned} \int \frac{dp}{2\pi} e^{ip(X-x)}|x'\rangle &= \int \frac{dp}{2\pi} e^{ip(x'-x)}|x'\rangle = \delta(x'-x)|x'\rangle \\ &= \delta(x'-x)|x\rangle = |x\rangle\langle x|x'\rangle \end{aligned} \tag{B.3}$$

and hence the operator $|x\rangle\langle x|$ equals the integral expression on the left. Inserting this into (B.2) we obtain:

$$\begin{aligned}
|x\rangle\langle x'| &= \int \frac{dp}{2\pi} e^{ip(X-x)} D(\frac{x-x'}{\sqrt{2}}) = \int \frac{dp}{2\pi} e^{ip(\frac{\hat{a}^\dagger+\hat{a}}{\sqrt{2}}-x)} e^{\hat{a}^\dagger \frac{x-x'}{\sqrt{2}} - \hat{a}\frac{x-x'}{\sqrt{2}}} \\
&= \int \frac{dp}{2\pi} e^{\hat{a}^\dagger \frac{x-x'+ip}{\sqrt{2}} - \hat{a}\frac{x-x'-ip}{\sqrt{2}}} e^{-ip(x+x')/2} \\
&= \int \frac{dp}{2\pi} D(\frac{x-x'+ip}{\sqrt{2}}) e^{-ip(x+x')/2} \qquad \text{(B.4)}
\end{aligned}$$

where the disentangling theorem was used in the second line. With the help of (B.4) and (4.1.14) we can express the projection on the vacuum in the following manner (note that the vacuum state is not the same as $x = 0$):

$$\begin{aligned}
|vac\rangle\langle vac| &= \int dxdx' |x\rangle\langle x|vac\rangle\langle vac|x'\rangle\langle x'| \\
&= \int dxdx' |x\rangle\langle x'|\langle vac|x'\rangle\langle x|vac\rangle \\
&= \int \frac{dxdx'dpdp'}{(2\pi)^2} D(\frac{x-x'+ip}{\sqrt{2}}) e^{-ip(x+x')/2} e^{-\frac{1}{2}\left|\frac{x'-x+ip'}{\sqrt{2}}\right|^2} e^{-ip'(x+x')/2} \\
&= \int \frac{dxdx'dpdp'}{(2\pi)^2} D(\frac{x-x'+ip}{\sqrt{2}}) e^{-i(p+p')(x+x')/2} e^{-\frac{1}{4}\left[(x-x')^2+p'^2\right]} \\
&= \int \frac{dydy'dpdp'}{2(2\pi)^2} D(\frac{y+ip}{\sqrt{2}}) e^{-i(p+p')y'/2} e^{-(y^2+p'^2)/4} \\
&= \int \frac{dydpdp'}{2(2\pi)} D(\frac{y+ip}{\sqrt{2}}) \delta(\frac{-p-p'}{2}) e^{-(y^2+p'^2)/4} \\
&= \int \frac{dydp}{2\pi} e^{-(y^2+p^2)/4} D(\frac{y+ip}{\sqrt{2}}) \qquad \text{(B.5)}
\end{aligned}$$

relabelling the variable 'y' $\rightarrow$ 'x' concludes the proof of the lemma■

Now we generalise the generating function of sec. 4.1 to many modes. As in that section we have a collection of harmonic oscillator modes $\{a_i\}$ and a Bogoliubov transformation given by (4.1.11). At first we consider the case without measurements. We let index o run over the output modes, while i runs over all modes. The generating function is defined by:

$$\begin{aligned}
F &\equiv \mathrm{Tr}_{i\setminus o}\left[{}_{out}\langle vac| \left(\prod_o e^{\delta_o \hat{a}_o}\right) U \left(\prod_i e^{\beta_i \hat{a}_i^\dagger}\right) |vac\rangle\langle vac| \left(\prod_i e^{\alpha_i \hat{a}_i}\right) U^\dagger \left(\prod_o e^{\gamma_o \hat{a}_o^\dagger}\right) |vac\rangle_{out} \right] \\
&= \langle vac| \left(\prod_i e^{\alpha_i \hat{a}_i}\right) U^\dagger \left(\prod_o e^{\gamma_o \hat{a}_o^\dagger} |0\rangle_o\langle 0| e^{\delta_o \hat{a}_o}\right) U \left(\prod_i e^{\beta_i \hat{a}_i^\dagger}\right) |vac\rangle \\
&= e^{\frac{1}{2}\Sigma} \times \langle vac| \left(\prod_i D_i(-\alpha_i)\right) U^\dagger \left(\prod_o D_o(\gamma_o)|0\rangle_o\langle 0|D_o(-\delta_o)\right) U \left(\prod_i D_i(\beta_i)\right) |vac\rangle \qquad \text{(B.6)}
\end{aligned}$$

where $\Sigma \equiv \sum_i(\alpha_i^2+\beta_i^2)+\sum_o(\gamma_o^2+\delta_o^2)$. All the parameters of F are real; differentiation w.r.t. α_i, β_i determine the input matrix element, while γ_o, δ_o determine the output.

We define $w_o \equiv (x_o+ip_o)/\sqrt{2}$, $dW \equiv \prod_o \frac{d^2w_o}{\sqrt{2}\pi} = \prod_o \frac{dp_o dx_o}{2\pi}$ and $\Sigma_o \equiv \sum_o |w_o|^2$. Making use of the above lemma and the transformation rule (4.1.12) we then obtain the form of F which is implemented in our programs:

$$F = e^{\frac{1}{2}\Sigma} \times \int dW e^{-\frac{1}{2}\Sigma_o} K \tag{B.7}$$

with the kernel:

$$\begin{aligned} K &= \langle vac| \left(\prod_i D_i(-\alpha_i)\right) U^\dagger \prod_o D_o(\gamma_o) D_o(w_o) D_o(-\delta_o) U \left(\prod_i D_i(\beta_i)\right) |vac\rangle \\ &= \langle vac| \left(\prod_i D_i(-\alpha_i)\right) \\ &\left(\prod_{o,i} D_i(\gamma_o b_{oi}^* - \gamma_o c_{oi}) D_i(w_o b_{oi}^* - w_o^* c_{oi}) D_i(-\delta_o b_{oi}^* + \delta_o c_{oi})\right) \\ &\left(\prod_i D_i(\beta_i)\right) |vac\rangle \end{aligned} \tag{B.8}$$

Now we should like to extend this formula to also include measurements. We consider a setup in which the measured modes are distinct from the output modes and where the only measurement outcomes we condition on are the ones corresponding to (4.1.17), i.e. the presence or absence of a click in the detector. All measurements are on a single mode. More general cases can be treated with generating functions, but this will suffice for our purposes. Introducing two more indices l, d to index respectively the subsets of modes for which measurement yields a click and the subsets of modes for which measurement yields no click, (B.7) is modified to become (B.9).

$$
\begin{aligned}
F \;=\; \langle vac| & \left[\prod_i D_i(-\alpha_i)\right] \\
& \left[\prod_{o,i} D_i(\gamma_o b^*_{oi} - \gamma_o c_{oi})\right] \\
& \left[\prod_{o,i} \int \frac{d^2 w_o}{\sqrt{2}\pi} e^{-\frac{1}{2}|w_o|^2} D_i(w_o b^*_{oi} - w^*_o c_{oi})\right] \\
& \left[\prod_{d,i} \int \frac{d^2 w_d}{\sqrt{2}\pi} e^{-\frac{1}{2}|w_d|^2} D_i(w_d b^*_{di} - w^*_d c_{di})\right] \\
& \left[\prod_{l} \mathbb{1} - \int \frac{d^2 w_l}{\sqrt{2}\pi} e^{-\frac{1}{2}|w_l|^2} \prod_i D_i(w_l b^*_{li} - w^*_l c_{li})\right] \\
& \left[\prod_{o,i} D_i(-\delta_o b^*_{oi} + \delta_o c_{oi})\right] \\
& \left[\prod_i D_i(\beta_i)\right] |vac\rangle
\end{aligned}
\tag{B.9}
$$

This is the expression which has been implemented in the programs. In the implementation the expression is always expanded out. The integral in each term is pulled out so that the vacuum expectation is evaluated first and the resulting quadratic function is integrated afterwards, as described in steps 1–3 of sec. 4.1.

Appendix C

Entanglement Connection and Creation with Beam Splitters

Here we give short derivations to put on firm ground the procedure for entanglement connection of sec. 5.1 and the entanglement generation of sec. 6.2.1.

Connection

We consider the setup of fig. C.1 and require a single click in one detector only for successful connection.

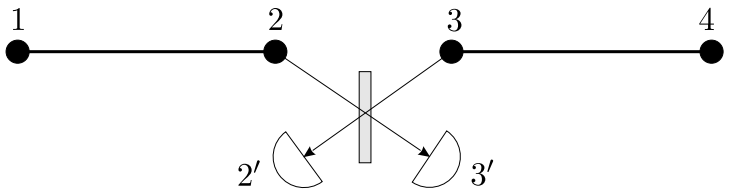

Figure C.1: Entanglement connection or creation. Modes 1,2 and 3,4, are initially entangled.

For simplicity let us assume that the left detector clicks. The projection operator corresponding to this outcome is $\hat{a}^\dagger_{2'}|vac\rangle\langle vac|\hat{a}^\dagger_{2'}$. Now the beam splitter takes vacuum to vacuum (it is passive) and transforms $\hat{a}_2 \rightarrow \frac{1}{\sqrt{2}}(\hat{a}_{2'} + \hat{a}_{3'})$ and $\hat{a}_3 \rightarrow \frac{1}{\sqrt{2}}(\hat{a}_{2'} - \hat{a}_{3'})$. Taking the inverse of this transformation, we see that our measurement is equivalent to a projection onto the state $\frac{1}{\sqrt{2}}(\hat{a}^\dagger_2 + \hat{a}^\dagger_3)|vac\rangle = |\Psi^+\rangle_{23}$.

If the initial state of modes 1234 is $|\Psi^+\rangle_{12} \otimes |\Psi^+\rangle_{34}$ we then obtain the unnormalised final state from:

$$
\begin{aligned}
{}_{23}\langle\Psi^+|\left[|\Psi^+\rangle_{12}\otimes|\Psi^+\rangle_{34}\right] &= \frac{1}{2\sqrt{2}}{}_{23}\langle vac|\left[(\hat{a}_2+\hat{a}_3)(\hat{a}_1^\dagger+\hat{a}_2^\dagger)(\hat{a}_3^\dagger+\hat{a}_4^\dagger)\right]|vac\rangle_{all} \\
&= \frac{1}{2\sqrt{2}}(\hat{a}_1^\dagger+\hat{a}_4^\dagger)|vac\rangle \qquad \text{(C.1)}
\end{aligned}
$$

renormalising, this state is exactly $|\Psi^+\rangle_{14}$ as desired.

In the case where the right detector clicks, the output state of modes 1,4 will be $|\Psi^-\rangle$ which can be transformed to $|\Psi^+\rangle$ by a local phase shift of mode 1.

Generation

Now consider the entanglement generation setup in fig. 6.1b. After interaction between the input pulse and the atoms, the joint state of atomic ensemble and Stokes output light is a two-mode squeezed state. When the excitation probability is small $p_c \ll 1$ the state is:

$$|\xi\rangle = (\sqrt{1-p_c}+\sqrt{p_c}\hat{a}_A^\dagger\hat{a}_L^\dagger)|vac\rangle \qquad \text{(C.2)}$$

The conditioning scheme is the same as in fig. C.1 with modes 1,4 being the atomic modes and modes 2,3 being the Stokes light modes. Hence, as before, a click in the left detector corresponds to projection onto $|\Psi^+\rangle_{23}$. To find the output state of the atomic modes, we repeat the calculation (C.1) with modes 1,2 and 3,4 in the new input state given by (C.2). We get:

$$
\begin{aligned}
&{}_{23}\langle\Psi^+|\left[|\xi\rangle_{12}\otimes|\xi\rangle_{34}\right] \\
&= \frac{1}{\sqrt{2}}{}_{23}\langle vac|\left[(\hat{a}_2+\hat{a}_3)(\sqrt{1-p_c}+\sqrt{p_c}\hat{a}_1^\dagger\hat{a}_2^\dagger)(\sqrt{1-p_c}+\sqrt{p_c}\hat{a}_3^\dagger\hat{a}_4^\dagger)\right]|vac\rangle_{all} \\
&= \frac{\sqrt{p_c}}{\sqrt{2}}(\hat{a}_1^\dagger+\hat{a}_4^\dagger)|vac\rangle \qquad \text{(C.3)}
\end{aligned}
$$

to lowest order in p_c. Renormalising gives $|\Psi^+\rangle_{14}$ as desired.

Note from (C.3) that the probability for the left detector to click is $p_c/2$. Thus the total probability to get a single click — and therefore for the generation to succeed — is p_c. On the other hand, we made the assumption that $p_c \ll 1$. If this condition is relaxed, errors of order $O(p_c)$ will appear in the output state of modes 1,4 and the state will no longer be a perfect Bell state. In fact, if we expand the generated entangled state (found by the generating function method) to lowest order in p_c, we obtain:

$$
\begin{pmatrix}
0 & 0 & 0 & 0 \\
0 & \frac{1}{2}-\frac{p_c}{4} & \frac{1}{2}-\frac{p_c}{4} & 0 \\
0 & \frac{1}{2}-\frac{p_c}{4} & \frac{1}{2}-\frac{p_c}{4} & 0 \\
0 & 0 & 0 & \frac{p_c}{2}
\end{pmatrix} \qquad \text{(C.4)}
$$

Appendix D

Solutions for Perturbation

Referring to sec. 5.3 in this appendix we give the parametrisations of the density matrix at each distance level for perturbation in the coefficients c_1, c_2 and c_3 of (5.2.2). We state the recurrence relations for each parameter and give the solutions.

It happens that only the phase of $c1$ enters into the solutions. It will be enough for our purposes to know the solution when this phase is zero, and hence we do not find the general solution for an arbitrary phase of c_1.

Proceeding along the lines of sec. 5.3 we find:

Perturbation in c_1

Assuming that $c_1 \ll 1$, when the phase is zero, we find the following parametrisation of the density matrix:

$$\rho_i = \begin{pmatrix} 1-2f_i+(2f_i-1+2g_i)c_1^2 & 0 & 0 & (1-2f_i)c_1 \\ 0 & f_i-g_ic_1^2 & f_i-g_ic_1^2 & 0 \\ 0 & f_i-g_ic_1^2 & f_i-g_ic_1^2 & 0 \\ (1-2f_i)c_1 & 0 & 0 & (1-2f_i)c_1^2 \end{pmatrix} \tag{D.1}$$

The parameter f_i does not come from the perturbation. It is present because we are using non-counting detectors, as discussed in sec. 5.4, and obeys the same recurrence relation regardless of which coefficient we are performing the perturbation in. The recurrence for f_i was stated and solved in sec. 5.3; for completeness we give the solution again below. For the parameter g_i we find:

$$\begin{aligned} g_{i+1} &= \frac{4f_i(4+g_i)+11f_i^3-20f_i^2-4}{2f_i(f_i-2)^2} \\ &= \frac{4(1+2^{1+i}+2^{2i})g_i-2^{2+3i}+2^{2+2i}+3}{2(2^{1+i}+1)^2} \end{aligned} \tag{D.2}$$

After a change of variable to $\tilde{g}_i \equiv 2(1+2^i)^2 g_i$ this recurrence may be solved in *Mathematica*, given the initial conditions (we start from a perfect entanglement generation step, i.e. from the Bell state $|\Psi^+\rangle$). The solutions for f_i, g_i are:

$$f_i = \frac{1}{2^i+1} \tag{D.3a}$$

$$g_i = \frac{-2^{1+3i} + 3\cdot 2^{1+2i} + 5\cdot 2^i - 9}{3\cdot 2(2^i+1)^2} \tag{D.3b}$$

Perturbation in c_2

Assuming that $c_2 \ll 1$, the parametrisation is:

$$\rho_i = \begin{pmatrix} 1-2f_i+(2g_i+k_i)c_2^2 & 0 & 0 & 0 \\ 0 & f_i - g_i c_2^2 & f_i - h_i c_2^2 & 0 \\ 0 & f_i - h_i c_2^2 & f_i - g_i c_2^2 & 0 \\ 0 & 0 & 0 & -k_i c_2^2 \end{pmatrix} \tag{D.4}$$

with f_i as before and the other recurrence relations:

$$k_{i+1} = \frac{2(k_i - f_i)}{2 - f_i} = \frac{2(2^i+1)k_i - 2}{2^{i+1}+1} \tag{D.5a}$$

$$\begin{aligned} g_{i+1} &= \frac{-2f_i^3 + f_i(-2+2g_i-5k_i) + 2k_i + 3f_i^2(2+k_i)}{f_i(f_i-2)^2} \\ &= \frac{2(2^{2i}+2^{1+i}+1)g_i - 2^{2+3i} + 2^{2+2i} + 2}{(2^{1+i}+1)^2} \end{aligned} \tag{D.5b}$$

$$\begin{aligned} h_{i+1} &= \frac{2(1+f_i^2 - g_i + 2h_i - k_i + f_i(-2+g_i-h_i+k_i))}{(f_i-2)^2} \\ &= \frac{2\cdot 3(2^i+1)h_i + 2^{1+2i}}{3(2^{i+1}+1)} \end{aligned} \tag{D.5c}$$

The recurrence relations are solved in *Mathematica* after changing variables to $\tilde{k}_i \equiv (2^i+1)k_i$, $\tilde{g}_i \equiv (2^i+1)^2 g_i$ and $\tilde{h}_i \equiv 3\cdot(2^i+1)h_i$. The solutions are:

$$f_i = \frac{1}{2^i+1} \tag{D.6a}$$

$$g_i = -\frac{2}{3}\frac{2^{3i} - 3\cdot 2^{2i} - 2^i + 3}{(2^i+1)^2} \tag{D.6b}$$

$$h_i = \frac{2^{i+1}(2^i-1)}{3(2^{i+1}+2)} \tag{D.6c}$$

$$k_i = -2\frac{2^i-1}{2^i+1} \tag{D.6d}$$

Perturbation in c_3

The parametrisation for perturbation in c_3 is identical to the parametrisation when expanding in c_2.

Remark on uniqueness of solutions

For all the recursion relations above the solutions are unique since, when they are rewritten with the given variables changes they become linear inhomogeneous difference equations with constant coefficients and a form of the inhomogeneity which yields unique solutions. For example for perturbation in c_2:

$$\tilde{g}_{i+1} = 2\tilde{g}_i - 2^{2+3i} + 2^{2+2i} + 2 \tag{D.7}$$

There is a one to one correspondence between the original and the new variables, and so the initial recurrence relations have unique solutions.

Although we have solved the recurrences in *Mathematica*, solutions can be obtained by hand by the method of undetermined coefficients.

Appendix E

Additional Figures

In this appendix we collect figures in which the conditional fidelity obtained from simulation is compared with the conditional fidelity from our pertubative calculations.

The first four figures show simulations of the two-pass protocol of sec. 6.3. The parameters, are $\kappa = 2$, $\eta = 0.1$ (except for the top left $\eta = 0$), and from top left to bottom right: $r = 0$, $r = 0.01$, $r = 0.05$, $r = 0.1$.

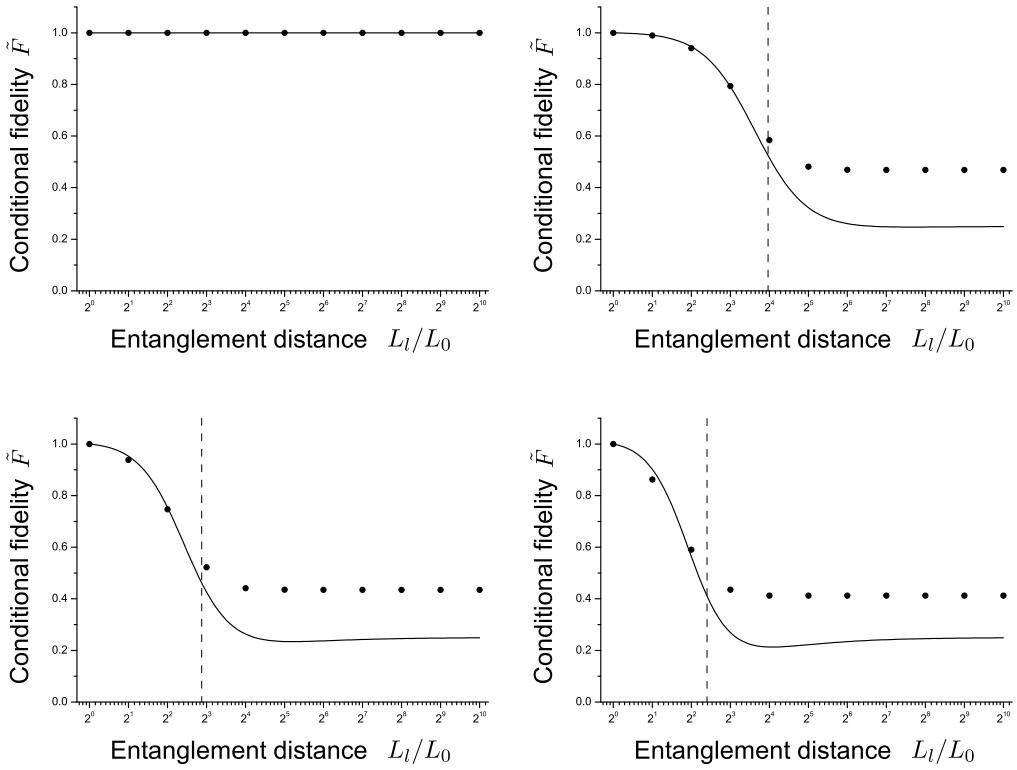

The next five figures show simulations of the one-pass protocol of sec. 6.4. From top left to bottom the parameters $[s, \kappa, g]$ are: $[10^9, 1.00, 1.00]$, $[10^6, 1.00, 1.00]$, $[10^3, 1.00, 1.00]$, $[10, 1.01, 0.96]$, $[1, 1.17, 0.83]$.

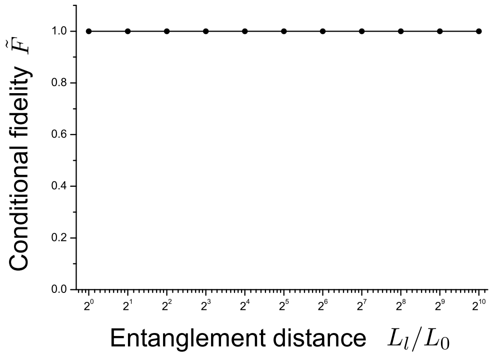

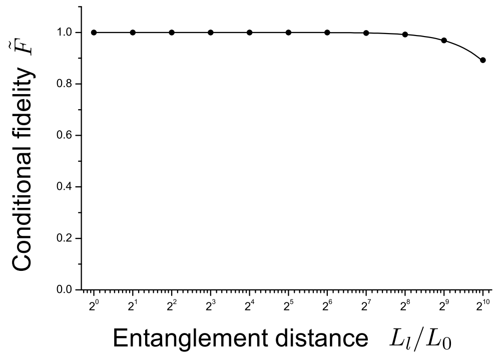

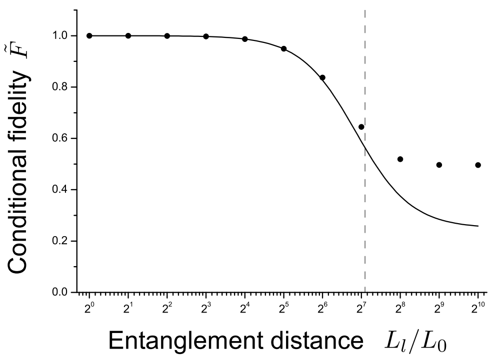

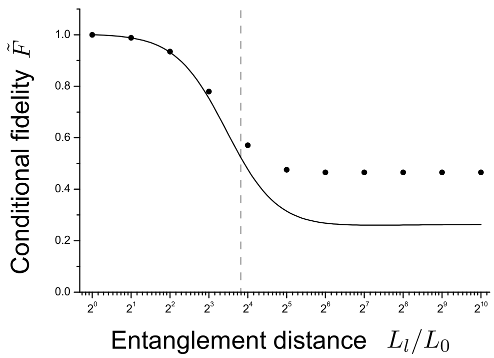

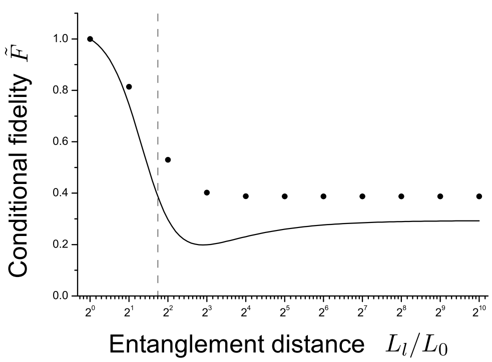

Appendix F

List of Programs

In this appendix we list the *Mathematica* programs that were used in obtaining the analytical and numerical results presented in the thesis. The total amount of code is considerable, and therefore we do not to print it. Within two month from the submission date of this thesis, the source will be available online, for the benefit of the examiners, at http://www.fys.ku.dk/ jona/speciale/.

We give a list of the *Mathematica* notebook files containing the most important procedures and calculation which were used in obtaining the results presented in this work. Online, the files are organised in folders according to the headlines below.

Code should always be well commented. Uncommeted code is largely illegible to anyone but the author, and will be so also for the programmer after short time. We have attempted to comment all code thoroughly.

Subroutines

generatingFct.nb : Provides modules to compute the generating function for a given Bogoliubov including measurements with non-resolving detectors transformation.

outputMatrix.nb : Provides modules to compute the output density matrix from a Bogoliubov transformation, given the generating function for the transformation and the input state.

repIteration.nb : Provides modules for obtaining the density matrix at each level of a repeater, given the initial state after entanglement generation and the generating function for the entanglement connection.

parallelReps.nb : Provides modules for simulation of channel mixing, to obtain the communication rate.

DLCZ-repeater

dlczEntGen.nb : Computes the generating function and output matrix from entanglement generation.

dlczGenFct.nb : Computes the generating function for entanglement connection.

dlczIter.nb : Simulates the DLCZ-repeater.

dlczRates.nb : Computes communication rates for the DLCZ-repeater.

Two-pass repeater

twopasslarmModeRedux.nb : Computes the mode reduction of the full state transfer Bogoliubov transformation.

twopasslarmGenFct.nb : Computes the generating function for entanglement connection.

twopasslarmIter.nb : Simulates the two-pass repeater.

twopasslarmRate.nb : Computes communication rates for the two-pass repeater.

twopasslarmAnalytic.nb : Implements the pertubative approach to the two-pass repeater, using the general solution for pertubation.

One-pass repeater

onepassfeedGenFct.nb : Computes the generating function for entanglement connection.

onepassfeedIter.nb : Simulates the one-pass repeater.

onepassfeedRate.nb : Computes communication rates for the one-pass repeater.

onepassfeedAnalytic.nb : Implements the pertubative approach to the one-pass repeater, using the general solution for pertubation.

Perturbation

pertGenFct_general.nb : Computes the generating function for entanglement connection using the mode reduced general full state transfer Bogoliubov transformation.

pertFidel_general.nb : Derives and solves the recurrence relations in each of the parameters in the perturbation, hence obtaining the full solution to the perturbation.

The numerical precision which was used in calculations was $MachinePrecision $\approx$ 16 digits.

Bibliography

[1] J.S.Bell: "Speakable and unspeakable in quantum mechanics" collected papers 2nd ed., Cambridge University Press 2004.

[2] C.H.Bennet *et al*: "Purification of noisy entanglement and faithful teleportation via noisy channels", Phys. Rev. Lett. 76, 722, 1996.

[3] H.-J.Briegel *et al*: "Quantum repeaters: The role of imperfect local operations in quantum communication", Phys. Rev. Lett. 81, 5932, 1998.

[4] J.-L. Chen *et al*: "Geometric observation for Bures fidelity between two states of a qubit", Phys. Rev. A 65, 024303, 2002.

[5] Z.Chen: "Characterization of maximally entangled two-qubit states via the Bell-CHSH inequality", quant-ph/0402007, 2004.

[6] L.Childress *et al*: "Fault-tolerant quantum communication based on solid-state photon emitters", Phys. Rev. Lett. 96, 070504, 2006.

[7] D.Deutsch *et al*: "Quantum privacy amplification and the security of quantum cryptography over noisy channels", Phys. Rev. Lett. 77, 2818, 1996.

[8] L.-M.Duan *et al*: "Long-distance quantum communication with atomic ensembles and linear optics", Nature 414, 413, 2001.

[9] L.-M.Duan *et al*: Supplementary information for Nature 414, 413, 2001.

[10] L.-M.Duan *et al*: "Quantum communication between atomic ensembles using coherent light", Phys. Rev. Lett. 85, 5643, 2000.

[11] A.K.Ekert: "Quantum cryptography based on Bell's theorem", Phys. Rev. Lett. 67, 661, 1991.

[12] C.C.Gerry, P.L.Knight: "Introductory quantum optics", Cambridge University Press, 2005.

[13] R.P.Feynmann: "Simulating physics with computers", Int. J. Theor. Phys. 21, 1982.

[14] S.Glancy *et al*: "Implementation of a quantum phase gate by the optical Kerr effect", quant-ph/0009110, 2000.

[15] D.Gottesmann, I.L.Chuang: "Demonstrating the viability of universal quantum computation using teleportation and single-qubit operations", Nature 402, 390-393, 1999.

[16] E.Hecht: "Optics" 4th ed., Addison Wesley, 2002.

[17] B.Julsgaard: "Entanglement and quantum interaction with macroscopic gas samples", Ph.D. thesis, University of Århus, Denmark, 2003.

[18] B.Julsgaard *et al*: "Experimental demonstration of quantum memory for light", Nature 432, 482, 2004.

[19] E.Knill *et al*: "A scheme for efficient quantum computation with linear optics", Nature 409, 46, 2001.

[20] P.W.Milonni, J.H.Eberly: "Lasers", Wiley and Sons, 1988.

[21] C.A.Muschik *et al*: "Efficient quantum memory and entanglement between light and atomic ensemble using magnetic fields", Phys. Rev. A 73, 062329, 2006.

[22] M.A.Nielsen, I.L.Chuang: "Quantum computation and quantum information", Cambridge University Press, 2000.

[23] A.Poppe *et al*: "Practical quantum key distribution with polarization entangled photons", Optics Express 12, 3865, 2004.

[24] U.V.Poulsen, K.Mølmer: "Quantum beam splitter for atoms", Phys. Rev. A 65, 033613, 2002.

[25] M.G.Raymer *et al*: "Seperability criterion for separate quantum systems", Phys. Rev. A 67, 052104, 2003.

[26] K.J.Resch *et al*: "Distributing entanglement and single photons through an intra-city, free-space quantum channel", Optics Express 13, 202, 2005.

[27] J.J.Sakurai: "Modern quantum mechanics" rev. ed., Addison Wesley Longman 1994.

[28] J.Sherson *et al*: "Light qubit storage and retrieval using macroscopic atomic ensembles", Phys. Rev. A 74, 011802, 2006.

[29] P.W.Shor: "Polynomial-time algorithms for prime factorization and discrete logarithms on a quantum computer", SIAM J. on Computation vol. 26, no. 5, 1997.

[30] T-C.Wei *et al*: "Maximal entanglement versus entropy for mixed quantum states", Phys. Rev. A 67, 022110, 2003.

Index